The performance of residential micro-cogeneration coupled with thermal and electrical storage

by

John Kopf, **B.Eng., Aerospace Engineering, Carleton University, 2010**

A thesis submitted to the
Faculty of Graduate and Postdoctoral Affairs
in partial fulfillment of the requirements for the degree of

Master of Applied Science in Mechanical Engineering

Ottawa-Carleton Institute for Mechanical and Aerospace Engineering
Department of Mechanical and Aerospace Engineering
Carleton University
Ottawa, Ontario
August, 2012

The undersigned hereby recommends to the
Faculty of Graduate and Postdoctoral Affairs
acceptance of the thesis

The performance of residential micro-cogeneration coupled with thermal and electrical storage

submitted by **John Kopf**, **B.Eng., Aerospace Engineering, Carleton University, 2010**

in partial fulfillment of the requirements for the degree of

Master of Applied Science in Mechanical Engineering

Professor Ian Beausoleil-Morrison, Thesis Supervisor,
Department of Mechanical and Aerospace Engineering

Professor Craig Merrett,
Department of Mechanical and Aerospace Engineering

Professor William O'Brien,
Department of Civil and Environmental Engineering

Professor Matei Radulescu,
Department of Mechanical Engineering, University of Ottawa

Professor Metin Yaras, Chair,
Department of Mechanical and Aerospace Engineering

Ottawa-Carleton Institute for Mechanical and Aerospace Engineering
Department of Mechanical and Aerospace Engineering
Carleton University
August, 2012

Abstract

Over 80% of residential secondary energy consumption in Canada and Ontario is used for space and water heating. Peak electricity demands resulting from residential energy consumption increase the reliance on fossil-fuel generation stations. Distributed energy resources can help to decrease the reliance on central generation stations. Presently, distributed energy resources such as solar photovoltaic, wind and bio-mass generation are subsidized in Ontario.

Micro-cogeneration is an emerging technology that can be implemented as a distributed energy resource within residential or commercial buildings. Micro-cogeneration has the potential to reduce a building's energy consumption by simultaneously generating thermal and electrical power on-site. The coupling of a micro-cogeneration device with electrical storage can improve the system's ability to reduce peak electricity demands. The performance potential of micro-cogeneration devices has yet to be fully realized. This research addresses the performance of a residential micro-cogeneration device and it's ability to meet peak occupant electrical loads when coupled with electrical storage.

An integrated building energy model was developed of a residential micro-cogeneration system: the house, the micro-cogeneration device, all balance of plant and space heating components, a thermal storage device, an electrical storage device, as well as the occupant electrical and hot water demands. This model simulated the performance of a micro-cogeneration device coupled to an electrical storage system within a Canadian household.

A customized controller was created in ESP-r to examine the impact of various system control strategies. The economic performance of the system was assessed from the perspective of a local energy distribution company and an end-user under hypothetical electricity export purchase price scenarios. It was found that with certain control strategies the micro-cogeneration system was able to improve the economic performance for both the end user and local distribution company.

To my family

Acknowledgments

First and foremost I would like to express my gratitude for the support and guidance from my supervisor Dr. Ian Beausoleil-Morrison. The past two years have been a great learning experience in many areas of my life which I will look back upon fondly, and none of it could have been possible without his commitment to take me on as a graduate student. His balance of providing support, challenges, and motivation at the right times always had my best interests in mind.

I would like to acknowledge the funding and support of this research by Natural Resources Canada's Clean Energy Fund Program and by the Natural Sciences and Engineering Research Council of Canada through my supervisor's Discovery Grant.

I would like to thank Dr. Ken Darcovitch and Dr. Ben Kenney at the National Research Council's Institute for Chemical Process and Environmental Technology for their experimental work with lithium-ion batteries. Thank you as well to Mark Douglas and Geoff Johnson of Natural Resources Canada's CANMET Energy Division for their experimental work with fuel cells.

Great thanks to all of my colleagues at the Sustainable Building Energy Systems Laboratory at Carleton University, I could not have asked for a better team. Thank you to Courtney Edwards, Skai Edwards, Geoff Johnson, Briana Kemery, Stephen McMurtry, Andrea Pietila, Patrice Pinel, Neil Saldanha, and Adam Wills, who all took the time to provide their expertise and support. Thank you for the tea breaks, barbecues, bike trips, wine and cheeses, and homemade beers, and thank you to those who took the time to review sections of my thesis.

A special thank you to all of my friends and family who have been understanding and supportive throughout this endeavour.

Finally, I would like to express my sincerest appreciation for my girlfriend, Lindsay Los. Her continued support and encouragement was crucial to my success, and her selfless love never ceased despite my physical and often mental absence. Getting to know her has made this experience more enjoyable than I could have ever imagined.

Table of Contents

List of Tables

List of Figures

Nomenclature

Abbreviations

AC	alternating current
BOP	balance of plant
BPS	building performance simulation
CHP	combined heat and power
CV	control volume
DC	direct current
DHW	domestic hot water
DOD	depth of discharge
EGHX	exhaust-gas-to-water heat exchanger
EPP	export purchase price
EU	end user
FC	fuel cell
FCPM	fuel cell power module
FD	finite difference
FIT	Feed-in Tariff
GHG	greenhouse gas

HHV	higher heating value
HOEP	Hourly Ontario Energy Price
HRV	heat recovery ventilator
HVAC	heating, ventilation and air-conditioning
ICE	internal combustion engine
IESO	The Independent Electricity System Operator
microFIT	micro Feed-in Tariff
LDC	local distribution company
LHV	lower heating value
li-ion	lithium-ion
NG	natural gas
OCV	open circuit voltage
OPA	Ontario Power Authority
PCU	power conditioning unit
PEMFC	proton exchange membrane fuel cell
PV	photovoltaic
RES	residential electric storage
SE	Stirling engine
SH	space heating
SOC	state of charge
SOFC	solid oxide fuel cell
TOU	time-of-use

Math Symbols

A	area	$[m^2]$
C_p	specific heat capacity	$[J/kgK]$
h	convective heat transfer coefficient	$[W/m^2K]$
I	current	$[A]$
$\widetilde{I}$	current (phasor)	$[A]$
k	thermal conductivity	$[W/mK]$
m	mass	$[kg]$
$\dot{m}$	mass flow rate	$[kg/s]$
q	heat flow	$[W]$
q''	heat flux	$[W/m^2]$
q'''	heat source	$[W/m^3]$
R	resistance	$[\Omega]$
T	temperature	$[^oC$ or $K]$
t	time	$[seconds]$
U	heat loss coefficient	$[W/m^2K]$
V	volume	$[m^3]$
$\widetilde{V}$	voltage (phasor)	$[V]$
$\widetilde{Z}$	impedance (complex)	$[\Omega]$

Greek Symbols

α	thermal diffusivity	$[m^2/s]$

Δt or δt	time interval	$[seconds]$
δx, δy, δz	spatial intervals in x, y and $z-$directions	$[m]$
Δx, Δy, Δz	width, depth, and height of a control volume	$[m]$
θ	temperature	$[^oC$ or $K]$
ρ	density	$[[kg/m^3]]$

Subscripts and superscripts

a, b or b, a	electricity transferred between nodes
CHP	cogeneration supplied electricity
G	generation component electricity
$grid$	grid supplied electricity
$HVAC$	HVAC electrical load
I	current node
$I-1$,$I+1$	neighbouring nodes
L	load component electricity
$non-HVAC$	occupant electrical load (e.g. appliances)
$plant$	plant interaction
T	transfer component electricity
t	current time step
$t+\delta t$	future time step
x	in the x-direction

Chapter 1

Introduction and Research Objectives

1.1 Introduction

The total worldwide marketed energy consumption in 2007 was 540 EJ, one fifth of which was consumed by residential and commercial buildings (14% residential, 7% commercial) (U.S. Energy Information Administration 2010). Residential and commercial buildings accounted for 31% of the total Canadian secondary energy use in 2008 (NRCan 2012), as shown in Figure 1.1.

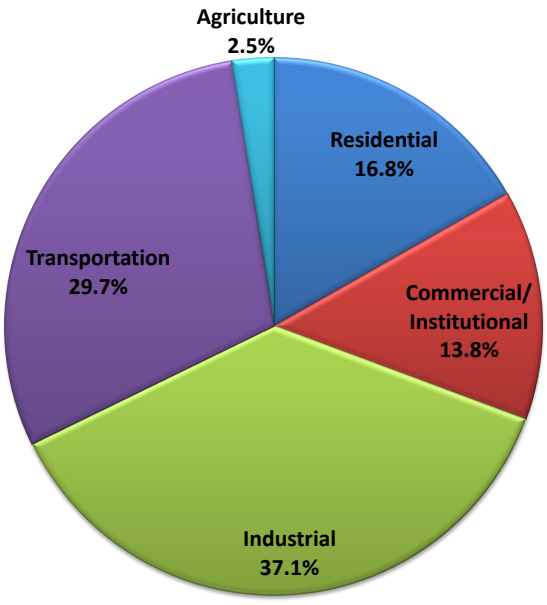

Figure 1.1: Fractional secondary energy use based on end-use for Canada (2008). Percentage of the total energy use (8720 PJ). Data from NRCan (2012).

Over 80% of the residential sector secondary energy use and over 55% of the commercial sector secondary energy use in Canada is used for space heating (SH) and water heating (NRCan 2012). Some have likened the design shift towards energy efficient residential and commercial buildings to the tapping of a new energy source, suggesting that between new developments and retrofits energy use for space heating and water heating could be cut by 50% (Capehart et al. 2011).

Cogeneration or combined heat and power (CHP) is the simultaneous production of thermal and electric power in a single thermodynamic cycle (Pehnt et al. 2006; Kolanowski 2011). There is a large amount of heat created in the thermodynamic cycles used to convert fossil fuel, nuclear, geothermal, and solar energy into electricity. Not all of this heat can be efficiently utilized for electricity production, thus heat from these processes can be recovered and used to meet space heating and water heating demands for a building.

Cogeneration has been utilized in power generation stations worldwide since the early 1900's (Hu 1985; Kolanowski 2011). However, the primary objective of power generation stations is electricity production and consequently the majority of waste heat from these plants is often under-utilized. Micro-cogeneration is a commercially available technology that exploits the efficiency advantages of cogeneration on a smaller scale than large power generation stations. A variety of devices and sizes are currently available and are suitable for use in residential and commercial buildings.

Micro-cogeneration is an emerging technology with the potential to minimize peak electricity demand (Beausoleil-Morrison 2008). Micro-cogeneration can be implemented as a distributed energy resource by installing devices in residential and commercial buildings, where they can be used to generate electricity and meet consumer heating loads simultaneously. One advantage of micro-cogeneration devices is that they can be modulated, as opposed to other distributed sources such as solar and wind that are weather reliant. Also, because their useful heat output can be used in situ (e.g. in the household), modern systems can have overall efficiencies of over 85% (sum of electrical and thermal production).

The current performance of residential micro-cogeneration systems could potentially be improved by coupling with electrical and thermal storage systems (Beausoleil-Morrison 2008). Residential space heating and electrical demands show very little coincidence, and so to fully exploit both the thermal and electrical power produced by a cogeneration unit, some method of thermal storage and residential electrical

storage (RES) is necessary.

To capture the combined interactions between a residential micro-cogeneration device coupled to a RES system, as well as the interactions between these systems and the containing building, it is ideal to model all three of these systems simultaneously in a single simulation tool. A number of building performance simulation (BPS) software tools have been in constant development since the 1970's, with over 400 tools available today (DOE 2011). Many of these are highly specialized and geared towards specific purposes (e.g. psychometric analysis, daylighting, building envelope, etc.). The ESP-r building simulation software (ESRU 2000) is well suited for complex building systems and is capable of simulating integrated models of heating, ventilation, and air-conditioning (HVAC) and electrical systems contained within a building envelope.

1.2 Research Objectives

Previous residential micro-cogeneration research has used building energy models to assess the performance of various micro-cogeneration technologies and their potential to reduce energy consumption and greenhouse gas emissions in Canada (Beausoleil-Morrison 2008). A micro-cogeneration model for simulating the performance of fuel cell devices was developed in Beausoleil-Morrison et al. (2007). This model has only been well used to simulate the performance of solid oxide fuel cells, however is also capable of modelling proton exchange membrane fuel cell devices. A RES model of a lithium ion battery device was developed in Saldanha (2010), though only simulated lithium ion cell data was previously available to calibrate this model.

The objectives of this research are to:

- model the performance of a residential micro-cogeneration device coupled with a RES system;
- examine the economic potential of the system from the perspective of an end-user and a local energy distribution company;
- assess the system feasibility in the current electricity market as well as in hypothetical scenarios so as to advise on a potential future policy for this technology.

These objectives can only be realized by means of an integrated modelling approach. This research will be based on a dynamic building model of a typical Canadian

residence containing a micro-cogeneration based HVAC system and a RES system. In this way the building and plant interactions are captured (e.g. heat losses from the hot water storage tank will enter the building, thus reducing the building's heat demand). This allows for a more accurate comparison to a typical Canadian household, where the conventional HVAC systems may contain very different components compared to a micro-cogeneration + RES system. The ESP-r building energy simulation tool will be used for developing this model and simulating the performance of the micro-cogeneration device coupled to a RES system in a Canadian household.

An existing fuel cell micro-cogeneration model will be improved upon to facilitate its use with proton exchange membrane fuel cell devices. This model will also be calibrated with experimental data from a current state-of-the-art proton exchange membrane fuel cell prototype device. An existing RES model of a lithium ion battery device will be calibrated with recent experimental data for a lithium ion battery cell.

Previous residential micro-cogeneration research has relied on generated data for incorporating non-HVAC occupant electrical loads, or has used monitored data with a typical temporal resolution of 5-15 minutes. This treatment can often neglect the magnitude of peak electrical power draws. A recent load monitoring project logged annual residential occupant electrical loads at one minute intervals to provide realistic profiles for use with building energy simulation (Saldanha and Beausoleil-Morrison 2012). The performance of the micro-cogeneration + RES system will be simulated at a fine temporal resolution (one minute) to match the resolution of the electrical load profiles. Thus, it will also be possible to examine the capability of the system to meet peak electrical loads.

Coupling the building envelope, micro-cogeneration based HVAC system and RES system in an integrated model also facilitates the development of combined system control strategies. The effects of these various strategies on the overall system performance can then be compared to a typical Canadian residence as well.

1.3 Thesis Outline

To meet these objectives the thesis is divided as follows:

Chapter 2 provides a summary of the literature reviewed for this research, including Canadian energy use, the Ontario electricity market, micro-cogeneration devices,

previous micro-cogeneration + RES system research, electrical energy storage, and an introduction to building performance simulation.

Chapter 3 provides an introduction to the ESP-r simulation tool, including the methods used to model the building envelope, plant and electrical systems.

Chapter 4 describes the models developed in this research to simulate the performance of a Canadian household containing a residential micro-cogeneration + RES system. The procedure used to couple these models and all model inputs are given as well.

Chapter 5 describes a customized system controller developed in this research, as well as the metrics used to measure the performance of a household containing a micro-cogeneration + RES system compared to a conventional household.

Chapter 6 summarizes the results of the micro-cogeneration + RES system based on the performance of the model and the metrics chosen.

Chapter 7 draws conclusions and provides recommendations for future work.

Chapter 2

Literature Review

The literature reviewed for this research is presented in five sections. Section 2.1 provides an overview of energy use in Canada and Ontario. Section 2.2 provides a brief description of the Ontario electrical power grid. Section 2.3 discusses the modelling of micro-cogeneration systems. Section 2.4 discusses electrical storage. Finally, Section 2.5 introduces the topic of BPS as a tool useful for the analysis of various facets of building systems. This leads into Chapter 3 which provides more detail on the specific BPS tool used in this research.

2.1 Canadian Energy Use

Residential and commercial buildings accounted for 31% of the total secondary energy consumption in Canada in 2008 (NRCan 2012). The residential secondary energy consumption based on energy source for Canada and Ontario is shown in Figure 2.1. Approximately 90% of residential energy consumption in Canada, and over 90% in Ontario, was from natural gas and electricity. This value is similar for the commercial sector, though electricity comprises a slightly larger fraction.

The secondary energy consumption based on end-use in the Ontario residential sector is shown in Figure 2.2. Approximately 80% of the energy consumed by the Ontario residential sector was used for space heating and water heating. This value and the fractions for space heating and water heating are nearly identical for all of Canada. These values are slightly lower in the commercial sector, where only 55% of the energy consumed was for space heating and water heating.

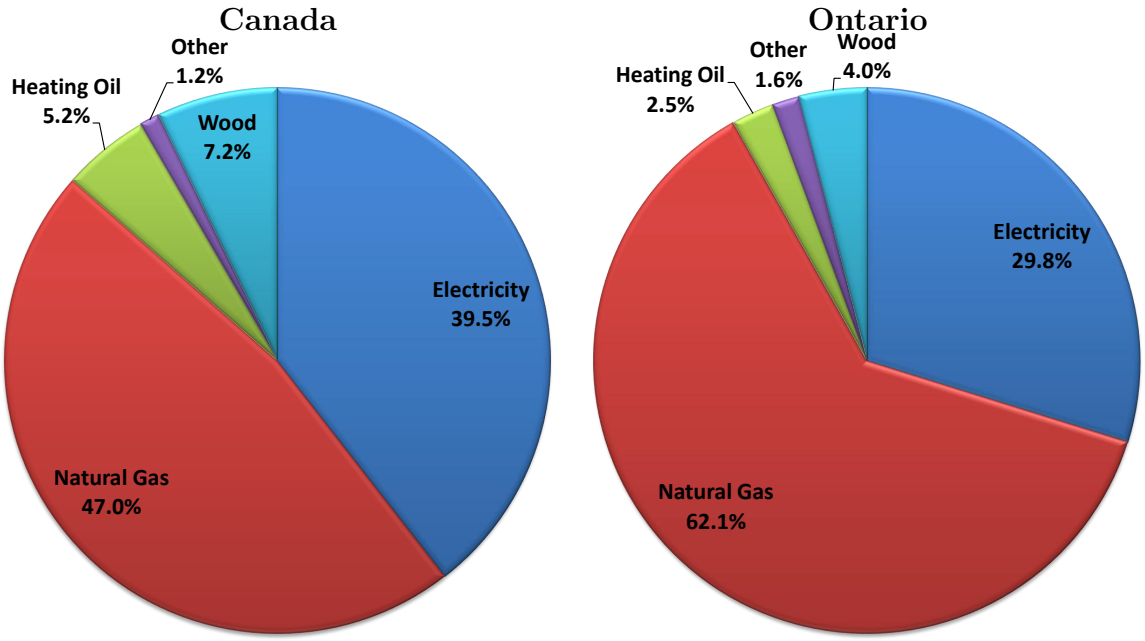

Figure 2.1: Fractional residential energy consumption based on energy source for Canada and Ontario (2008). Data from NRCan (2012).

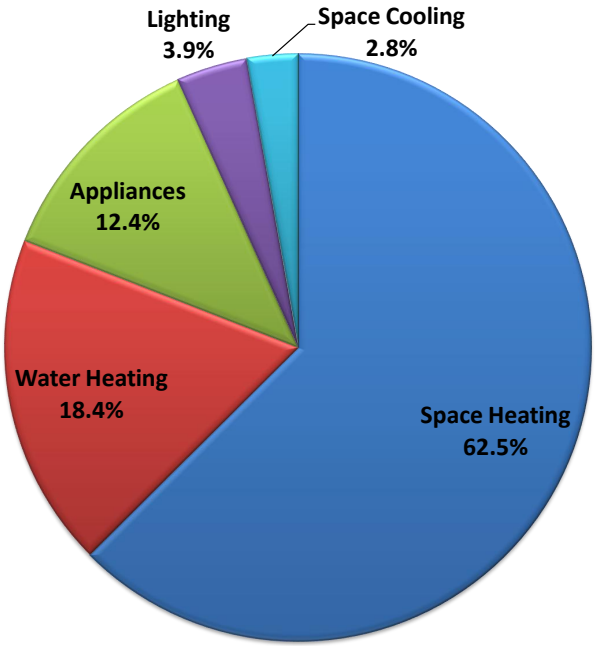

Figure 2.2: Fractional secondary energy consumption based on end-use for the Ontario residential sector (2008). Data from NRCan (2012).

2.2 The Ontario Electricity Grid

There are multiple power generation stations which are dispatched to meet electricity demands in Ontario. Figure 2.3 shows the contrast between Ontario and Canadian electric generation by source. Due to the different technologies installed, not all power generation stations are cost-effective to run at all times. Nuclear and hydro-electric power generation stations are not typically capable of varying their generation below a certain minimum output. For this reason, most nuclear and hydro-electric suppliers in Ontario have contracts with the Ontario Power Authority (OPA) to supply a fixed minimum amount of electricity at all times. Fossil fuel power generation stations are more expensive to operate than nuclear and hydro-electric, and are used primarily to meet peak electricity demands.

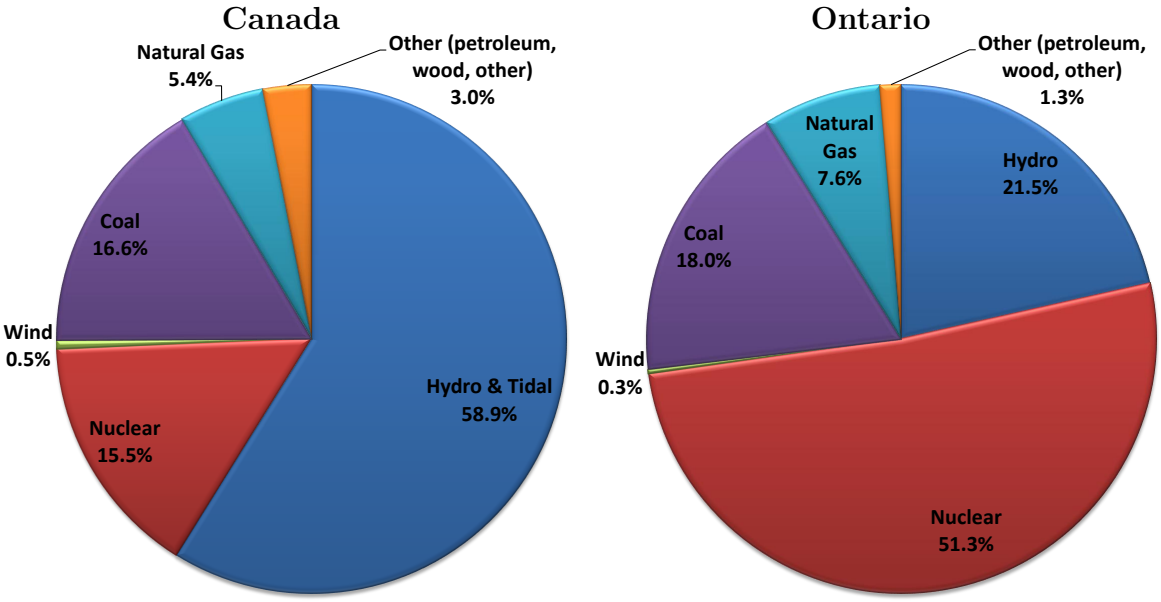

Figure 2.3: Electric generation based on energy source in Canada and Ontario (2008). Data from NRCan (2012).

The Independent Electricity System Operator (IESO) manages the supply and demand of electricity in Ontario. An electrical demand forecast is drawn by the IESO each day. Generators send their offers to supply electricity for one-hour time-slots based on their operating costs. The offer contains information on how much energy a generator can sell and what price they would like to receive for it (IESO 2011). More expensive fossil fuel power generation stations may be dispatched at

hours of peak demand. The hourly fluctuation in generation sources for a typical winter day in Ontario is shown in Figure 2.4. The difference shown between the supply and demand of electric power is a result of grid losses and interjurisdictional energy trading (i.e. imports and exports with neighbouring provinces and states).

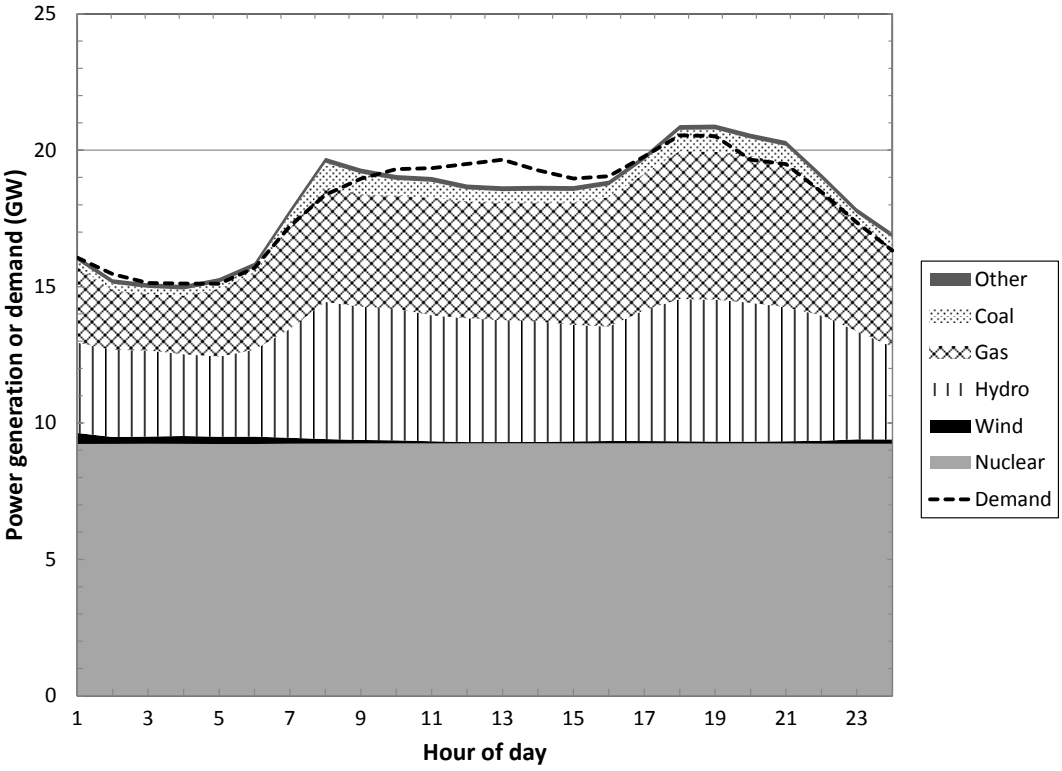

Figure 2.4: Ontario electricity demand and supply by generation source on a typical winter weekday. Data from IESO (2012). "Other" indicates petroleum, wood waste, and biomass generation.

Local distribution companies (LDCs) such as Hydro Ottawa pay the wholesale market price as determined by the IESO at each hour. This wholesale market price is known as the Hourly Ontario Energy Price (HOEP) and it varies throughout the day as different generators are dispatched. The HOEP is a reflection of electricity demand across Ontario, and has a strong correlation with the outdoor air temperature and the day of the week. During hours of peak electrical demand this price can be over four times greater than the purchase price of electricity for end-users (EUs). Examples of the seasonal and diurnal variations of the HOEP are shown for a hot summer day and a cold winter day in Figure 2.5.

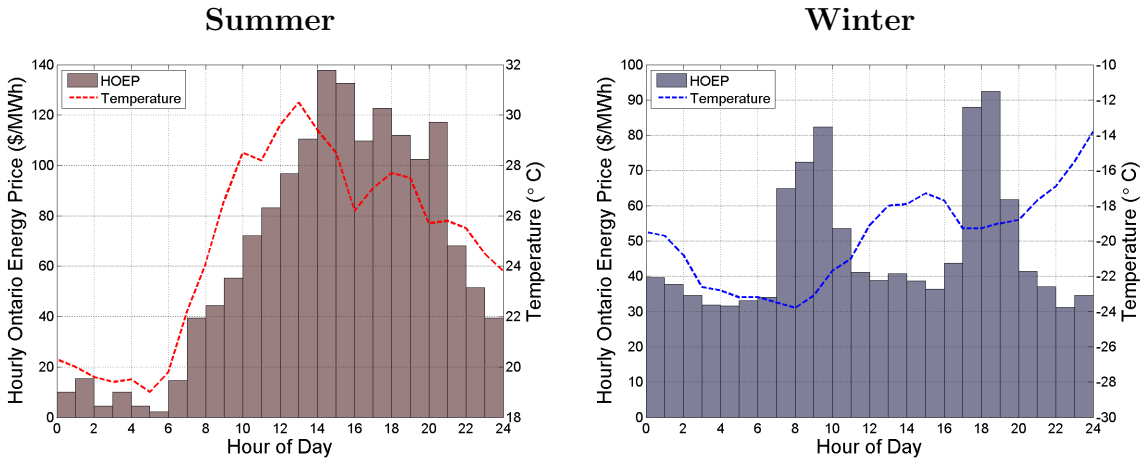

Figure 2.5: Fluctuations in the HOEP for one summer day, July 8, 2008, and one winter day, January 3, 2008.

The total annual electricity consumption based on sector use in Ontario is presented in Figure 2.6. Over 75% of the electricity consumed in Ontario is attributed to residential and commercial buildings (IESO 2011).

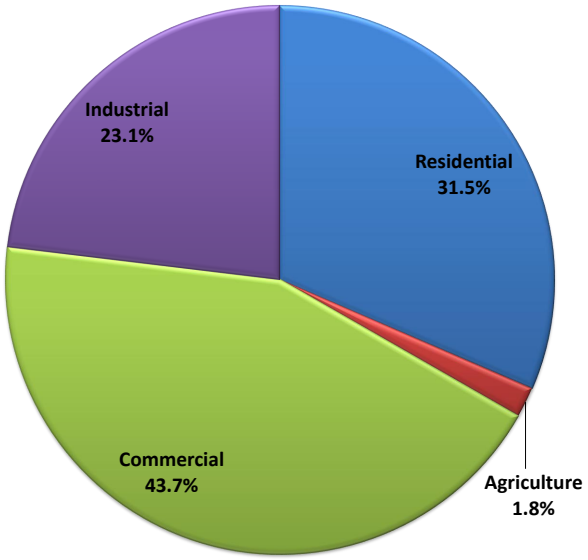

Figure 2.6: Fractional electricity use sector on end use in Ontario (2008). Percentage of total annual electricity consumption (546 PJ). Data from NRCan (2012).

Distributed energy resources such as solar photovoltaic (PV) and wind have the potential to reduce Ontario's reliance on fossil fuel generation during times of peak

electrical demands. The OPA has developed the Feed-in Tariff (FIT) and micro Feed-in Tariff (microFIT) programs to encourage the use of renewable energy sources such as PV and wind, as well as bio-gas, landfill gas, and waterpower (Ontario Power Authority 2010).

In the FIT and microFIT programs, owners are paid a fixed price for the electricity produced and in return are expected to incur connection, metering, and ongoing maintenance costs. The FIT program applies to generating facilities of any size greater than 10 kW, though waterpower and PV projects are subject to a maximum of 50 MW and 10 MW, respectively (Ontario Power Authority 2011). The microFit program is geared towards residential applications and applies to projects that are 10 kW or less. Generation sources such as PV and wind are weather dependent and therefore can be variable, intermittent, and unreliable during times of peak demand. Currently, there is no policy in place in Ontario for electricity exported from micro-cogeneration and battery storage devices. These technologies are discussed in greater detail in the following sections.

2.3 Micro-cogeneration

A variety of residential micro-cogeneration technologies are commercially available (Knight et al. 2005; Onovwiona and Ugursal 2006). The most common are the Stirling engine (SE), internal combustion engine (ICE), solid oxide fuel cell (SOFC) and proton exchange membrane fuel cell (PEMFC). Some solar and wood-waste cogeneration devices are also available though are less popular.

The electrical conversion efficiencies of micro-cogeneration devices vary for each of the technologies though for all technologies are low compared to modern central generation stations (Beausoleil-Morrison 2011). Current micro-cogeneration prototypes have electrical conversion efficiencies of 5-30% in terms of the net alternating current (AC) electrical output relative to the source fuel's lower heating value (LHV) (Entchev et al. 2004; Carbon Trust 2007; Beausoleil-Morrison 2008; Johnson and Beausoleil-Morrison 2012). Thermal conversion efficiencies of micro-cogeneration devices range from 30-80% in terms of net thermal output relative to the source fuel's LHV. Due to the on-site utilisation of the waste heat from this conversion process, the overall conversion efficiency of current devices can be as high as 85-90% (Onovwiona and Ugursal 2006; Beausoleil-Morrison 2008; Johnson and Beausoleil-Morrison 2012).

The proper sizing of a residential micro-cogeneration device is crucial to its successful application (Beausoleil-Morrison 2008). Sizing a device to supply all of a building's heating loads can lead to excessive electricity export at inopportune times. Conversely, sizing a device to supply all of a building's electrical loads will cause excess heat to be generated at times of high electrical but low thermal demands, necessitating some sort of heat rejection or storage. Devices are typically sized to provide only part of a building's electrical and heating demand (Knight et al. 2005).

Heat recovery in a micro-cogeneration device is accomplished either by an exhaust-gas-to-water heat exchanger (EGHX) or by a stack heat exchanger within a PEMFC stack cooling loop. Devices are typically coupled to a thermal storage tank to store the useful heat output and provide low temperature cooling water to the device's cooling loop. These systems also typically contain a supplementary space heating burner to ensure that the consumer heating loads are met when they exceed the capacity of the micro-cogeneration unit and storage tank.

The performance of micro-cogeneration systems within residential or commercial buildings has yet to be fully realized. It is still unclear how to optimally deploy and dispatch micro-cogeneration devices as a distributed energy resource within a centralized electricity grid. In relation to the deployment and dispatching, current research is also examining methods to optimize the control of micro-cogeneration devices from various perspectives (e.g. lowest cost, lowest energy consumption, lowest GHG emissions) (Gähler et al. 2008; Matics and Krost 2008; Houwing et al. 2009). It is important to know the current performance offered by prototype micro-cogeneration devices in order to best optimize future control strategies.

The modelling of micro-cogeneration systems is becoming increasingly popular, as it avoids the costs associated with experimental testing. Two models for simulating micro-cogeneration devices were developed in Beausoleil-Morrison et al. (2007). One of these models was integral to this research and will be discussed in the next section. The treatment of other model inputs such as occupant electrical loads, DHW loads, and any thermal and electrical storage devices, is also important in examining the overall performance of a micro-cogeneration system. A residential electrical storage (RES) model is introduced in Section 2.4, and the treatment of occupant electrical and DHW loads is discussed in Chapter 4.

2.3.1 Micro-cogeneration modelling

The goal of a micro-cogeneration model is to accurately predict the performance of a residential micro-cogeneration device. A mathematical model is used to represent the device's thermal and electrical performance, as well as the performance of any embedded components (e.g. air compressor, inverter, etc.). This model can be calibrated with data from the experimental testing of a specific device.

It is ideal to allow the device model to be coupled to other BOP components (e.g. pumps, fans, storage tanks), and to do so within an existing BPS tool so as to model an entire micro-cogeneration based HVAC system within a residential building. This means that models have to be capable of being implemented in a variety of situations, as well as in a range of time-steps typical of building performance simulation (10^1 - 10^3 *seconds*).

It was found that past micro-cogeneration models were not well suited for BPS applications (Beausoleil-Morrison et al. 2007). The majority of these models were either simplified performance map models, or complex models focussing on the chemical processes within fuel cell (FC) stacks or combustion engine fluid volumes. These complex models do not adapt well into BPS tools, as their simulation time-steps are usually much smaller than those encountered in BPS. Beausoleil-Morrison (2011) provides an overview of previous performance map models.

Recently, micro-cogeneration models for use in BPS tools were developed in Annex 42, a research project undertaken by the International Energy Agency's (IEA) Energy Conservation in Buildings and Community Systems (ECBCS) Programme. Two micro-cogeneration models were developed in the IEA/ECBCS Annex 42. One of these models represents combustion-based micro-cogeneration such as SE and ICE devices, while the other represents FCs such as SOFC and PEMFC devices. These models have been adapted into publicly released versions of BPS tools such as ESP-r and EnergyPlus. The following section describes the IEA/ECBCS Annex 42 FC model in greater detail.

Annex 42 fuel cell model

The FC model developed in the IEA/ECBCS Annex 42 programme consists of a group of models capable of representing the performance of a FC stack and its typical subsystems. A total of twelve subsystems are available (Beausoleil-Morrison et al. 2007), these are:

1. The fuel cell power module (FCPM);
2. The air supply blower;
3. The fuel supply compressor (if present);
4. A water pump (if required for steam reformation);
5. An auxiliary burner (if present, upstream of the EGHX);
6. An EGHX;
7. A battery system for electrical storage;
8. A power conditioning unit (PCU) for converting the fuel cell's direct current (DC) electrical output to alternating current (AC);
9. A dilution air system (if present, downstream of the EGHX) with optional heat recovery ventilator (HRV);
10. A heat exchanger in the stack cooling system;
11. An air cooler in the stack cooling system;
12. A stack cooling circuit pump.

The energy flows between the twelve subsystems of the FC model are shown in Figure 2.7. The FC model was drawn as shown in order to represent a number of potential SOFC and PEMFC systems and configurations. Not all model subsystems are required; components such as the blower, auxiliary burner, stack cooling system, etc., can be omitted.

An energy balance can be written for the control volume containing the fuel cell power module as:

$$\dot{H}_{fuel} + \dot{H}_{air} + \dot{H}_{liq-water} + \dot{H}_{dilution-air-in} + P_{el,ancillaries-AC} = P_{el} + \dot{H}_{FCPM-cg} + q_{s-cool} + q_{skin-loss} + \dot{H}_{dilution-air-out} \quad (2.1)$$

Where $\dot{H}_{fuel}$ is the total enthalpy flow rate $[W]$ of fuel into the control volume (downstream of the fuel compressor); $\dot{H}_{air}$ is the total enthalpy flow rate $[W]$ of air into the control volume (downstream of the blower); $\dot{H}_{liq-water}$ is the total enthalpy flow rate $[W]$ of the liquid water into the control volume (downstream of the water pump, if required for steam reformation); and $\dot{H}_{FCPM-cg}$ is the total enthalpy flow rate $[W]$ of the product gases that exit the control volume and enter the auxiliary burner.

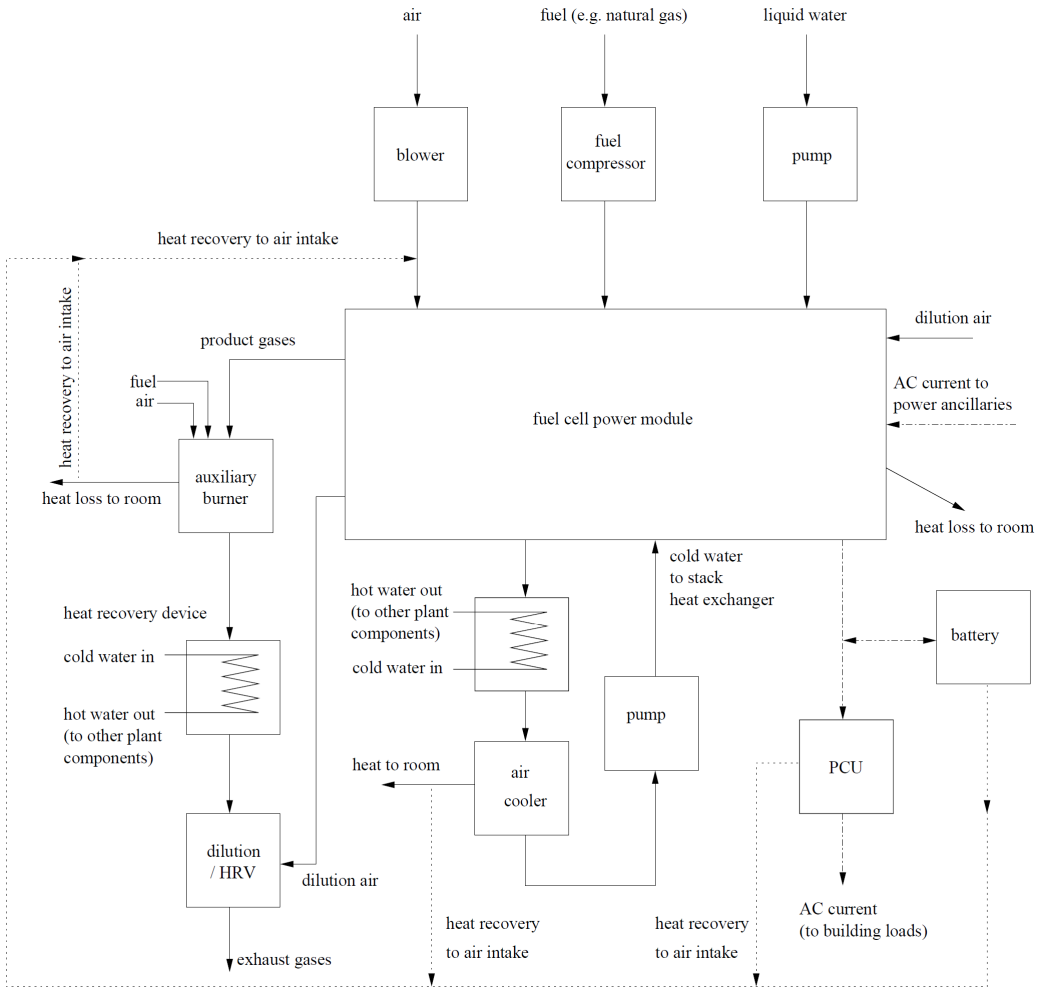

Figure 2.7: Topology of IEA/ECBCS Annex 42 fuel cell micro-cogeneration model. Used with permission from Beausoleil-Morrison et al. (2007).

q_{s-cool} is the heat to be extracted $[W]$ from the stack by the stack cooling system in order to control the temperature in a PEMFC stack and $q_{skin-loss}$ are the parasitic thermal losses from the control volume (convective and radiative).

P_{el} is the net DC electric power output and $P_{el,ancillaries-AC}$ is the power draw of the AC powered ancillary devices, both in $[W]$.

$\dot{H}_{dilution-air-in}$ and $\dot{H}_{dilution-air-out}$ are the total enthalpy flow rates $[W]$ of air drawn through the FC cabinet for cooling purposes.

The electrochemical performance of the fuel cell stack is not explicitly modelled. Instead, the electrical efficiency of the FCPM is modelled as a parametric function of the electrical power output requested by the user. This is given as:

$$\epsilon_{el} = \left[\epsilon_0 + \epsilon_1 \cdot P_{el} + \epsilon_2 \cdot P_{el}^2\right] \cdot \left[1 - N_{stops} \cdot D\right] \cdot \left[1 - MAX\left|\int_0 dt - t_{threshold}, 0\right| \cdot L\right] \quad (2.2)$$

Where the ϵ_i coefficients are calibration coefficients supplied by the user. P_{el} is the power produced by the fuel cell stack, less any DC ancillary power draw. The $[1 - N_{stops} \cdot D]$ term models the degradation associated with on/off cycling seen in some FC devices, where the D term is a user input value representing the fractional performance degradation associated with each start-stop cycle (can be omitted). The $[1 - MAX|\int_0 dt - t_{threshold}, 0| \cdot L]$ term represents the operational degradation sometimes associated with long run times, where the L term is a user input value representing the fractional performance degradation associated with operation time (can be omitted).

When configured for use with a PEMFC device, the heat recovered from the fuel cell stack is modelled as a parametric function of the electrical power output requested by the user and the temperature of cooling water entering the heat recovery heat exchanger, T_{w-in}. The heat recovered is given by:

$$q_{s-cool} = r_0 + r_1 \cdot P_{el}^{\alpha_0} + r_2 \cdot (T_{w-in} - T_0)^{\alpha_1} \quad (2.3)$$

Where r_i, α_i, and T_0 are calibration coefficients supplied by the user.

Equations 2.2 and 2.3 together govern the thermal and electrical outputs of the fuel model when configured for a PEMFC device.

The DC power produced by the FCPM has to be converted to AC by the PCU. The efficiency of the PCU is modelled as a quadratic fit of the PCU power input:

$$\eta_{PCU} = u_0 + u_1 \cdot P_{PCU-in} + u_2 \cdot P_{PCU-in}^2 \quad (2.4)$$

Where the u_i coefficients are calibration coefficients supplied by the user, and P_{PCU-in} is the DC power input to the PCU from the FCPM $[W]$. This is equal to P_{el} if the internal battery storage system is not in use.

The specific model control volumes and calibration inputs used will be discussed in greater detail in Chapter 4. A detailed description of the FC model and the treatment of each control volume is given in Beausoleil-Morrison et al. (2007).

2.3.2 Micro-cogeneration system studies

A number of modelling studies regarding various micro-cogeneration technologies have been conducted. The findings of some selected studies are discussed below.

Beausoleil-Morrison and Ribberink (2008) used an integrated modelling approach to examine the potential of a residential SOFC system to reduce energy consumption and greenhouse gas (GHG) emissions. These metrics were measured by comparing the natural gas use in a reference house with a conventional HVAC system to the same house with a SOFC-based system, with grid supplied electricity assumed to be supplied by a natural gas power generation station. The SOFC-based HVAC system developed is shown in Figure 2.8. The total energy use was compared by converting all grid electricity consumed to a volume of natural gas assuming a fossil-fuel powered central generating station. The SOFC unit was unable to modulate its output due to the high operating temperatures of SOFC devices. It was found that the experimental SOFC used to calibrate the FC model was oversized for residential applications, and that a large portion of the thermal energy was rejected. The household domestic hot water (DHW) demands were also not served by the SOFC's thermal output, which could lead to a further improvement upon the results.

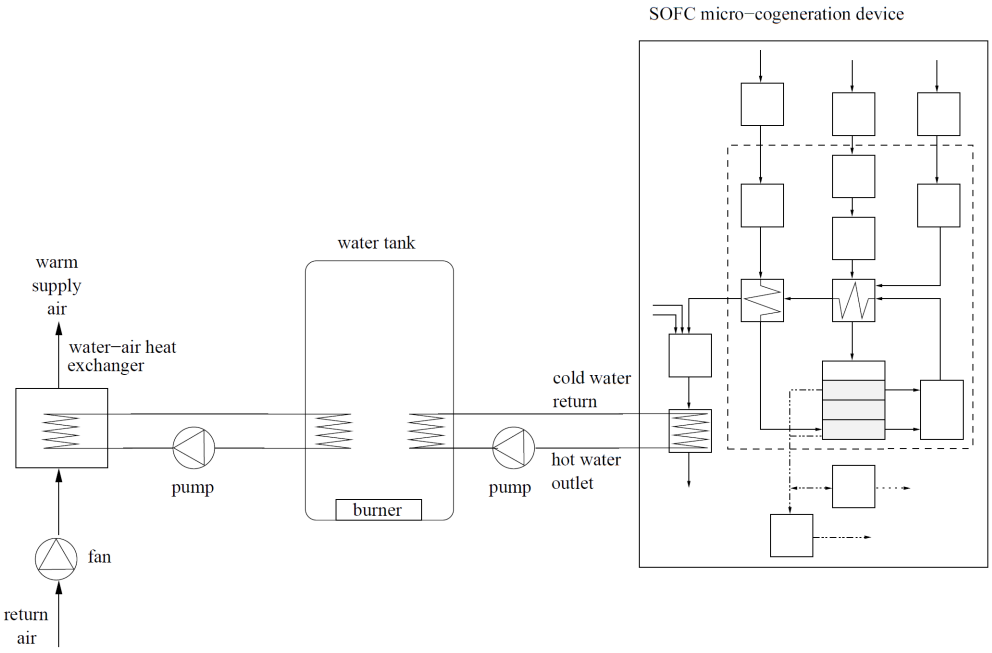

Figure 2.8: Example of a solid oxide fuel cell based HVAC system developed in Beausoleil-Morrison and Ribberink (2008). Used with permission.

Ribberink et al. (2007) also used BPS to model the performance of two different cogeneration devices, a SE and a SOFC, in a Canadian household. In this study the cogeneration unit provided thermal energy for both the space heating and DHW demands. The same SOFC unit was used to calibrate the model in this research as in Beausoleil-Morrison and Ribberink (2008). The energy consumption of the micro-cogeneration based HVAC system was compared to a conventional HVAC system by assuming all grid electricity was supplied by a natural gas fired combined cycle power plant. The GHG emission reduction was calculated by considering the displaced central power production for four different Canadian cities. It was found that the SOFC system increased the natural gas consumption compared to the reference house, though an improvement was seen in the GHG emissions for Ontario. The SE device had a negligible emission reduction and also slightly increased the natural gas consumption in comparison to the reference house.

Mottillo et al. (2006) simulated a complex residential hydrogen storage system containing a PEMFC and battery storage, as well as a PV system tied to an electrolyser and hydrogen storage cylinder. The electrolyser was used to convert excess power from the PV system to hydrogen, which fuelled the PEMFC when the PV output did not supply the occupant heating and electrical demands. The results of such an integrated system are difficult to attribute to one technology. However, it was found that a PV-battery system was more economical due to the renewable energy incentive program which subsidises PV produced electricity.

Beausoleil-Morrison (2008) summarized the work of a number of residential cogeneration systems. It was found that micro-cogeneration devices coupled to HVAC and DHW systems could reduce primary energy consumption by up to 33% and GHG emissions by up to 23% when compared to conventional household HVAC and DHW technologies. One of the suggestions from this work was the further investigation of coupling with alternative electrical storage systems to maximize the use of energy produced by cogeneration devices.

The modelling of an electrical storage device in BPS software is discussed in the next section.

2.4 Electrical Storage

Residential thermal and electrical demands vary from household to household and typically display very little coincidence. The space heating and electrical demands for a Canadian household over a typical winter day are illustrated in Figure 2.9. The space heating demands shown were developed in this research, and the occupant electrical demands are from a data collection project by Saldanha and Beausoleil-Morrison (2012). As the figure shows, space heating loads tend to peak in the morning and diminish throughout the day as solar gains heat the living space. It is also shown that electrical demand generally peaks in the late-afternoon and through the evening, with some small peaks in the morning. A sudden peak is seen in the space heating demand around 06h00, which corresponds to the transition from the household's nighttime temperature set point to the daytime set point.

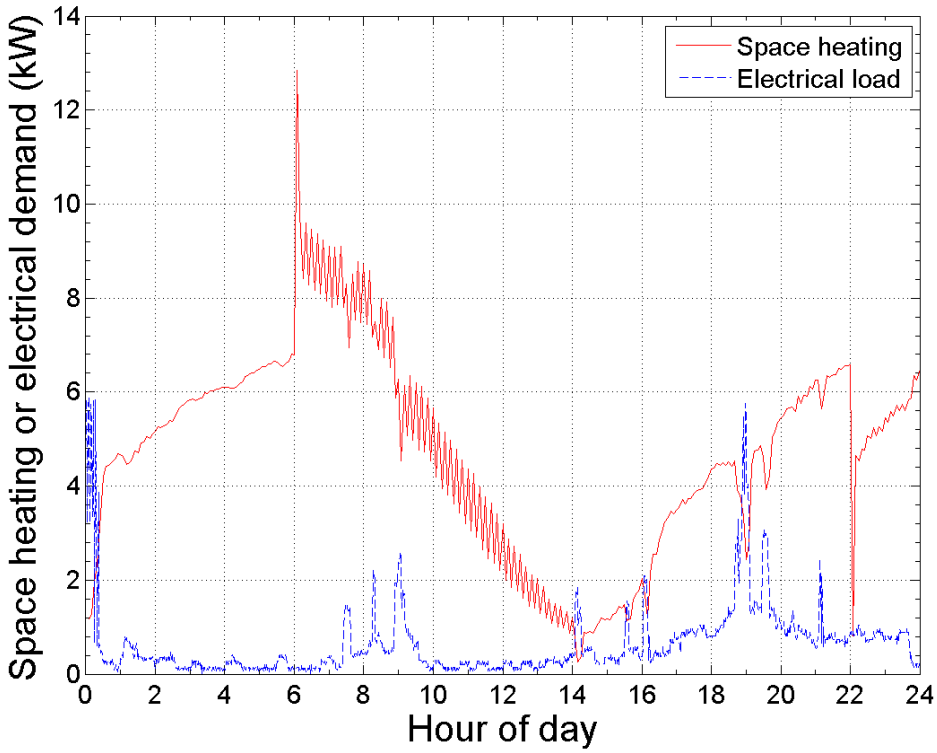

Figure 2.9: Space heating and electrical demands of a Canadian household over a typical winter day.

Due to the non-coincidence of residential thermal and electrical demands there

is a potential for RES to improve the overall performance of a micro-cogeneration device. This was also one of the conclusions from the IEA/ECBCS Annex 42 final report (Beausoleil-Morrison 2008).

There are a number of energy storage techniques which can absorb excess electrical power and store it in various forms, to be converted back to electricity when convenient. Some common forms of energy storage are potential (e.g. pumped hydro), mechanical (e.g. compressed air), kinetic (e.g. flywheel), thermal (e.g. liquid salt), chemical (e.g. electrolysis), electrochemical (e.g. lead-acid battery, lithium-ion battery), and electrical (e.g. supercapacitors).

Ibrahim et al. (2008) shows that electrochemical batteries are the most practical storage method for low to medium power applications, such as residential energy storage. Specifically, lead-acid batteries are frequently used in residential and portable applications due to the maturity of the technology. Lithium-ion (li-ion) batteries have more favourable characteristics compared to other electrochemical storage techniques. Saldanha (2010) provides an overview of electrochemical technologies and the advantage of li-ion technology.

To predict the performance of a battery-based RES system, as well as capture the interactions between the micro-cogeneration unit and RES, it is necessary to use a battery model developed for use in BPS. This model should simulate losses associated with the charge and discharge cycling and temperature-dependent performance of a battery based RES system, among other characteristics specific to the chosen battery type. Such a model was developed in ESP-r by Ribberink and Wang (2008), and a li-ion version of this was implemented by Saldanha (2010). The li-ion model is described in greater detail later in Section 4.3.1.

2.5 Building Performance Simulation

A BPS tool was used to develop the building energy model critical to this research. This model was used to simulate the thermal and electrical performance of a residential building containing a micro-cogeneration and RES device.

The use of an existing BPS tool in this research was attractive because the modelling of energy flows within the building envelope are already considered and have been extensively validated. Some of the energy flows that are considered within BPS tools include solar irradiaton, longwave radiation, thermal conduction through the

building envelope, ground heat transfer through the basement, air infiltration, etc.

Most BPS tools are also capable of simulating the performance of the HVAC system(s) supplying a building's thermal demands. This is typically accomplished by the sequential simulation of the building envelope and HVAC system performance, where the building envelope thermal demands are solved and then used as input requirements for the HVAC system. Some tools also contain facilities that can explicitly model specific plant (HVAC) network components and simultaneously simulate the performance of the building envelope and plant system as well as any interactions between the two. This type of explicit handling of the plant system is desirable when developing less conventional micro-cogeneration based HVAC systems.

Many of the current tools contain databases of common user inputs such as construction materials, weather data, existing plant and electrical component models, etc. This also streamlines the design iterations that can occur in the development of new and less conventional systems.

The BPS tool used to develop the building energy model for this research is described in the following chapter.

Chapter 3

ESP-r Simulation Methods

The ESP-r building simulation software (ESRU 2000) was first developed in the 1970's and has been in constant development since. ESP-r is an open-source software which developers worldwide are able to download and improve upon based on their knowledge and expertise. It has mostly been used as a research tool in academia, though simplified versions have stemmed from it and have been used for consulting (ESRU 2000).

ESP-r has various domains that are able to simulate different building processes such as building thermal demands, internal air flow, building electrical flow and HVAC plant systems. Finite difference (FD) schemes are used to simplify the non-linear conservation equations that govern the heat (energy), mass and momentum flow in the various building domains. A partitioned solution technique is employed where customized solvers are used to handle different simulation domains. The solutions of different domains are then compared and iterated upon if necessary. Using FD schemes circumvents the errors associated with earlier response function methods popular in early BPS programs. Response function methods depend on the principle of superposition to sum the independent responses of various building system components to a set of excitations, which means they neglect the coupled interactions that occur between building system components.

There are three main steps to developing any FD model, which are as follows;

1. Discretize the domain with a set of nodes. The node spacing depends on the model accuracy desired, as well as the placement of certain nodes at desired points. In BPS, important nodal locations for the thermal domain include the internal air volume, interior/exterior construction surfaces, air gaps, points where heat injection may take place such as radiant floor heating, etc. HVAC

and electrical flow domains are more straightforward, with nodes placed at each plant or electrical component.

2. Form the relevant conservation equations (energy, mass, and/or momentum) for each node in terms of the surrounding nodes.

3. Solve the equation set based on initial and boundary conditions. In BPS, boundary conditions for the thermal domain are usually given for the external surface as a set of known temperatures, humidities, wind velocities, etc., based on local weather conditions and solar irradiance data. Boundary conditions for the internal building zone can be given as thermostat (temperature and humidity) set points, with control logic initializing plant heat/cool injection when the internal zone is outside of those set points.

The use of ESP-r was integral to the research conducted, and so understanding the methods ESP-r uses to model building systems was necessary. Three main domains were utilized in this work: the building thermal domain as described in Section 3.1, the plant domain as described in Section 3.2, and the electrical flow domain as described in Section 3.3. An overview of the solution technique employed by ESP-r to solve these domains is provided in Section 3.4.

3.1 ESP-r Building Thermal Domain

This section describes the methods used by ESP-r to form the energy balance equations for the building thermal domain (e.g. thermal energy flow through wall constructions, foundation, windows, etc.) by addressing the first two steps listed above. First, an introduction to the FD formulation of the basic heat equation is provided in Section 3.1.1. A description of the system discretization method within ESP-r is then provided in Section 3.1.2. A more detailed description of the heat balance equations for various nodes within a building's thermal domain is provided in Section 3.1.3.

3.1.1 Finite difference formulation

ESP-r uses FD schemes to simplify the non-linear partial differential equations that govern the energy, mass and momentum flow in buildings, such as the Fourier heat

equation or the Navier Stokes equations. Specifically, the Taylor series expansion is used to approximate the derivatives of these equations.

The FD formulation for one-dimensional heat transfer using the Fourier heat conduction equation is illustrated in Appendix A. This energy balance represents the heat transfer across solid building envelope components.

This basic theory can be extended to represent three-dimensional conduction in a realistic construction if a three-dimensional volume is considered. However, as discussed in Section 3.1.2, ESP-r assumes one-dimensional conduction through the building envelope. Thus, the derivation shown in Appendix A is the foundation for all of the equations used to model the heat transfer through solid building envelope components. Assumptions such as a homogeneous, isotropic material with constant thermo-physical properties can also be dropped for more complex building envelopes.

3.1.2 System discretization

The accuracy of any numerical model is largely dependent on the discretization scheme used. Although rounding errors can arise and quickly compound as a result of the many equations comprising a FD scheme, modern computing power can deem these negligible (Clarke 2001). In the previous section, FDs were used to replace derivatives in the Fourier heat equation. These FD formulations are then solved at spatial increments across the building envelope and temporal intervals within the desired time frame to be analyzed. In general, increasing the number of increments (decreasing the increment size) improves accuracy, though it also increases the computational time required to solve the FD equations. Figure 3.1 represents an example of a discretized building wall section. ESP-r typically represents each homogeneous construction layer with 3 nodes (this can be increased if desired); one node is placed at each bounding surface and one in the middle of the construction layer. This gives a total of $2m+1$ nodes for each building envelope construction, where m is the number of material layers that comprise a specific construction.

A single node is used to represent the internal air volume of a building zone. However, a mass flow network can be defined to represent the flow through ducts and throughout the zone. In the simplest formulation of a single zone construction, with only a single construction material for each surface, the system discretization will appear as in Figure 3.2. Note that Figure 3.2 is a two-dimensional cross-section of a

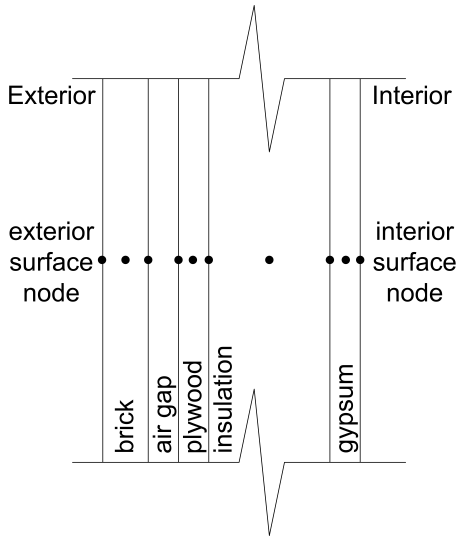

Figure 3.1: Example of default nodal arrangement for wall constructions in ESP-r. Adapted from Beausoleil-Morrison (2000).

basic building zone, therefore ceiling and floor constructions and discretizations are not shown. Also, the inter-zone airflow is shown as a potential example of an energy and mass transfer ESP-r is capable of modelling. However, this is only possible in the case of a multi-zone building.

Once the building envelope is appropriately discretized, the heat balance equations can then be written for each node type, as various nodes will experience different boundary conditions and modes of heat transfer (e.g. intra-constructional nodes only experience conduction, where surface nodes will also experience convection). Examples of these are also shown in Figure 3.2, and are discussed in greater detail in Section 3.1.3.

3.1.3 Heat balance formulation

The heat balance equation is formulated for a basic intra-constructional node and examples are then given on how this theory is extended to more complicated nodes with multiple modes of heat transfer.

Intra-construction nodes

ESP-r treats heat transfer through building envelope construction materials as one-dimensional with conductive heat transfer only (Clarke 2001). Figure 3.3 shows a

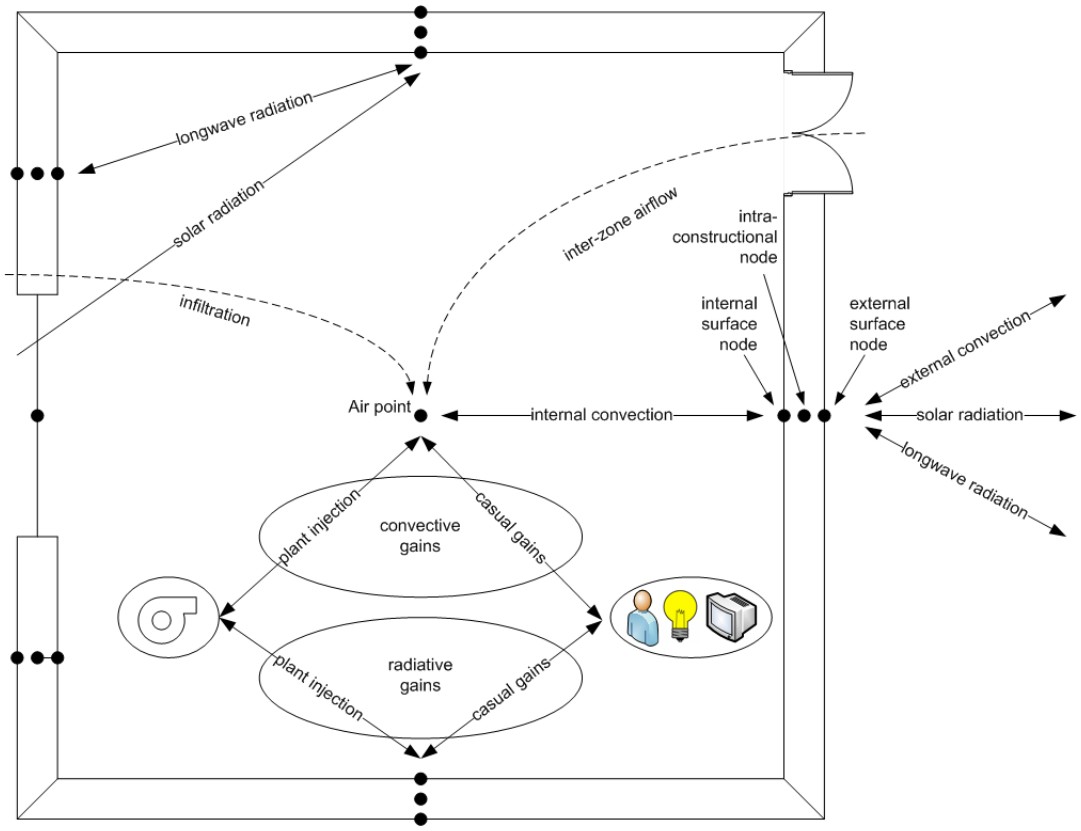

Figure 3.2: Example of a typical nodal arrangement for a building zone with a single wall construction material in ESP-r.

building construction element node I and its neighbouring nodes, with the greyed area of width Δx representing the control volume (CV) for node I. Note that each node has a depth Δy and height Δz associated with it, which corresponds to the total width and height of a particular wall section by default.

A heat balance can then be written for node I as follows:

$$\left\{ \begin{array}{c} \text{Storage of heat} \\ \text{within CV} \end{array} \right\} = \left\{ \begin{array}{c} \text{Net conduction} \\ \text{into CV} \end{array} \right\} + \left\{ \begin{array}{c} \text{Heat generation} \\ \text{within CV} \end{array} \right\} \tag{3.1}$$

where the storage of heat, heat generated within the CV and the net conduction into the CV can be computed as:

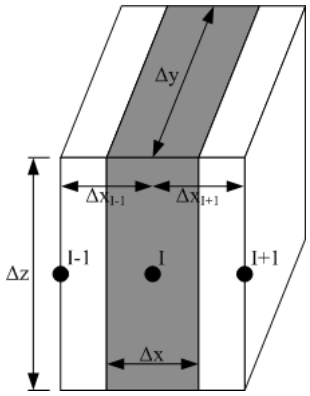

Figure 3.3: Nodal geometry for a building envelope control volume in ESP-r. Adapted from Beausoleil-Morrison (2000).

$$\left\{ \begin{array}{c} \text{Storage of heat} \\ \text{within CV} \end{array} \right\} = \rho C_p \frac{\partial T}{\partial t} \tag{3.2}$$

$$\left\{ \begin{array}{c} \text{Net conduction} \\ \text{into CV} \end{array} \right\} = -\frac{\partial q''_x}{\partial x} = -\left(\frac{\partial q''_{I-1}}{\partial x} + \frac{\partial q''_{I+1}}{\partial x} \right) \tag{3.3}$$

$$\left\{ \begin{array}{c} \text{Heat generation} \\ \text{within CV} \end{array} \right\} = q'''_{plant} = \frac{q_{plant}}{\Delta x \Delta y \Delta z} \tag{3.4}$$

Integrating over the entire control volume $\mathrm{d}V$ yields:

$$\int_{\delta V} \rho C_p \frac{\partial T}{\partial t} \, \mathrm{d}V = -\int_{\delta V} \left(\frac{\partial q''_{I-1}}{\partial x} + \frac{\partial q''_{I+1}}{\partial x} \right) \mathrm{d}V + \int_{\delta V} \frac{q_{plant}}{\Delta x \Delta y \Delta z} \, \mathrm{d}V \tag{3.5}$$

The net heat flux by conduction into the CV can be represented by one backwards and one forwards difference, respectively:

$$q''_{I-1} = -k_{I-1} \frac{T_I - T_{I-1}}{\Delta x_{I-1}} \tag{3.6}$$

$$q''_{I+1} = -k_{I+1} \frac{T_I - T_{I+1}}{\Delta x_{I+1}} \tag{3.7}$$

Similarly, the temperature derivative in the storage term can also be expressed as a backwards difference:

$$\frac{(\rho C_p \Delta x \Delta y \Delta z)}{\delta t}(T_I^{t+\delta t} - T_I^t) = \frac{k_{I-1}\Delta y \Delta z}{\Delta x_{I-1}}(T_I^t - T_{I-1}^t) + \frac{k_{I+1}\Delta y \Delta z}{\Delta x_{I+1}}(T_I^t - T_{I+1}^t) + q_{plant}^t \tag{3.8}$$

This is the fully explicit scheme similar to Equation A.4 developed in Appendix A. ESP-r uses the Crank-Nicolson method, which is a combination of the fully explicit scheme above, and the fully implicit scheme (not shown). Combining these two schemes and collecting terms gives:

$$\begin{aligned} &\left[\frac{2(\rho C_p)}{\delta t} + \frac{k_{I-1}}{\Delta x \Delta x_{I-1}} + \frac{k_{I+1}}{\Delta x \Delta x_{I+1}}\right] T_I^{t+\delta t} \\ &\quad - \left[\frac{k_{I-1}}{\Delta x \Delta x_{I-1}}\right] T_{I-1}^{t+\delta t} - \left[\frac{k_{I+1}}{\Delta x \Delta x_{I+1}}\right] T_{I+1}^{t+\delta t} - \frac{q_{plant}^{t+\delta t}}{\Delta x \Delta y \Delta z} \\ &= \left[\frac{2(\rho C_p)}{\delta t} - \frac{k_{I-1}}{\Delta x \Delta x_{I-1}} - \frac{k_{I+1}}{\Delta x \Delta x_{I+1}}\right] T_I^t \\ &\quad + \left[\frac{k_{I-1}}{\Delta x \Delta x_{I-1}}\right] T_{I-1}^t + \left[\frac{k_{I+1}}{\Delta x \Delta x_{I+1}}\right] T_{I+1}^t + \frac{q_{plant}^t}{\Delta x \Delta y \Delta z} \end{aligned} \tag{3.9}$$

Note that in Figure 3.1 it can be seen that many intra-constructional nodes fall on the boundaries between two different construction materials. In these cases it is necessary to take a volumetric weighted average of thermo-physical properties for neighbouring construction materials (Clarke 2001).

This energy balance forms the basis of the equations used by ESP-r for interior nodes within opaque construction components. Internal and external surface nodes require special treatment as convective and radiative heat transfer modes must be considered.

Internal and external surface nodes

For an interior surface node, such as the rightmost node in Figure 3.1, convection and radiation must also be considered. Similar to the intra-constructional node formulation above, this node will receive conductive heat transfer, though from the left node only. It will interact convectively with the internal air volume node to the right, and may also experience radiant heat transfer from solar irradiance, plant components, or casual gains. This node will also be subject to longwave radiation from surrounding

internal construction surfaces. All of these can be added to the right side of the original heat balance equation (3.1) as source terms. ESP-r uses a default correlation for convective heat transfer (buoyancy-driven), with options to use other correlations.

A default correlation is also for exterior surface nodes based on prevailing wind conditions. ESP-r assigns an area-weighting for longwave radiation exchange to internal surface nodes based on building geometry (exact view factors can be calculated if desired), and to external surface nodes based on ground and sky obstructions.

Air volume nodes

The heat balance equation for an internal air volume node consists of convective heat transfer terms with each bounding surface (i.e. the internal surface node of each wall construction bounding the air volume). Convective sources such as casual gains and plant injection interact directly with the air node. The energy balance also accounts for inter-zone airflow from neighbouring building zones and intra-zone air flow due to air infiltration through the building envelope. Constant or scheduled mass flow rates can be assigned to these air flows. A more detailed approach can be applied by including an air flow network to calculate infiltration rates and mass flow rates based on prevailing wind conditions and the thermal condition within each room.

3.1.4 Heat balance matrix

The heat balance (energy conservation) equations presented in Section 3.1.3 can be expressed in matrix notation for an entire building system as

$$\boldsymbol{A}\theta^{t+\delta t} = \boldsymbol{B}\theta^{t} + \boldsymbol{C} = \boldsymbol{Z} \tag{3.10}$$

$\boldsymbol{A}$ and $\boldsymbol{B}$ are matrices of coefficients for temperatures or heat injection terms at the future and present time-steps, respectively. $\theta^{t+\delta t}$ and θ^{t} are column vectors of nodal temperatures and plant injections at the future and present time-steps, respectively. $\boldsymbol{C}$ is a column matrix of known excitations for both the present and future time row (casual gains, etc.). When solving these matrix equations, discussed further in Section 3.4, the current nodal temperatures and heat injections will all be known, and so $\boldsymbol{B}$ and $\boldsymbol{C}$ can be combined into a single column matrix $\boldsymbol{Z}$.

A detailed description of the building envelope energy balances and equations for each node type are provided in Clarke (2001) and Beausoleil-Morrison (2000).

3.2 ESP-r Plant Network Domain

The previous sections described ESP-r's treatment of building thermal modelling without regarding the means by which heat is injected or extracted from the building zone. The temperature within a building zone can be left to free float or a desired temperature range may be specified within the building control, in which case the required heating and cooling loads will be an output of the building thermal simulation. These heating and cooling requirements can then be used in a separate simulation to predict the performance of a building HVAC system. However, to fully capture the control logic between building and plant, as well as the coupled interactions between the two systems, it is beneficial to model the building and plant systems simultaneously.

The following is a brief introduction into the methods used by ESP-r to model the plant network within a building system. Consistent with its treatment of the building thermal domain, ESP-r uses a simultaneous solution technique to solve the energy balance equations within the plant network domain. This differs from many of the popular sequential modelling software tools used for simulating plant networks such as TRNSYS (TRNSYS 2000). A finite difference control volume approach similar to that developed in the building thermal domain is used to solve the heat and mass balance equations that govern the energy transfers within the plant network. Nodes in the plant network represent specific plant components, as shown in Figure 3.4. A single component may be defined by multiple nodes depending on its complexity.

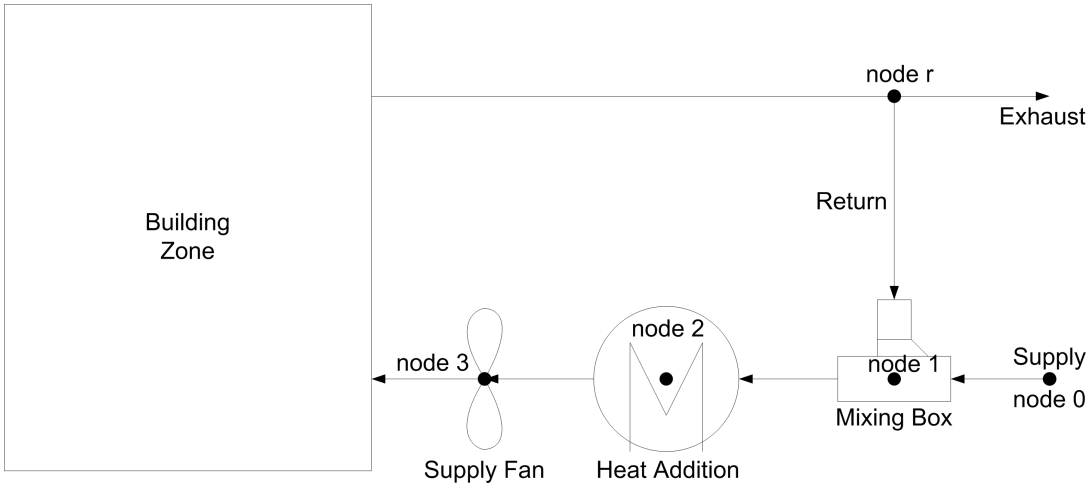

Figure 3.4: Example of basic plant network schematic in ESP-r.

The basic form of the energy (heat) and mass balance equations solved by ESP-r for each plant node are given as:

$$\left\{ \begin{array}{c} \text{Net heat flow} \\ \text{into CV} \end{array} \right\} + \left\{ \begin{array}{c} \text{Heat generation} \\ \text{within CV} \end{array} \right\} = \left\{ \begin{array}{c} \text{Storage of heat} \\ \text{within CV} \end{array} \right\} \tag{3.11}$$

$$\left\{ \begin{array}{c} \text{Total mass flow rate} \\ \text{entering the system} \end{array} \right\} = \left\{ \begin{array}{c} \text{Total mass flow rate} \\ \text{exiting the system} \end{array} \right\} \tag{3.12}$$

The energy balance in equation (3.11) above can be written for the discretized plant system in Figure 3.4 as follows:

For node 1: $$\dot{m}_0 C_{p0}(T_0 - T_1) + \dot{m}_r C_{pr}(T_r - T_1) + q_{e1} = \frac{\bar{C}_1 m_1 \partial T_1}{\partial t} \tag{3.13a}$$

For node 2: $$\dot{m}_1 C_{p1}(T_1 - T_2) + q_{e2} + \phi_2 = \frac{\bar{C}_2 m_2 \partial T_2}{\partial t} \tag{3.13b}$$

For node 3: $$\dot{m}_2 C_{p2}(T_2 - T_3) + q_{e3} = \frac{\bar{C}_3 m_3 \partial T_3}{\partial t} \tag{3.13c}$$

where m_i is the mass flow rate of the air/vapour mixture coming from node i $[kg/s]$; C_{pi} is the fluid specific heat capacity at node i $[J/kgK]$; q_{ei} is the heat exchange between the surroundings and node i $[W]$; $\bar{c_i}$ is the mass averaged specific heat capacity of node i $[J/kgK]$; ϕ_i is the heat injection at node i $[W]$ and m_i is the total mass for node i $[kg]$ including contained air and water (may also be shown as a volume multiplied by a volume averaged density).

The heat loss q_{ei} can be represented by each node's heat loss coefficient as:

$$q_{ei} = UA(T_e - T_i) \tag{3.14}$$

where U is the node's total heat loss coefficient $[W/m^2K]$; A is component's total surface area $[m^2]$ and T_e is the temperature of the environment $[K]$.

Equation (3.12) can be written to represent the air and water vapour mass balances for the plant system of Figure 3.4 as follows:

For node 1:
$$\dot{m}_{a,0} + \dot{m}_{a,r} - \dot{m}_{a,1} = 0 \tag{3.15a}$$
$$\dot{m}_{v,0} + \dot{m}_{v,r} - \dot{m}_{v,1} = 0 \tag{3.15b}$$
For node 2:
$$\dot{m}_{a,1} - \dot{m}_{a,2} = 0 \tag{3.15c}$$
$$\dot{m}_{v,1} - \dot{m}_{v,2} = 0 \tag{3.15d}$$
For node 3:
$$\dot{m}_{a,2} - \dot{m}_{a,3} = 0 \tag{3.15e}$$
$$\dot{m}_{v,2} - \dot{m}_{v,3} = 0 \tag{3.15f}$$

For humidifiers, dehumidifiers, and other components where vapour addition or extraction may occur, the mass balance would instead equal the rate of vapour addition or extraction.

Similar to the treatment of the building thermal energy balance, the Crank-Nicolson semi-explicit, semi-implicit forms of the equations can be written to form three matrix equations; one for energy balances; one for air mass flow balances and one for vapour mass flow balances. The general form of the plant system energy balance matrix will be:

$$\boldsymbol{A\theta}^{t+\delta t} = \boldsymbol{B\theta}^{t} + \boldsymbol{C} \tag{3.16}$$

Analogous to the building thermal energy balance, the matrix equations $\boldsymbol{B}$ and $\boldsymbol{C}$ can be combined into a single matrix, as values for the previous time-step will be known. Similarly, the general form of the plant system mass balance will be:

$$\boldsymbol{D\varphi}^{t+\delta t} = \boldsymbol{E\varphi}^{t} + \boldsymbol{F} \tag{3.17}$$

where the right hand side of the equation again can be combined into a single row matrix. In the case of two phase flow of an air/water vapour mixture there will be two mass balances, one for air and one for water vapour, as shown in Equations 3.15 for the system shown in Figure 3.4.

A variety of plant component models are available in ESP-r. Each component has its own coefficient generator which forms the energy and mass balance equations for all of the nodes that represent the component. Most component models require user input for components parameters. For example, a centrifugal fan or pump may require a rated flow rate and the power consumed at rated conditions. A more complicated

model, such as the fuel cell model described in Section 2.3.1, may require dozens of calibration coefficients. The order in which the equations for each component are placed in the plant matrix equations is determined by how the components are connected within the plant network.

Plant variables may also be controlled via user-defined control functions. There are a number of plant variables that can be modulated via a plant or building control function. A control function in ESP-r is defined by: sensor location, actuator location, controller type and control law (Hensen 1991). Details on available plant components, control types and laws are given in Hensen (1991). The control functions available in ESP-r were not used to control the plant network components in this research and are not elaborated upon further. The control functions developed are described in Chapter 5.

3.3 ESP-r Electrical Flow Network Domain

This section describes the methods used by ESP-r to solve the energy balance equations for the electrical flow network. In order to properly analyze the performance of a micro-cogeneration unit and RES system within the building being modelled, it is necessary to couple the electrical output of the cogeneration unit to the time-varying electrical draws within the building.

The modelling technique used for the building thermal and plant domains described in Section 3.1 and Section 3.2 respectively is extended to the modelling of an electrical system in ESP-r. The electrical network is discretized by a series of nodes and conservation equations are then applied between nodes. These equations are then solved by a similar finite difference control volume approach as seen previously. In the case of the electrical flow network, nodes are placed at current junctions between electrical loads and sources. The conservation equation applied is Kirchhoff's current law, which is given for node i in a system of n nodes as:

$$\sum_{j=1}^{n} \widetilde{I}_{i,j} = 0 \tag{3.18}$$

Here $\widetilde{I}$ is the complex quantity given by $\widetilde{I} = I \cdot (\cos\theta + j \sin\theta)$, as both alternating current (AC) and direct current (DC) may need to be expressed in a building electrical flow network. Kirchhoff's law can be expressed for generation (G), transmission (T),

and load (L) currents as:

$$\sum_{j=1}^{n} \widetilde{I}_{Gi,j} + \sum_{j=1}^{n} \widetilde{I}_{Ti,j} - \sum_{j=1}^{n} \widetilde{I}_{Li,j} = 0 \tag{3.19}$$

For the simplified household electrical system shown in Figure 3.5 nodes would correspond to the two branching points of the system shown.

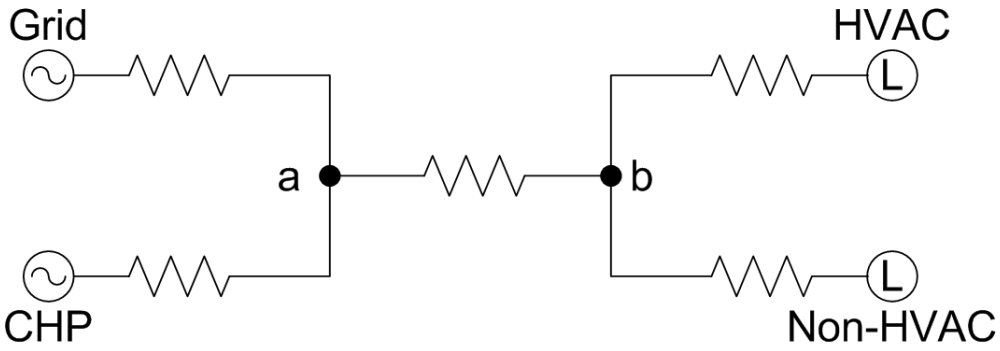

Figure 3.5: Example of a basic electrical network schematic in ESP-r.

Writing Kirchhoff's Law for this system gives:

For junction a: $$\widetilde{I}_{G,grid} + \widetilde{I}_{G,CHP} + \widetilde{I}_{Ta,b} = 0 \tag{3.20a}$$

For junction b: $$\widetilde{I}_{Tb,a} - \widetilde{I}_{L,HVAC} - \widetilde{I}_{L,non-HVAC} = 0 \tag{3.20b}$$

Gathering all generation and load terms to one side and using Ohm's law to represent the transmitting currents gives

For junction a: $$\widetilde{I}_{G,grid} + \widetilde{I}_{G,CHP} = (\widetilde{V}_a - \widetilde{V}_b)\widetilde{Y}_{a,b} \tag{3.21a}$$

For junction b: $$\widetilde{I}_{L,HVAC} - \widetilde{I}_{L,non-HVAC} = (\widetilde{V}_b - \widetilde{V}_a)\widetilde{Y}_{b,a} \tag{3.21b}$$

where $\widetilde{Y}_{a,b}$ is the inverse of impedance [S or $1/\Omega$]. Although a matrix equation set can be developed similar to the building and plant networks with the current equations shown, boundary conditions for loads and generation from the cogeneration unit would have to be given in terms of current flows. However, these conditions are typically given in terms of power flow.

Multiplying all terms by voltage (to give power flow instead of current flow), the equations are then manipulated to gather generation and load power flows on each side to give a solvable equation set. For an AC network of n nodes there are $2n$ equations, an equation set for both real and reactive power, and $2n$ unknowns, the voltage magnitudes and phase angles at each node.

Further details regarding the electrical flow network are given in Kelly (1998) and Clarke (2001).

3.4 ESP-r Partitioned Solution Technique

The building heat balance matrix shown in Section 3.1.4 can be solved without further manipulation. However, due to the sparse nature of this matrix it is advantageous to employ matrix partitioning to reduce solution time (Clarke 2001). A partitioning technique is used to divide the overall thermal balance into separate matrices representing each surface.

The matrix equations for plant and electrical networks, given in sections 3.2 and 3.3 respectively, are formed in a similar way to the building heat balance equations. However the overall size of these matrices will be small in comparison to the building thermal equations, and so no partitioning technique is employed.

For the plant network, the energy and mass balance matrix equations are solved separately to reduce the overall matrix size as well as sparsity (Hensen 1991). The first phase (air) and second phase (water vapour, if defined) mass flows are solved prior to the plant energy balance, and an iteration process is invoked to ensure that strongly coupled variables match (e.g. the amount of water vapour added during a humidification process, and the heat transfer due to the vapour addition). If an air (mass) flow network is also defined for one or more building zones, this is solved prior to the plant network first phase mass flow.

Further information on specific solution techniques employed by ESP-r in each of these domains can be found in Clarke (2001). Specific information for the plant and electrical flow network solutions can be found in Hensen (1991) and Kelly (1998), respectively.

Chapter 4

Modelling Methodology

The performance of a micro-cogeneration device coupled with a residential electrical storage (RES) system was assessed using an integrated building model developed in ESP-r. The building envelope model was developed in the ESP-r building thermal domain described in Section 3.1. Contained within the building envelope were the plant and electrical models of the micro-cogeneration + RES system. These models were developed in the plant and electrical domains described in Section 3.2 and Section 3.3, respectively.

As mentioned in Section 3.4, the energy balances for each of the models are solved separately in each domain. This is due to the fact that the boundary conditions from one domain are often the results from another domain's solution (e.g. the casual gains due to the heat loss from HVAC components depend on the current HVAC operating point). In this way, Sections 4.1, 4.2, and 4.3 describe the building, plant and electrical models, respectively. The necessary boundary conditions and energy profiles used are described in Section 4.4.

4.1 Building Envelope Model

A building model of a typical Canadian household was necessary to examine the impact of the micro-cogeneration + RES system in a Canadian setting. Single detached homes account for almost 60% of Canada's residential housing stock, with an average floor area of 154 m^2 (NRCan 2012). Most houses in Canada have a lightweight wood-based construction built on top of a cast-in-place concrete basement.

A building envelope model of a typical Canadian single detached home was developed in ESP-r (see Fig. 4.1). The modelled house has a two-storey wood-frame

construction; a liveable area of 210 m^2; a cast-in-place concrete basement; and is built to the R-2000 energy efficiency standard (NRCan 1994). Four thermal zones were used to represent the house, each containing a single air volume node representing the entire air volume for that zone (assumed to be at the same thermal state). The attic, attached garage, and basement were represented as individual thermal zones, while the two storeys of the living space were combined into a single zone. The main living space is the only zone conditioned by the HVAC system. The basement would typically receive some conditioning though it was found that the heat loss from the micro-cogeneration unit provided sufficient heating. Some of the building model characteristics are given in Table 4.1.

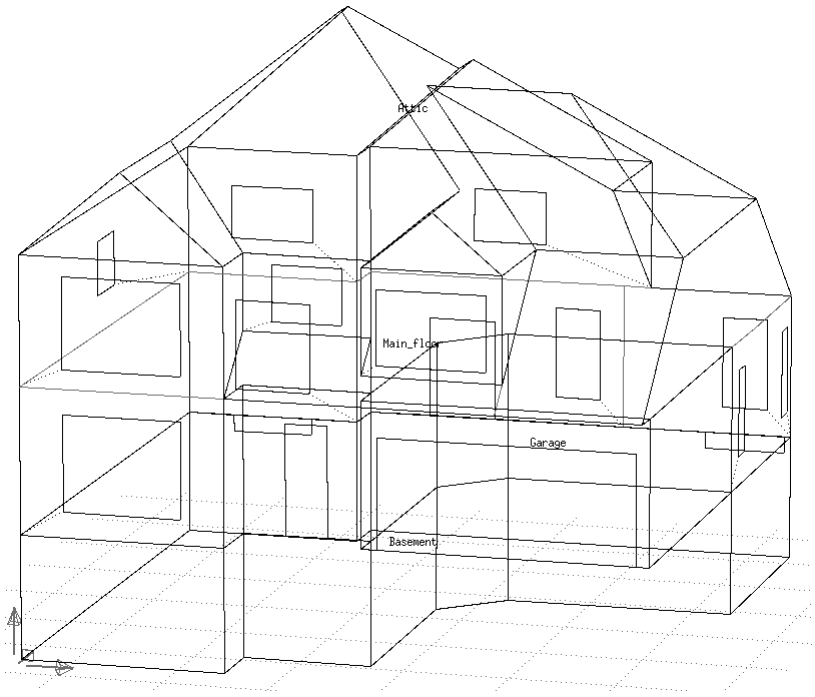

Figure 4.1: Wire-frame of the house model developed in ESP-r.

4.2 Plant Network Model

A plant network model was required to accurately predict the performance of a micro-cogeneration device and all balance of plant (BOP) components serving the device. A

House model property	Value	Units
Conditioned floor area	210	m^2
Wall U-value	0.24	W/m^2K
Basement wall U-value	0.34	W/m^2K
Ceiling U-value	0.15	W/m^2K
Window U-value	1.90	W/m^2K
Window area	35.0	m^2
Airtightness[1]	1.50	ach

[1] Measured at 50 Pa depressurization

Table 4.1: Selected characteristics of the house model developed.

number of micro-cogeneration device models are available for use in ESP-r. The models all require inlet/outlet connections to model the cooling water and heat recovery loops present in real devices.

A thermal storage device was also necessary to store the heat recovered from the micro-cogeneration unit. This was to account for the non-coincidence of residential thermal and electrical demands. The goal of the plant network was to efficiently utilize the thermal energy generated by a micro-cogeneration unit while illustrating a practical HVAC system that is feasible with current technologies. The plant network was required to serve four main purposes:

1. Provide cooling water to a micro-cogeneration unit.
2. Store the thermal output of a micro-cogeneration unit.
3. Provide a household with DHW at an adequate temperature.
4. Maintain thermal comfort of a living space via a space heating system.

A plant network model of a micro-cogeneration device, thermal storage tank and all BOP components was developed in the plant domain of ESP-r and is illustrated in Figure 4.2. The main features of the plant network are a component model for a micro-cogeneration unit and a large thermal storage tank model. A proton exchange membrane fuel cell (PEMFC) was chosen as the micro-cogeneration unit for this work. This was due to the favourable electric-to-thermal power ratio, high overall efficiency,

and modulating capabilities of PEMFCs (Knight et al. 2005). The PEMFC model used in this research is discussed further in Section 4.2.1.

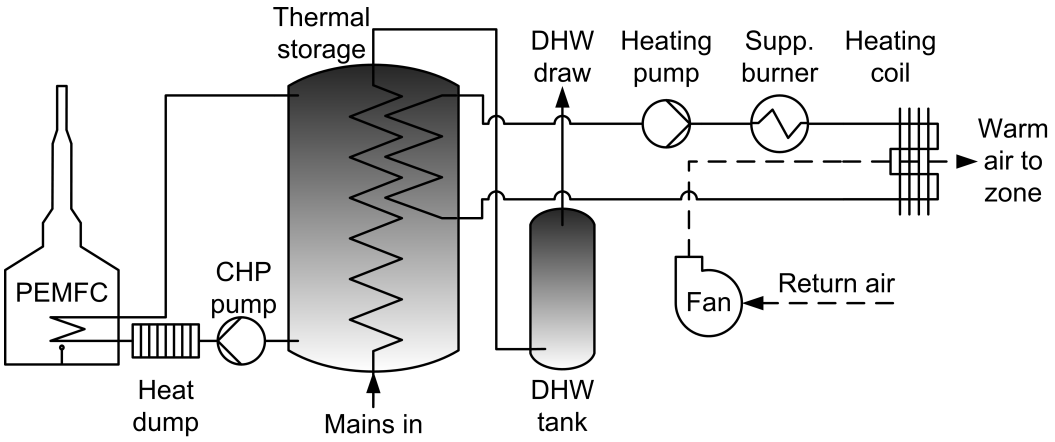

Figure 4.2: Plant model with micro-cogeneration device and thermal storage.

The thermal storage (tank) component model chosen is capable of modelling up to three sets of inlets/outlets, two of which are immersed-coil heat exchangers. The tank model used and the selection of inlet/outlet placement (see Fig. 4.2) is discussed in greater detail in Section 4.2.2.

The DHW draw was modelled using a flow source component that is capable of reading DHW flow rates from an external file at any time-step (this does not have to match the simulation time-step). The DHW draw profiles are discussed later in Section 4.4.2.

The SH loop follows a typical configuration and is not elaborated upon further. Flow rates and power draws for the SH components were adapted from Ribberink et al. (2007) and Beausoleil-Morrison and Ribberink (2008) and are shown in Table 4.4. A heat rejection device was also required upstream of the PEMFC component and is elaborated upon in the next section.

4.2.1 Proton exchange membrane fuel cell model

The main component of the plant system developed is the PEMFC cogeneration model. The Annex 42 fuel cell model discussed in Section 2.3.1 was used to model the performance of a commercial FC cogeneration device. To simulate the performance of

BOP component property	Value	Units
SH pump rated flow rate	9	L/min
SH pump power draw[1]	20	W
SH fan rated flow rate	600	L/s
SH fan power draw[1]	50	W
Supp. burner capacity	15.0	kW
Supp. burner efficiency[2]	85.0	-
DHW tank burner capacity	23.0	kW
DHW tank burner efficiency[2]	85.0	-

[1] Power consumption at rated conditions.
[2] Efficiencies for the supplementary burner and DHW tank burner are in terms of thermal energy output (MJ) relative to the input fuel's higher heating value (HHV).

Table 4.2: Plant network component data for balance of plant components.

a realistic PEMFC a number of calibration parameters are required for the model. The data used to calibrate the PEMFC model in this work was obtained experimentally by Johnson and Beausoleil-Morrison (2012).

The PEMFC unit to which the model was calibrated (see Fig. 4.3) has a maximum rated power output of 1 kW_{AC} electric and 1.2 kW thermal. The actual thermal output was found to be slightly greater with a maximum of 1.5 kW (Thorsteinson et al. 2011). The PEMFC electrical output can also be modulated down to 270 W when there is little or no thermal or electrical demand. The details of the calibration can be found in Johnson and Beausoleil-Morrison (2012). The calibration was performed according to the procedure described for the Annex 42 cogeneration models in Beausoleil-Morrison (2007).

The power conditioning unit (PCU) for the experimental PEMFC device was found to have a relatively constant efficiency at all power settings. Selected performance characteristics at the minimum and maximum power operating points are shown in Table 4.3. At the maximum power setting (1 kW_{AC}) the power draw of the PEMFC AC ancillary devices was 31 W. One of these devices was the cogeneration

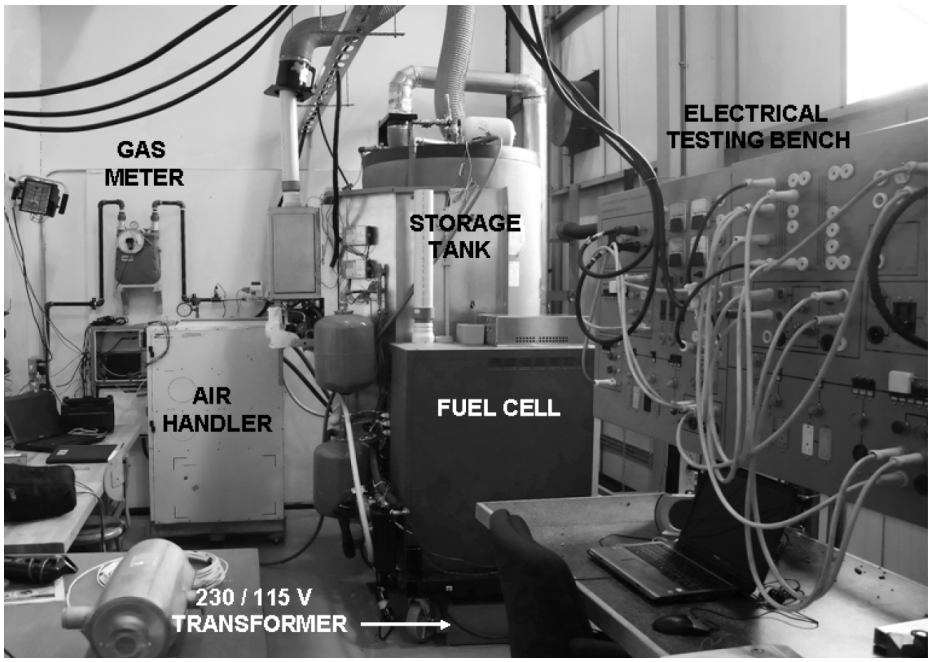

Figure 4.3: HYTEON 1 kW_{AC} proton exchange membrane fuel cell experimental rig. Used with permission from Thorsteinson et al. (2011).

pump pictured separately in the plant system (pump upstream of FC unit, Fig. 4.2). For this reason the electrical draw of this component is not included in the electrical network discussed in Section 4.3, as the PEMFC had already accounted for it.

Information regarding the PEMFC performance is presented in Thorsteinson et al. (2011). The experimental set-up, procedure and specific calibration parameters for the PEMFC are described in Johnson and Beausoleil-Morrison (2012).

4.2.2 Thermal storage model

The majority of thermal storage (tank) models available in ESP-r are well-mixed models. These assume that the entire water volume within the tank is at the same thermal state. Recently, a few tank models capable of modelling stratification have been implemented into ESP-r, aided by the development and modelling of solar thermal systems.

A tank model capable of simulating stratification between water layers inside the tank volume was developed for the transient system simulation (TRNSYS) program (TRNSYS 2000). This model, known as the Type 60 model, was developed by Newton

PEMFC property	Value at min. set-point	Value at max. set-point	Units
DC power production	314	1113	W
Net AC power production	270	980	W
Net thermal production	387	1590	W
Fuel flow	0.089	0.299	m^3/hr
PCU efficiency	0.93	0.91	-
AC Ancillary draw	21	31	W
Room heat loss	303	421	W
Electrical efficiency[1]	0.30	0.32	-
Thermal efficiency[2]	0.43	0.53	-

[1] Electrical efficiency is in terms of net AC electrical output (MJ) relative to the input fuel's lower heating value (LHV).
[2] Thermal efficiency is in terms of thermal output relative to the input fuel's lower heating value (LHV).

Table 4.3: HYTEON proton exchange membrane fuel cell performance data from Johnson and Beausoleil-Morrison (2012).

(1995) and was selected as the tank model for this work. The ESP-r version of Type 60 was implemented by Thevenard and Haddad (2010) and is capable of modelling up to three sets of open inlets/outlets or immersed coil heat exchangers.

The Type 60 model simulates stratification by dividing the tank's water volume into separate nodes (up to 100) and solving the energy balances between these nodes within an internal simulation. This internal simulation can occur several times within each plant domain time-step. The TRNSYS implementation was validated in Cruickshank and Harrison (2004), among many others, and the later ESP-r implementation was tested and validated in Thevenard (2007, 2009). A detailed description of the Type 60 model is provided in Newton (1995).

It was not certain prior to the development of the plant network whether the system flow rates would result in stratification. Various inlet/outlet and immersed coil heat exchanger combinations were explored before settling on the final plant network shown in Figure 4.2. The final layout was selected for the following reasons:

1. Immersed coil heat exchanger selected for SH loop to minimize heat loss to the

BOP component property	Value	Units
SH pump rated flow rate	9	L/min
SH pump power draw[1]	20	W
SH fan rated flow rate	600	L/s
SH fan power draw[1]	50	W
Supp. burner capacity	15.0	kW
Supp. burner efficiency[2]	85.0	-
DHW tank burner capacity	23.0	kW
DHW tank burner efficiency[2]	85.0	-

[1] Power consumption at rated conditions.
[2] Efficiencies for the supplementary burner and DHW tank burner are in terms of thermal energy output (MJ) relative to the input fuel's higher heating value (HHV).

Table 4.4: Plant network component data for balance of plant components.

tank when the backup SH burner is fired.

2. Immersed coil heat exchanger selected for DHW loop to avoid having to maintain the large thermal storage tank at the recommended 60^oC temperature (ASHRAE 2011). This would have also interfered with the cooling water requirement of the cogeneration unit.
3. Open inlet/outlet selected for cogeneration loop to maximize the amount of heat which can be recovered from the PEMFC. This also improved the overall system performance by drawing cooling water for the cogeneration unit from the coldest (bottom) section of the storage tank.

A cylindrical tank was used for this work. Some of the basic model inputs are shown in Table 4.5. The model required a tank heat loss coefficient (UA), which was calculated to correspond to 10 cm of fibreglass insulation. Model defaults were accepted for the pitch and diameter of the immersed heat exchangers, as an optimization of these was not feasible within the scope of this work.

Tank Property	Value	Units
Height	1.0	m
Volume	500	L
Heat loss coeff.	0.38	W/m^2K
Number of nodes	10	-
Internal time-steps	2	-

Table 4.5: Stratified tank model characteristics.

4.3 Electric Flow Model

An electrical flow model was necessary to predict the electric power transfer from the PEMFC to the RES system and the power loss associated with this process. The model was also used to sum all building electrical flows within the integrated building model. For this research the electrical flows include the PEMFC generation, HVAC and BOP loads, non-HVAC occupant loads (fridge, stove, dryer, etc.) and any grid interactions.

The solution of the electrical domain within ESP-r occurs after the solution of the building and plant domains at each simulation time-step to ensure the system is fully bound. For example, the electrical loads of the PEMFC and BOP components will be the result of the solution in the building and plant domains.

The electrical network developed in this work is shown in Figure 4.4. Two nodes are used to model the network: one representing the AC bus and one representing DC bus. The AC bus connects all standard household electrical flows (non-HVAC loads, BOP loads, grid interaction), while the DC bus serves the battery only. Electrical component models of a rectifier and inverter are used to transfer power to and from the DC bus, respectively. A lithium-ion (li-ion) battery model was used to model the electrical storage in this work. The battery model is described in greater detail in Section 4.3.1.

The BOP loads within the electrical network are a result of the plant domain solution. The PEMFC electric generation and the battery charge/discharge power are passed from the system controller described in Chapter 5. The non-HVAC occupant loads are read from an external file containing annual electricity demand data.

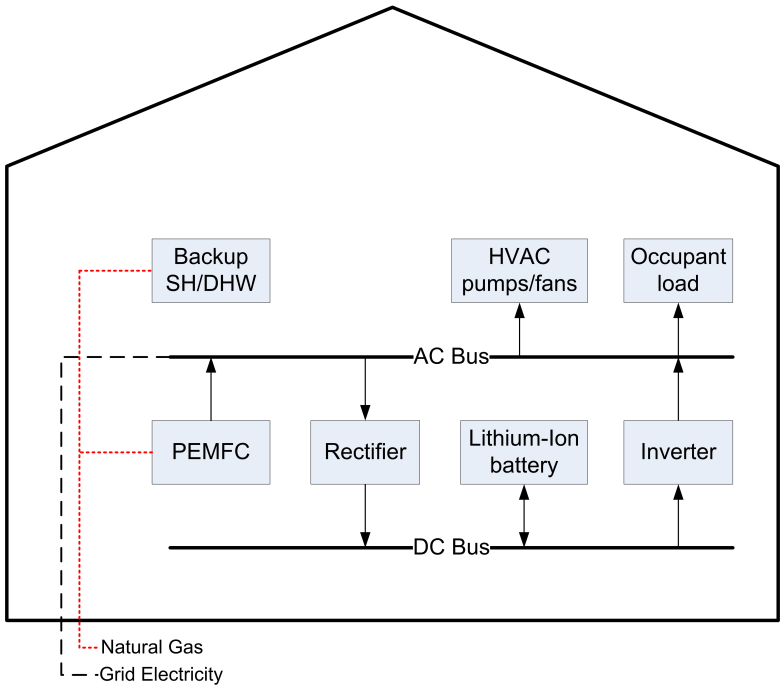

Figure 4.4: Electrical network model with lithium-ion battery storage.

These loads were taken from a data collection project and are elaborated upon in Section 4.4.3. Constant efficiencies were used for both the rectifier and inverter components.

4.3.1 Lithium-Ion battery model

The li-ion battery model used in this research was developed by Saldanha (2010). This model uses a resistor-capacitor network to represent the open circuit voltage (OCV) of a single cell, as proposed by Gao et al. (2002). The model has been implemented in the electrical domain of ESP-r (Section 3.3) for use with modelling RES systems.

The number of individual battery cells connected in series and parallel is specified as a model input. At each time-step the final voltage, temperature and depth of discharge (DOD) is calculated for an individual cell given the initial DOD and temperature. The single cell result is then multiplied by the number of cells in series and parallel to give the overall system voltage and current, respectively.

The model accounts for the losses due to cycling, and also includes a battery management system routine that is called at each simulation time-step. This mimics a realistic battery storage system, ensuring that at each time-step every cell within

the battery is within its specified operating temperature, voltage, and power limits.

Experimental li-ion cell data from Darcovich and Kenney (2012) was used to calibrate the battery model. Some of the model inputs for the li-ion battery are shown in Table 4.6. A detailed description of the li-ion model and the required calibration inputs is provided in Saldanha (2010).

Battery property	Value	Units
Capacity (single cell)	37.7	$A \cdot h$
DOD=0% (V) (single cell)	4.17	V
DOD=100% (V) (single cell)	3.00	V
Max. discharge current (cell)	150.8	A
Max. discharge voltage (cell)	4.17	V
Number of cells in series	14	-
Number of cells in parallel	4	-
Total battery capacity	8.80	$kW \cdot h$
Maximum allowable DOD	0.0	%
Minimum allowable DOD	100.0	%
Maximum temperature	60.0	^oC
Minimum temperature	-40.0	^oC

Table 4.6: Lithium-ion battery model characteristics.

4.4 Boundary Conditions and Energy Use Profiles

The boundary conditions used to solve the energy and mass balance equations for the PEMFC + RES system are described in this section. These are required prior to the simulation of the building thermal, plant, and electrical domains used in this research. All simulations conducted in this research were for an annual time frame, and so a set of complete annual data was required for the conditions on each of these domains.

ESP-r assumes an initial thermal state of each building, plant and electrical node within the model (usually 20^oC). The models are then simulated for a specified

number of 'start-up' days prior to the simulation time frame to obtain a realistic temperature distribution.

4.4.1 Building thermal domain conditions

To solve the building heat balance equations (Section 3.1) boundary conditions are required at internal air volume nodes in the form of casual gains data (i.e. internal heat gains from equipment and occupancy) and at external building nodes in the form of weather data. Annual weather data from 2008 for Ottawa, Canada, was used for this research as this is the most current complete weather data available for Ottawa (Environment Canada 2008).

Internal heat gains from HVAC equipment (e.g. PEMFC, thermal storage tank, DHW tank) are a result of the plant domain solution. Internal heat gains from non-HVAC equipment (e.g. fridge, stove, dryer) are inferred from the electrical consumption of this equipment, as described in Section 4.4.3. This is the most accurate way to model these gains, as the majority of all electricity used in non-HVAC equipment will end up as thermal energy within the building.

In most Canadian residences the HVAC equipment is located in the basement and non-HVAC equipment is located in the main living space. For this reason, the internal heat gains from HVAC and non-HVAC equipment were added to the basement and main living space air volumes, respectively.

4.4.2 Plant domain conditions

The boundary condition requirements for the plant network are in the form of energy and mass flow set points of the various plant components (e.g. pump/fan flow rates, burner heat injection). The operating points for the PEMFC unit and all BOP components are required at each plant time-step. These are all passed from the system controller developed specifically for this work, which is described in Chapter 5.

The demand on the SH loop of the plant system (Fig. 4.2) is a result of the thermal energy requirements of the building thermal domain solution. The thermal demand on the DHW loop requires a method to treat residential DHW demand flow rates.

ESP-r has available plant components capable of modelling constant or stochastic DHW draws. A more accurate way of treating the DHW draws is to read monitored or generated annual DHW demand profiles from an external file, ideally at the same

temporal resolution as the simulation. The latter method was selected for this work, and is described in the following section.

Domestic hot water draws

DHW consumption for Canadian residences was monitored in Perlman and Mills (1984) and Wiehagen and Sikora (2002). Both found the average daily consumption to be approximately 235 L/day. More recently it was suggested that the consumption for the average Canadian residence is closer to 300 L/day (Knight et al. 2007).

Monitored annual DHW data is scarce (Knight et al. 2007) and so a generated DHW demand profile was used. A set of generated profiles based on a probabilistic model was developed in the IEA Solar Heating and Cooling Programme (SHC) Task 26 by Jordan and Vajen (2001). These profiles have since been compared to a number of monitored profiles in Knight et al. (2007) and found to be representative of realistic demands.

For this research a 300 L/day DHW demand profile with a one minute temporal resolution was adapted from Jordan and Vajen (2001). A sample for one day of the DHW demands is shown in Fig. 4.5.

4.4.3 Electric domain conditions

There are two boundary condition requirements for the electrical network developed in this work: the annual occupant non-HVAC electrical load and the battery charge/discharge power.

The losses of the rectifier/inverter system are a function of the battery demand. The BOP component loads and PEMFC electrical output at each electrical network time-step are a result of the plant domain solution based on the current plant operating point.

The battery power demand is an output of the system controller developed, discussed in Chapter 5. The annual non-HVAC load profiles used were taken from a monitoring project of twelve Ottawa area houses, and are discussed in the following section.

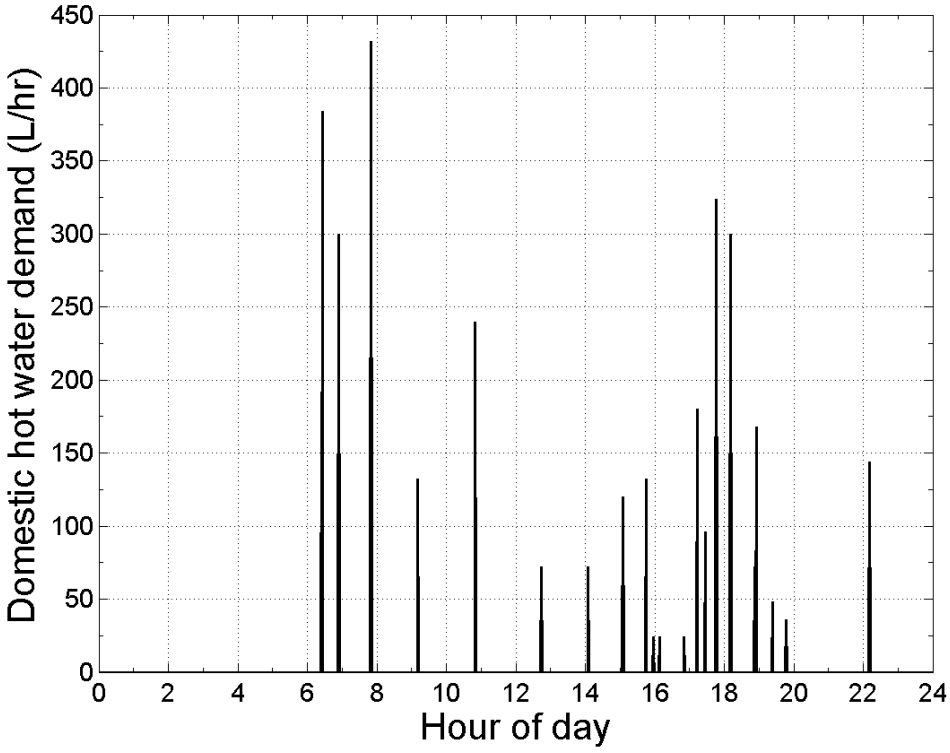

Figure 4.5: Residential domestic hot water demand profile for a typical day.

Occupant electrical loads

The household HVAC loads in the model are taken into consideration via the electrical consumption of the plant network components. Non-HVAC occupant electrical loads (e.g. fridge, stove, washer) must be taken into account to accurately assess the performance of the PEMFC + RES system.

Similar to the DHW demand profiles, occupant electrical demand profiles are traditionally represented by two methods: empirical data collection or model generated data. The models used to generate electrical data are becoming increasingly complex, with some taking the desired livable area, number of occupants and various electrical appliances as inputs. However, these models can lack the ability to represent varying occupant behaviour and peak demands (Saldanha 2010).

A comparison by Saldanha (2010) found that synthetically generated profiles can under-predict the magnitude of peak electrical loads by as much as half in comparison to monitored loads. It was also shown that previous data collection projects,

the majority of which had temporal resolutions of 5-15 minutes, fail to capture the amplitude of peak electrical loads as well. A sample of monitored one-minute data from Saldanha (2010) and the effect of averaging the data over 15 minutes is shown in Figure 4.6.

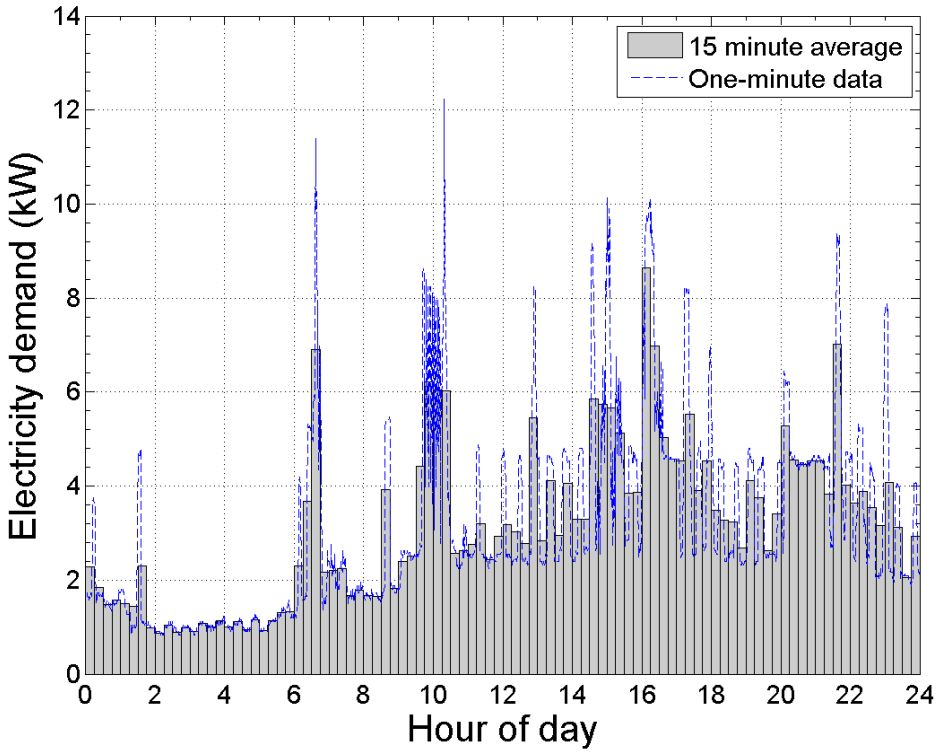

Figure 4.6: Monitored household non-HVAC electrical data for a typical day.

The occupant load profiles used in this research were from Saldanha and Beausoleil-Morrison (2012); a data collection project where the non-HVAC electrical loads were monitored in twelve Ottawa-area houses at one-minute time increments. The houses monitored were selected to represent various house types, vintages, and sizes. Four of the twelve annual load profiles were used for this work. The information on the four profiles used is shown in Table 4.7.

House label	Size (m^2)	Number of occupants	Total load (GJ)	Non-HVAC load (GJ)
H4	170	4	21.9	18.2
H6	130	3	25.3	23.4
H11	100	3	33.5	30.1
H12	140	4	42.6	39.5

Table 4.7: Annual electricity consumption in four Ottawa-area houses (Saldanha and Beausoleil-Morrison 2012)

Chapter 5

Controls and Performance Metrics

Having selected component models and configured a plant system capable of modelling the performance of a residential PEMFC + RES system, a set of controls governing the system operation was required. A customized controller was developed within ESP-r to interact with the plant and electrical networks, providing control signals to many components simultaneously.

A set of metrics by which to gauge the performance of the PEMFC + RES system was also required. The performance metrics influenced which operation strategies were explored for the system, and are described in this chapter. The metrics chosen compared the performance of the developed system to a household with a conventional HVAC system and with electricity supplied by the central electrical grid.

The custom controller developed for this work is described in Section 5.1. The performance metrics used are discussed in Section 5.2.

5.1 Custom Plant and Electrical Network Controller

Both the plant and electrical networks developed in this research require control inputs for their various components at each simulation time-step.

The only electrical network components in ESP-r which require control inputs are battery models. No control functions are currently offered in ESP-r for providing control inputs to the batteries, as the models are relatively new. This was done in Beausoleil-Morrison et al. (2006) and Saldanha (2010) by developing custom control functions within the ESP-r source code.

Many plant components in ESP-r require at least one control signal (e.g. On/Off signal, flow rate for a variable pump or fan, flux for a heat injection device). A number of plant control options, known as control functions, are available in ESP-r. The control functions are called at each time-step before the solution of the plant domain energy balances.

All plant control functions in ESP-r have the same requirements:

1. **Sensor location:** This can be any plant component or building domain node, and can also sense external weather conditions (e.g. wind speed, humidity, etc.).

2. **Actuator location:** For plant controls, this must be a node within a plant component.

3. **Control type and law:** The controller type defines what nodal variables are sensed and actuated (e.g. temperature, mass flow, flux, enthalpy, etc.). The control law defines the sensor-actuator interaction (e.g. On/Off, P, PI, PID, etc.).

The current control laws and sensor/actuator combinations in ESP-r are not well suited for controlling a complex plant systems. Time delayed controls or multiple conditions for an actuator are currently impossible. Current sensor/actuator options are limited to sensing and actuating single nodal variables (e.g. sense the inlet temperature at a burner connection node, actuate the flux at the burner combustor node). Each sensor/actuator pair can also only have a single control law defining their operation.

A custom controller component which manages both plant and electrical network components was developed in ESP-r, similar to the controllers developed in Beausoleil-Morrison et al. (2006) and Edwards (2011). The controller provides control signals at each time-step to a number of plant components (PEMFC, pumps, fans, burners) as well as the li-ion battery component within the electrical network.

The control strategies implemented for the PEMFC + RES system are described below. The control of the DHW components is described in Section 5.1.1. The control of the SH components is described in Section 5.1.2. The control of the PEMFC and components serving the PEMFC is described in Section 5.1.3. Finally, the control of the RES system is described in Section 5.1.4.

5.1.1 Domestic hot water heating control

The control logic of the DHW loop in the plant network developed is similar to that of conventional systems. The DHW control logic within the custom controller is shown in Figure 5.1. The mass flow rates for the loop are set by the DHW demand profile, so no control signal for the flow rate is required. The DHW storage tank was maintained at $60^oC \pm 2^oC$ (e.g. tank temperature is allowed to drop to 58^oC, at which point the burner heats the tank to 62^oC) to mimic the sensor lag in household DHW systems.

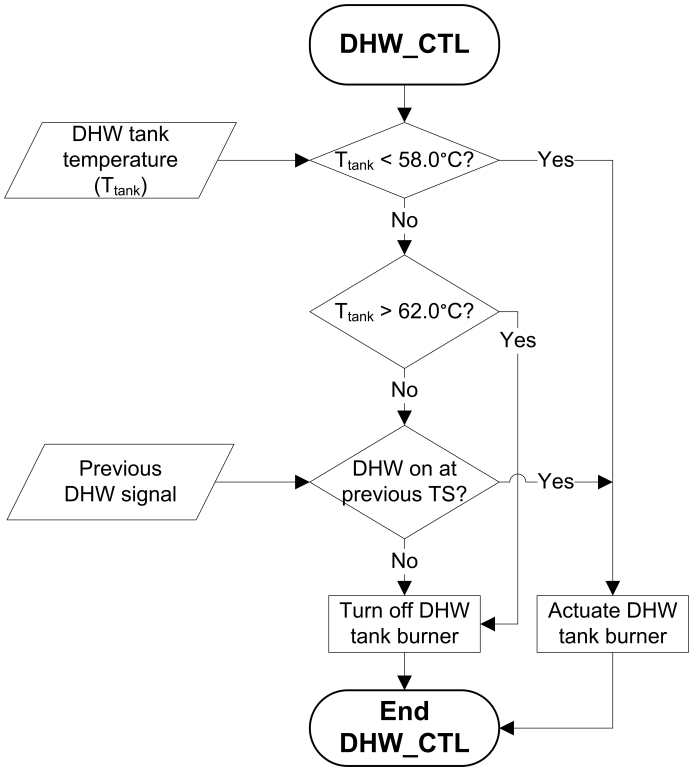

Figure 5.1: Control logic for the plant network domestic hot water loop.

5.1.2 Space heating control

The control method developed for the SH loop of the plant network worked to maximize the use of stored thermal energy recovered from the PEMFC unit. A time-delayed SH control was implemented. Thus, the plant system attempted to provide zone heating primarily from stored thermal energy and minimize the use of the supplementary burner.

The sensor and actuator locations within the SH loop are shown in Figure 5.2. The sensors are located at the main living space node (return air temperature) and at the heating coil outlet node (return water temperature). Actuators are located at the SH pump and fan nodes (flow rates) as well as the supplementary burner node (heat injection).

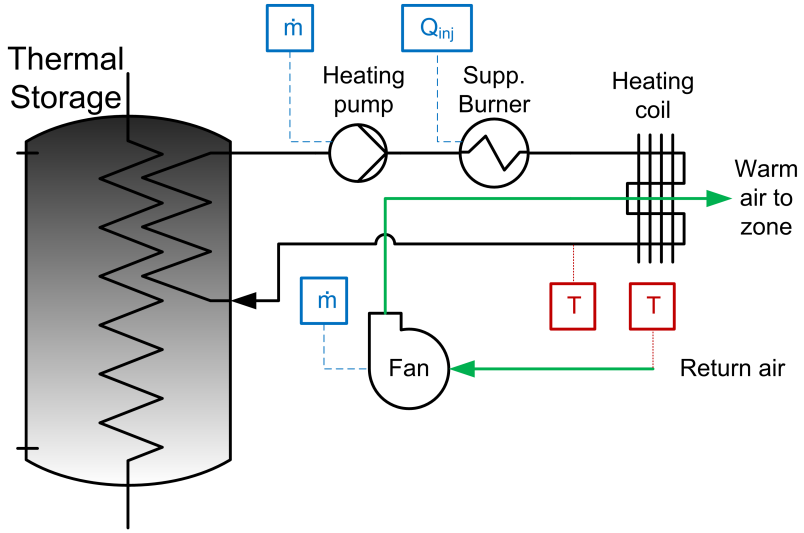

Figure 5.2: Actuated and sensed components within the plant network space heating loop.

The control logic for the SH loop components is shown in Figure 5.3. The winter heating set-point for the main living space is $21.5^oC \pm 1.0^oC$ during the daytime, with an overnight setback to $19.5^oC \pm 1.0^oC$.

When the main living space temperature falls below 20.5^oC the SH pump and fan are cycled on at their rated flow rates until the zone temperature increases to 22.5^oC. If after 15 minutes the zone temperature has not increased to its upper set-point the supplementary burner is cycled on at full capacity for the remainder of the heating cycle.

5.1.3 Fuel cell control

The control of the PEMFC loop of the plant network was determined by the current PEMFC output power. All the BOP components within the loop are reactionary to the PEMFC's current thermal output, as well as the thermal state of the supply

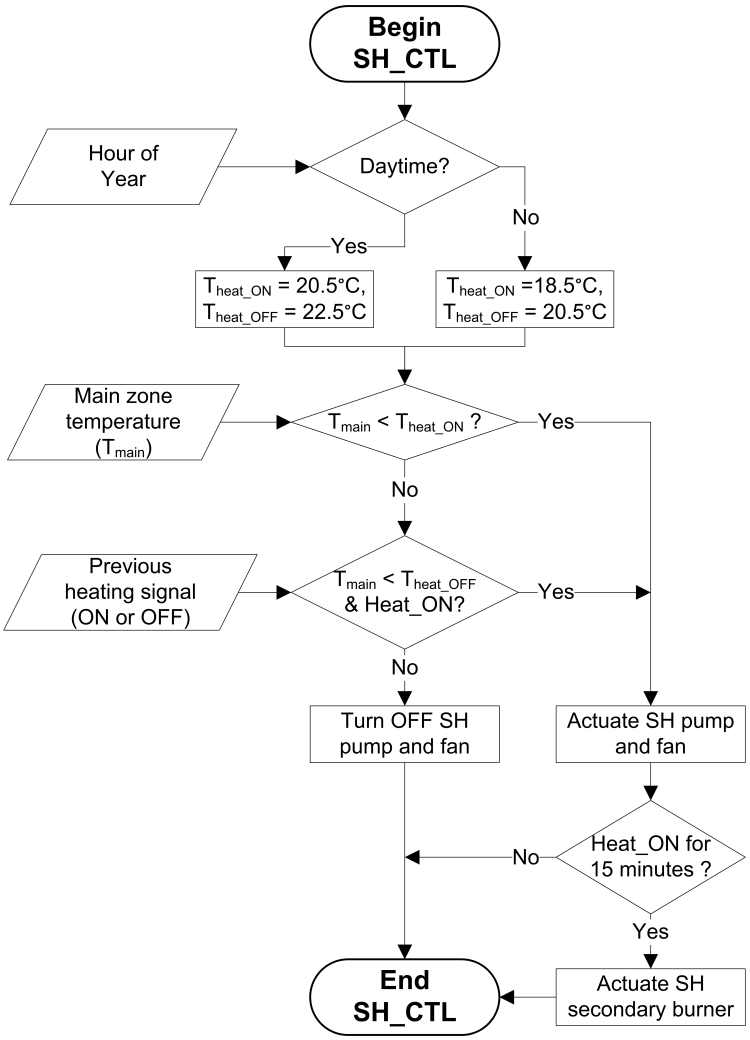

Figure 5.3: Control logic for the plant network space heating loop.

water to the unit.

The sensor and actuator locations for the PEMFC loop are shown in Figure 5.4. Temperature sensors are located at the inlet to the PEMFC and heat dump components. Actuators are located at the PEMFC FCPM (power output), heat dump (heat rejection), and pump components (flow rate).

The control logic for components within the PEMFC loop is shown in Figure 5.5. The experimental PEMFC unit contained an internal pump which maintained the outlet water temperature (T_{FC_out}) close to 70^oC. Similarly, the flow rate of the PEMFC external pump in the plant network model was varied in order to maintain

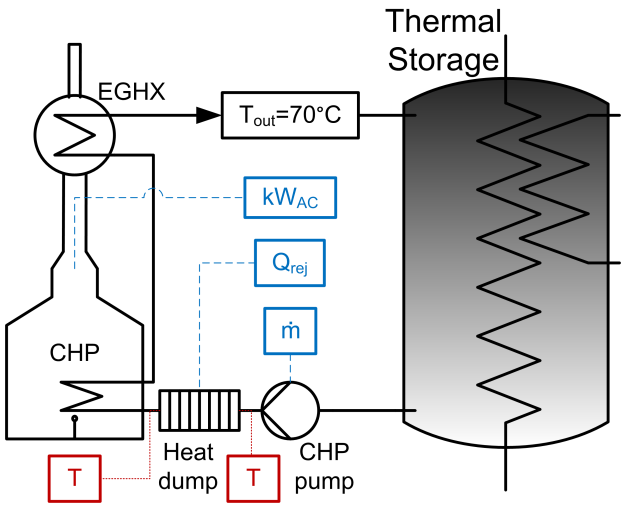

Figure 5.4: Actuated and sensed components within the plant network PEMFC loop.

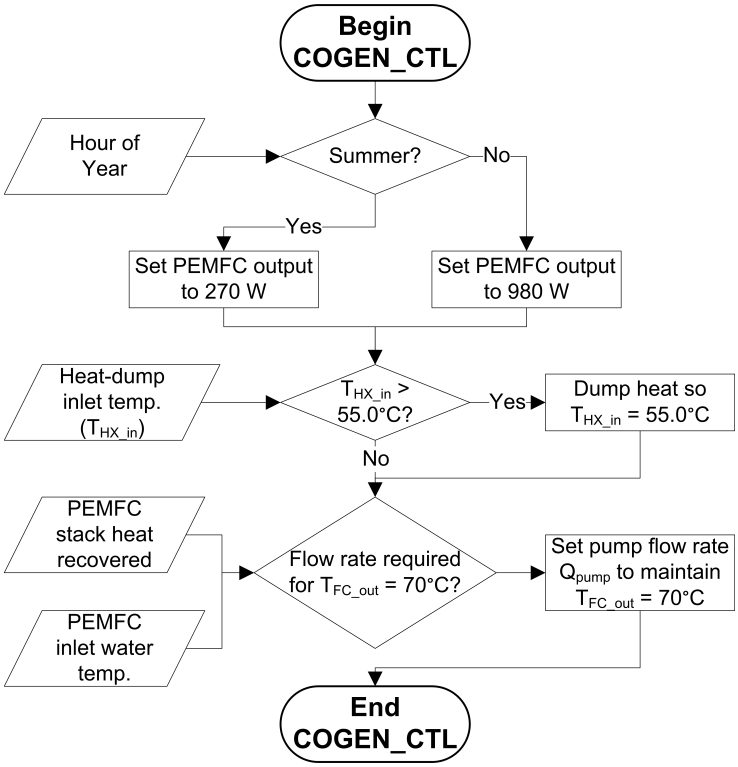

Figure 5.5: Control logic for the plant network PEMFC loop.

the PEMFC outlet temperature at 70^oC. The maximum PEMFC inlet temperature was limited to 55^oC in order to mimic experimental conditions and manufacturer

suggestions. If the heat dump inlet temperature (T_{HX_in})was greater than 55^oC a variable heat rejection occurred to maintain a PEMFC inlet temperature of 55^oC.

The most important controlled variable in the PEMFC loop was the PEMFC power output. The power output of the PEMFC was low compared to the average electricity demand of Canadian households (Saldanha and Beausoleil-Morrison 2012). Therefore, the power output of the PEMFC was not varied; a constant power output of the maximum 980 W was used for the winter heating season, which was throttled down to the minimum 270 W output during the summer cooling season.

5.1.4 Battery control

The li-ion battery model within the electrical network also required an external control signal. The custom controller provided the battery charge/discharge power (or set the power output to zero for idle).

A number of different battery control strategies were examined. Both constant discharge and electrical load following strategies were examined for their potential to reduce on-peak electricity demand. A summary of the different control strategies implemented is shown in Table 5.1. These strategies will be referred to as their names seen in the leftmost column.

5.1.5 Controller implementation

The control functions described for the four main subsystems (DHW, SH, PEMFC, RES) were developed in a customized controller. The controller was implemented using a Fortran subroutine within the ESP-r source code. The Fortran source code of the customized controller can be found at the online ESP-r source code repository.[1]

5.2 Performance Metrics

Having developed a model to simulate a PEMFC + RES system and a custom controller with strategies to reduce the on-peak energy consumption, a set of metrics was necessary to compare performance of the developed system to conventional residential HVAC systems.

[1]http://espr.svn.cvsdude.com/esp-r/branches/John_Kopf/src/esruplt/COGEN_CTL.F.

Battery control law	Description
B1	No battery use
B2	Constant 1.25 kW discharge on-peak, immediate 1.0 kW charge off-peak[1]
B3	Constant 1.25 kW discharge on-peak, delayed 2.0 kW charge off-peak[2]
B4	Electric load-following on-peak, excess electricity is exported [3]
B5	Electric load-following on-peak and mid-peak, excess electricity is exported [3]
B6	Electric load-following on-peak and mid-peak, excess electricity charges RES system [3]
B7	Load-following + 1 kW discharge on-peak
B8	Load-following + 1 kW discharge on-peak, mid-peak charge during winter TOU periods
B9	7.5 kW charge during minimum off-peak HOEP, 7.5 kW discharge during maximum on-peak HOEP

[1] Unless otherwise specified, the battery is idle during mid-peak periods.
[2] All control scenarios after this, with the exception of B9, make use of the delayed charge.
[3] If the electrical load is less than the PEMFC output.

Table 5.1: Battery control laws available within the customized controller.

A base case model with a conventional heating system was developed to provide a performance baseline from which to make all comparisons. The same building model was used for the base case, with the heating demands served by a condensing furnace instead. The DHW tank and draw profiles were also used for the base case, though there was no thermal storage tank to preheat the mains water prior to entering the DHW tank. A summary of the energy flows for the base case and the PEMFC +

Energy type	Base case system	PEMFC + RES system
Natural gas	Condensing furnace	PEMFC
	DHW tank burner	DHW tank burner
		SH supplementary burner
Electricity	Occupant loads	Occupant loads
	AC & circulation fan	AC & BOP component loads
	Grid import	Grid import/export
		PEMFC generation
		Battery charge/discharge

Table 5.2: Building energy flows for the base case and PEMFC + RES system.

RES system is shown in table Table 5.2.

The purpose of the metrics used in this research was to provide a quantitative comparison between the base case and the PEMFC + RES system, as well as each of the variant occupant load profiles and control strategies. To better inform on energy policies, such as a standard offer procedure for electricity exports from battery or micro-cogeneration devices, the cost of energy was chosen as the main metric for this research. An annual balance period was used to show the year-round performance of the system.

The cost performance metrics from the perspective of the end-user (EU) and the local energy distribution company are described in greater detail in sections 5.2.1 and 5.2.2, respectively.

The total annual electricity and natural gas consumptions were also examined. However, as mentioned in Chapter 2 it is important to look not only at the total energy production but also at the time of energy use offset.

5.2.1 Annual cost - End user

The economic performance of the residential PEMFC + RES system was examined from the EU perspective. This included both electricity and natural gas costs. Natural gas pricing data for Ontario in 2012 was used to calculate the natural gas price in this research (Enbridge 2012). The total natural gas price for Ontario in 2012, including delivery and transportation charges, was 21.22 $¢/m^3$.

The purchase price of grid electricity for a residential consumer varies in Ontario. The time-of-use (TOU) rates and periods for 2012 are shown in Figure 5.6. The cost of electricity for weekends and holidays is always the off-peak price. The electricity cost for summer and winter weekdays varies with the time of day.

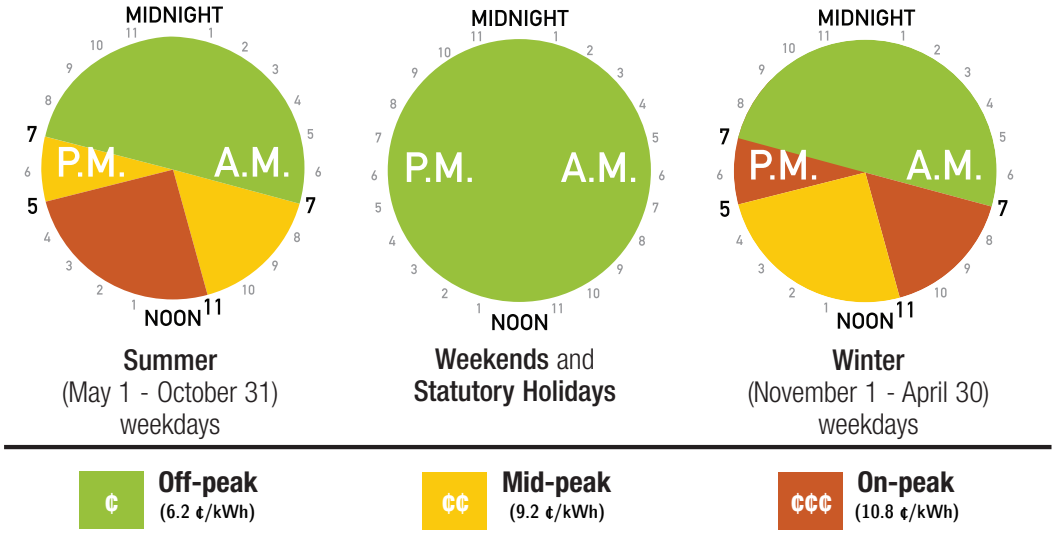

Figure 5.6: Ottawa time-of-use electrical rates and periods. Used with permission from Hydro Ottawa (2012)

This research examined the performance of the PEMFC + RES system with potential export purchase price (EPP) scenarios while ignoring local issues, as there is no way to quantify the cost performance of the system in the current market. EPP rates in Ontario are not currently favourable for micro-cogeneration (i.e. no standard offer in place), and electricity export from batteries is currently not allowed.

The scenarios explored varied the EPP which the consumer would receive for electricity exported to the grid. Three scenarios were adapted from Douglas (2012) and were explored for each of the control strategies described. These are shown in Table 5.3.

The cost of electricity mentioned for these three scenarios corresponds to the total cost, which includes the commodity price (see Fig. 5.6), the delivery price and other charges.

Scenario	Description
EPP1	Purchase price equal to cost of electricity.
EPP2	Purchase price less than the cost of electricity (50% of cost)
EPP3	Purchase price equal to cost of electricity, with a premium of 5 ¢/kWh paid for exports during on-peak periods.

Table 5.3: Hypothetical export purchase price scenarios explored for the end-user economic performance of the PEMFC + RES system.

5.2.2 Annual cost - Electric utility

The performance of the residential PEMFC + RES system was also examined from the perspective of a local distribution company (LDC), such as Hydro Ottawa. LDCs in Ontario (e.g. Hydro Ottawa) purchase electricity at the wholesale market price, known as the hourly Ontario energy price (HOEP) (IESO 2011). This price is set by the Independent Electricity System Operator (IESO) and is calculated as the hourly average of the five minute prices during that hour. These variations reflect the electricity supply and demand across Ontario.

It was assumed that from the LDC's perspective the value of electricity at each hour, whether consumed or generated by the household, would be equal to the current market price of electricity. Therefore, the cost for electricity imports and the EPP for electricity exports were both equal to the HOEP at each hour. In this way the usefulness of control strategies that employed an electrical load following discharge of the battery storage during peak hours could be examined.

5.2.3 Closing remarks

An integrated model of a Canadian household containing a residential PEMFC + RES system was developed in Chapter 4. This model was used to predict the performance of a PEMFC + RES system in a Canadian setting and under various levels of occupant loads.

The development of a customized controller within ESP-r was described in Section 5.1. This controller facilitated the testing of various control strategies and their impact on the PEMFC + RES system performance.

The methods to post-process ESP-r simulation results and metrics used to calculate the system performance were outlined in Section 5.2.

The thermal and electrical performance of the PEMFC + RES system, as well as the economic impact of each control strategy are given next in Chapter 6.

Chapter 6

Results

Chapter 4 described the development of an integrated model of a Canadian household containing a residential PEMFC + RES system. Chapter 5 reviewed the development of a customized controller for the PEMFC + RES system, and defined the metrics by which the system's performance was measured. With the completion of these research objectives, this chapter discusses the performance of the modelled system compared to a household with conventional HVAC and DHW systems.

Section 6.1 provides detailed results for the electrical performance of the PEMFC + RES system. Specifically, the function of the battery control scenarios is demonstrated over a daily basis. Section 6.2 provides detailed results for the thermal performance of the PEMFC + RES system. Finally, Section 6.3 summarizes the PEMFC + RES system performance for the metrics defined. This is done for all of the control scenarios developed and for each of the occupant load profiles examined.

6.1 Electrical Performance

The detailed electrical performance of the PEMFC + RES system is illustrated for each of the battery control scenarios developed in Section 5.1.4. The electrical balances are given for occupant load profile H11 over a typical day containing one charge-discharge cycle.

The electrical balance over one winter day for battery control scenario B1 is given in Figure 6.1. For the dotted line showing grid interaction, positive power values correspond to electricity imported from the grid and negative values correspond to electricity exported to the grid. As the figure shows, the generation throughout the day is constant as B1 does not use the RES system. This value corresponds to the

winter PEMFC electrical output of 980 W. It is also shown that for the plotted day the occupant loads peak from 14h00 to 17h00 with some lesser peaks from 06h00 to 11h00. It should be noted that the on-peak TOU periods for winter are from 07h00 to 11h00 and from 17h00 to 19h00.

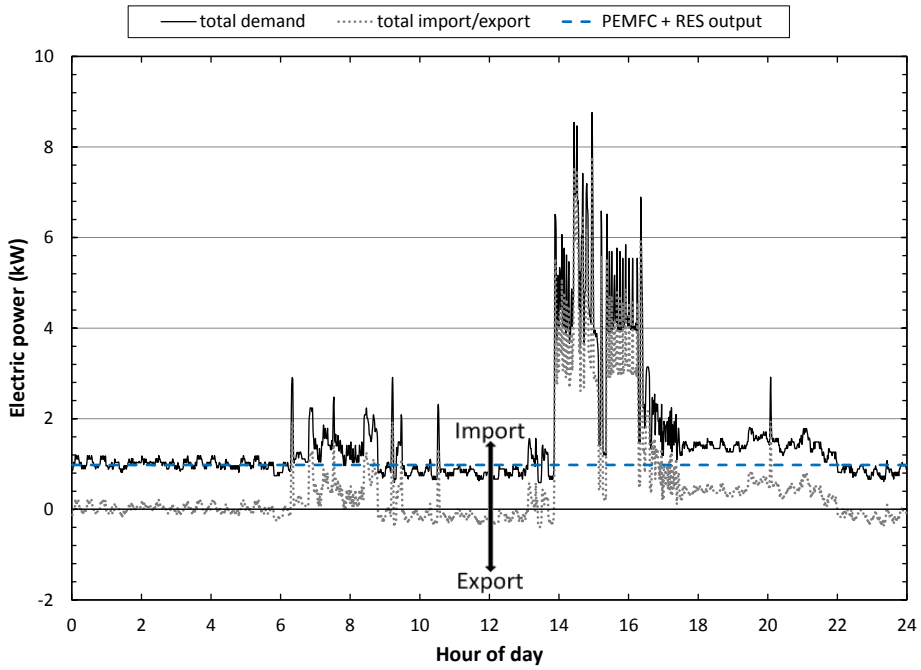

Figure 6.1: Electrical balance for occupant load profile H11 and battery mode B1 for January 16, 2008.

The electrical balance over one winter day for battery control scenario B2 is given in Figure 6.2. As the figure shows, the batteries are discharged during on-peak periods, which is seen as an increase in the total PEMFC + RES output during these periods. The associated battery state of charge (SOC) is given on the right axis of the figure. The RES system is charged once the off-peak period resumes at 19h00, even though the HOEP may still be high at these times. Scenario B3 attempts to avoid this.

The electrical balance over one winter day for battery control scenario B3 is given in Figure 6.3. This scenario is identical to B2, though the charging of the RES system is postponed until after midnight. It can also be seen that a higher charge rate is necessary as there is less available charge time before the end of the off-peak period.

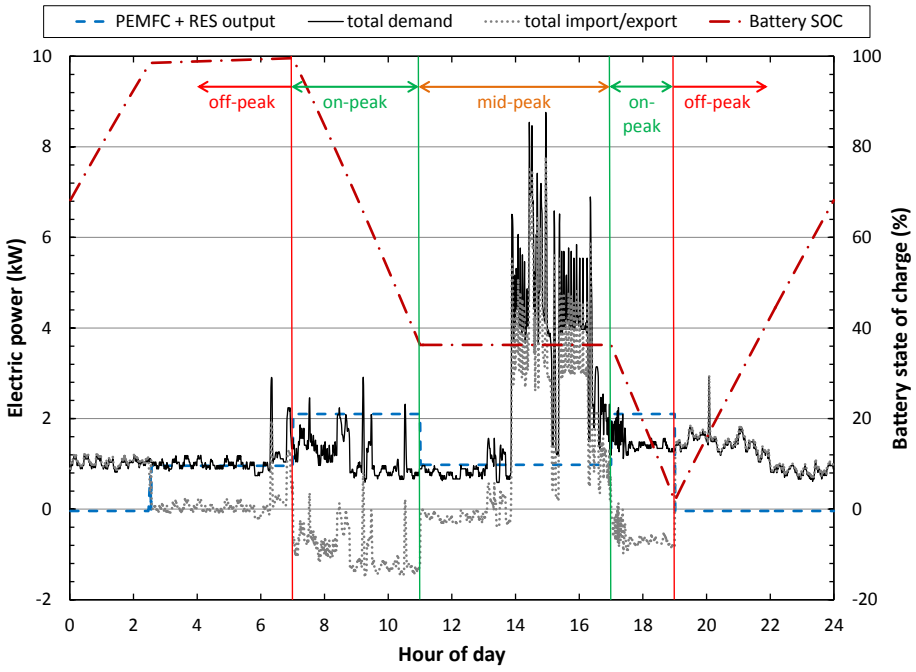

Figure 6.2: Electrical balance for occupant load profile H11 and battery mode B2 for January 16, 2008.

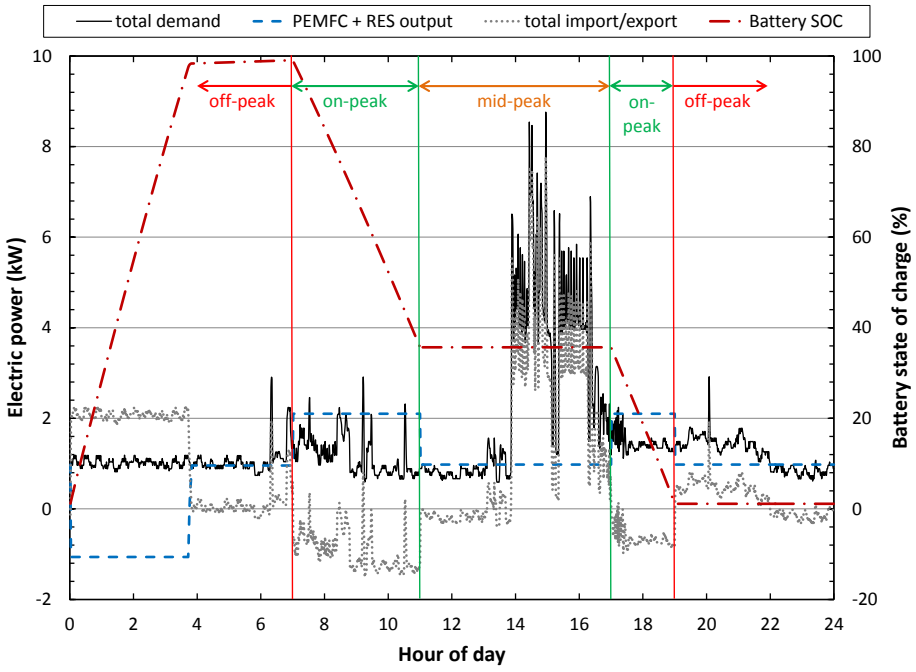

Figure 6.3: Electrical balance for occupant load profile H11 and battery mode B3 for January 16, 2008.

The electrical balance over one winter day for battery control scenario B4 is given in Figure 6.4. As the figure shows, there is no electricity imported from the grid during on-peak periods, which is the goal of a load-following control. Similar to B3, the off-peak charge is postponed until after midnight. It should be noted that the RES system demand for the given day is not sufficient to deplete the battery capacity. This suggests that the RES system may be over-sized for the goal of eliminating grid imports during on-peak periods only. The figure also shows that the battery SOC at the beginning of the charge cycle at 00h00 is 80%, meaning that the load-following operation during the previous day did not make full use of the battery's capacity.

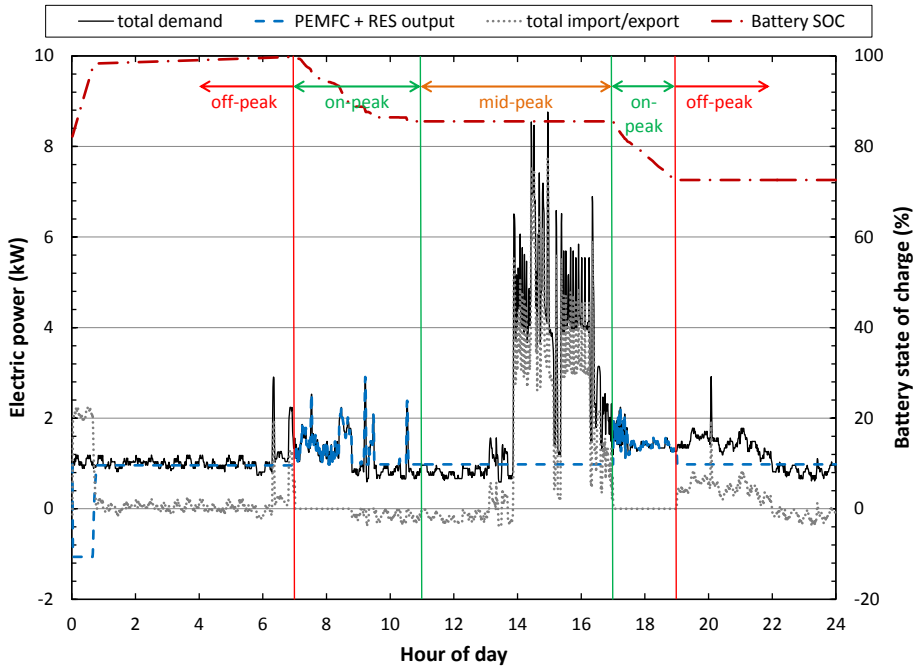

Figure 6.4: Electrical balance for occupant load profile H11 and battery mode B4 for January 16, 2008.

The electrical balance over one winter day for battery control scenario B5 is given in Figure 6.5. It can be seen that during on-peak and mid-peak periods no electricity is imported from the grid until 15h00. Compared to Figure 6.4 it can be seen that the load-following discharge during the mid-peak period is sufficient to fully deplete the battery's capacity. However, the battery SOC at the beginning of the charge cycle at 00h00 is 60%, meaning that the load-following operation during the previous day still did not make full use of the battery's capacity.

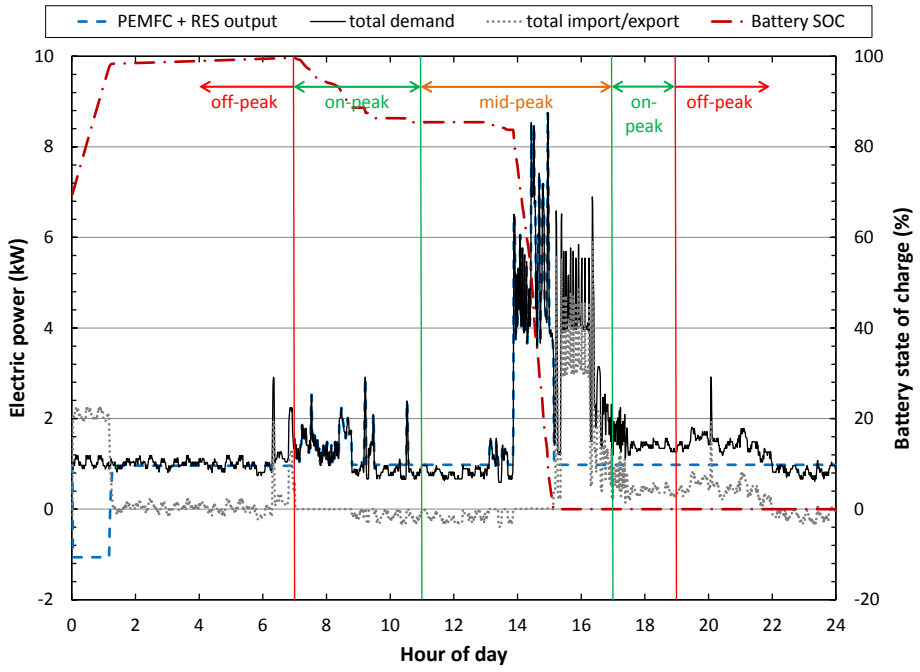

Figure 6.5: Electrical balance for occupant load profile H11 and battery mode B5 for January 16, 2008.

The electrical balance over one winter day for battery control scenario B6 is given in Figure 6.6. As the figure shows, the RES system discharge follows the electrical load during mid-peak and on-peak periods. The figure also shows that any excess PEMFC electrical power during mid-peak and on-peak periods is used to charge the RES system instead of being exported, which allows the PEMFC + RES system to serve the residential electrical loads for a greater length of time. However, due to the magnitude of peak electrical demands around 15h00 the result is not very different than that shown in Figure 6.5.

The electrical balance over one winter day for battery control scenario B7 is given in Figure 6.7. As the figure shows, the RES system discharge follows the electrical load during the on-peak period while simultaneously exporting 1 kW to the grid. The figure also shows that RES system is not able to sustain the load-following discharge through the second on-peak period. This suggests that for profile H11, the current RES system capacity may be slightly under-sized for scenario B7.

The electrical balance over one winter day for battery control scenario B8 is given in Figure 6.8. As the figure shows, the RES system discharge follows the electrical

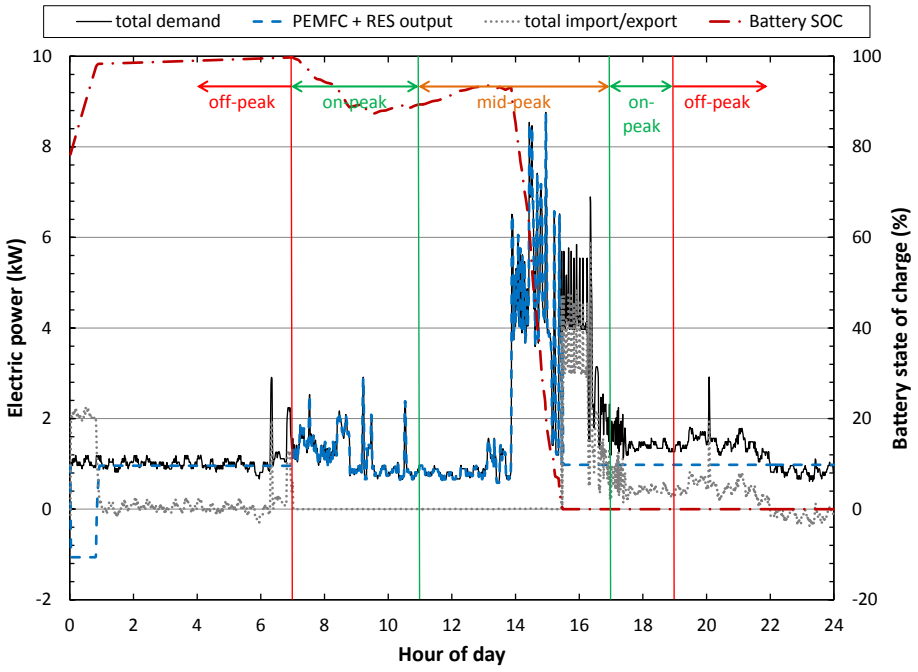

Figure 6.6: Electrical balance for occupant load profile H11 and battery mode B6 for January 16, 2008.

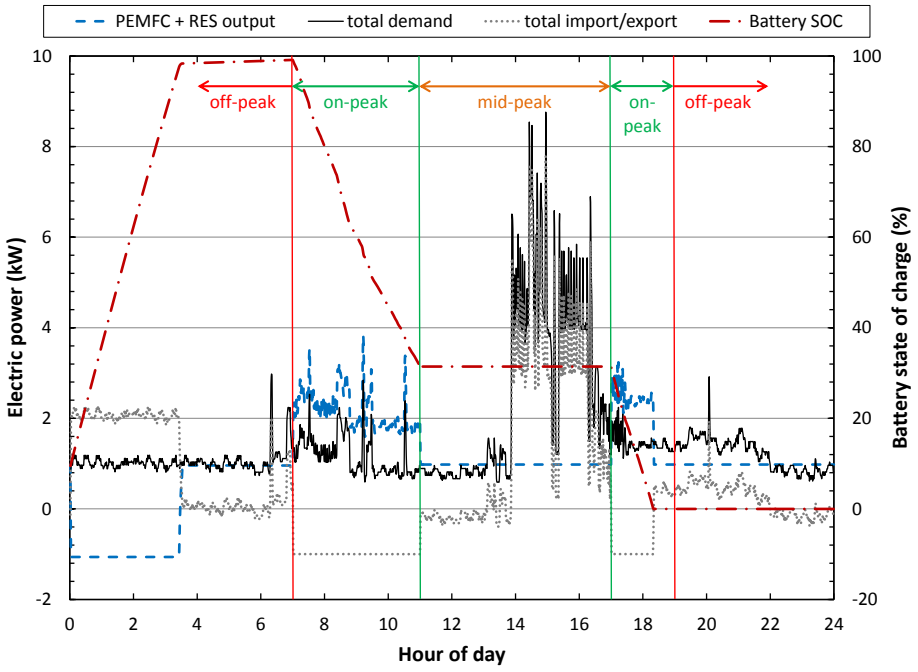

Figure 6.7: Electrical balance for occupant load profile H11 and battery mode B7 for January 16, 2008.

load during the on-peak period while simultaneously exporting 1 kW to the grid, identical to scenario B7. The figure also shows that the RES system is charged during the mid-peak TOU period to ensure that there is sufficient capacity for the second on-peak period. It can be seen that the RES system is over-charged during the mid-peak period, and is not able to discharge its remaining capacity during the second on-peak period. It is less economical to charge the battery in this way instead of doing so overnight when electricity is cheap for both the EU and LDC.

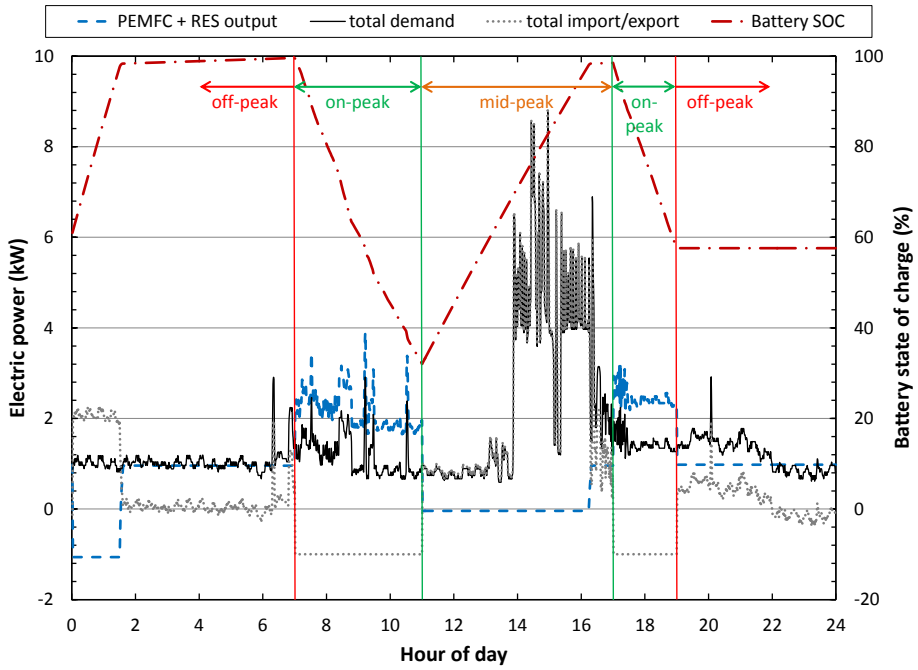

Figure 6.8: Electrical balance for occupant load profile H11 and battery mode B8 for January 16, 2008.

The electrical balance over one winter day for battery control scenario B9 is given in Figure 6.9. As the figure shows, the grid import increases at 04h00 and grid export increases at 08h00. This corresponds to the charging and discharging of the RES system for the hour of minimum and maximum HOEP, respectively. As expected, B9 has little effect on minimising a consumer's grid import/export, and instead focusses on maximising the cost performance from the LDC's point of view.

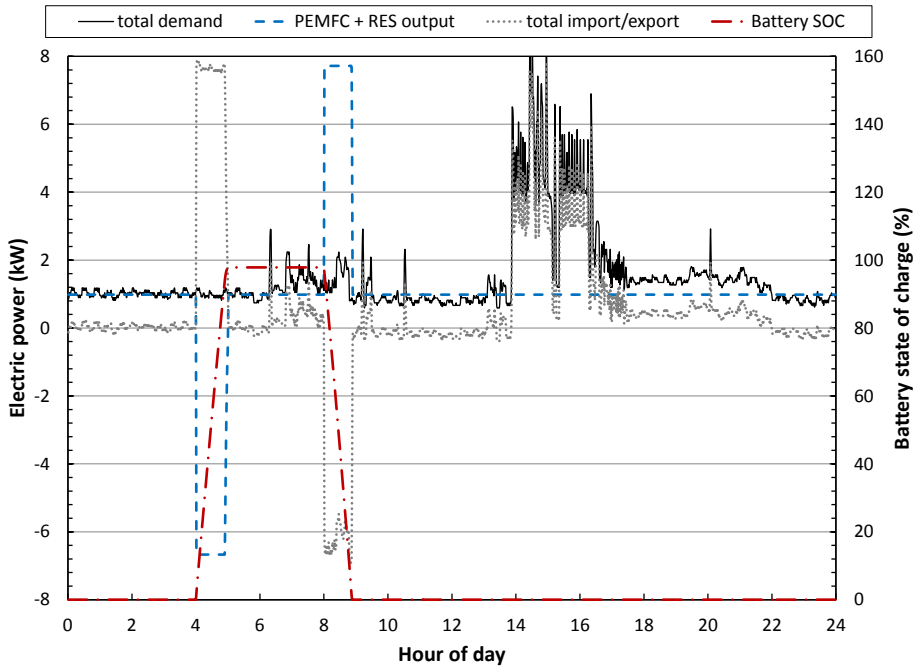

Figure 6.9: Electrical balance for occupant load profile H11 and battery mode B9 for January 16, 2008.

6.2 Thermal Performance

The PEMFC electrical output was not modulated in this research (see Chapter 5) and so the PEMFC thermal output remains constant as well. As a result of this, the thermal performance of the PEMFC + RES system does not vary between control scenarios. The thermal performance does however vary slightly with differing occupant non-HVAC load profiles as the casual gains from non-HVAC loads will offset the heating demands.

The household SH demands for a typical winter day are illustrated in Figure 6.10. As the figure shows, the storage tank temperature is not sufficient to provide all of the space heating to the main zone overnight and in the morning. There is little to no space heating demand from 11h00 to 19h00 as a result of solar irradiation and casual gains from non-HVAC loads. The storage tank temperature increases during this time and is able to provide the household's space heating demands from 19h00 to 20h00, after which the boiler is again fired regularly.

The household DHW demands for a typical winter day are illustrated in Figure 6.11. The DHW tank temperature is seen to be maintained around 60^oC. The

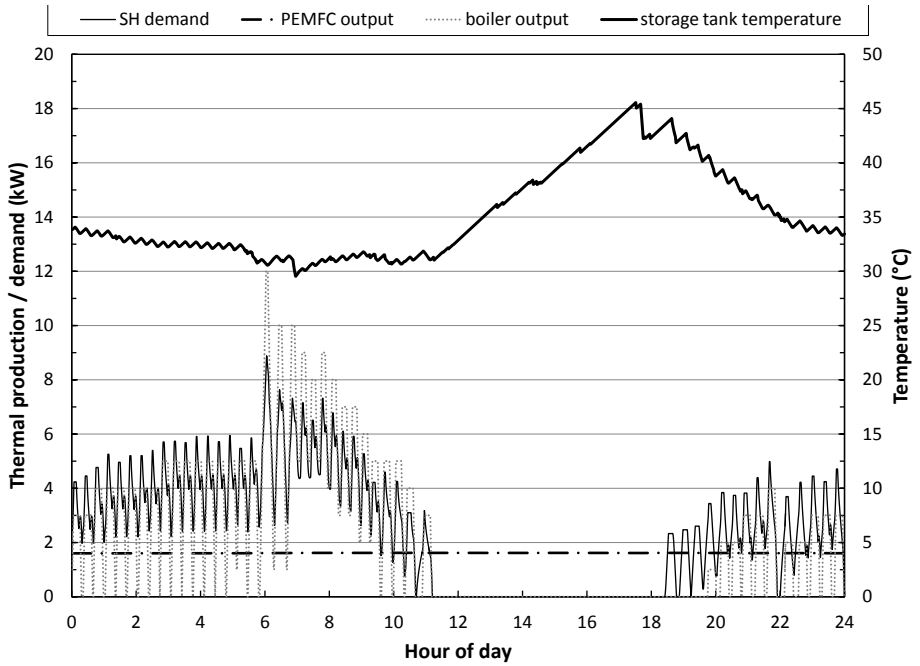

Figure 6.10: Household space heating demand and thermal storage tank temperature for January 16, 2008.

sharp increases in the DHW tank temperature correspond to the DHW tank burner firing to maintain the temperature set point. The DHW demand in Figure 6.11 is for the same day as the SH demand in Figure 6.10 so the combined effect of the SH and DHW demands can be seen by comparing the two figures.

6.3 House Variant Results

The simulation results are presented in two sections, one for each of the metrics described in Chapter 5. The results demonstrate the effectiveness of various control scenarios to minimize the annual household energy costs to the EU and the LDC. The results also demonstrate the ability of the PEMFC + RES system to serve various magnitudes of annual occupant non-HVAC loads. The nine battery control scenarios described in Section 5.1.4 were examined for each of the occupant load profiles from Section 4.4.3.

A comparison of the annual grid interaction of the PEMFC + RES system for profile H11 and all nine battery control scenarios is presented in Figure 6.12. As

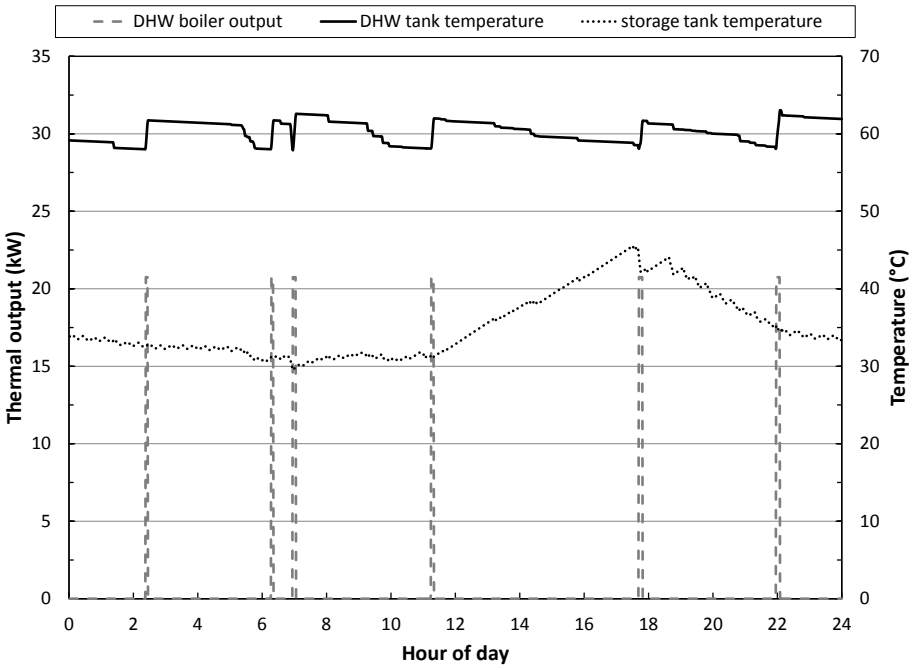

Figure 6.11: Household domestic hot water demand and domestic hot water tank temperature for January 16, 2008.

the figure shows, all nine control scenarios reduce the household's grid interaction in comparison to the base case. Scenario B1, with no RES system, is one of the cases with the least grid interaction, whereas scenarios B2, B3, B7, B8, and B9 use the RES system to export electricity during times of peak electrical demand. The annual PEMFC electrical production for all profiles and simulation variants was 23.4 GJ.

Figures for the annual grid interaction for profiles H4, H6 and H12 can be found in Appendix B. Comparing the annual grid interaction between these and profile H11 shown in Figure 6.12 it can be seen that for profiles with lower annual electricity demands (H4 and H6) the PEMFC + RES system tends to export more electricity. This is due to the greater number of occurrences where the PEMFC electrical output is greater than the total occupant load. Profile H12 has very little grid export for most control scenarios.

The economic performance of the PEMFC + RES system from the perspective of an EU is described next in Section 6.3.1.

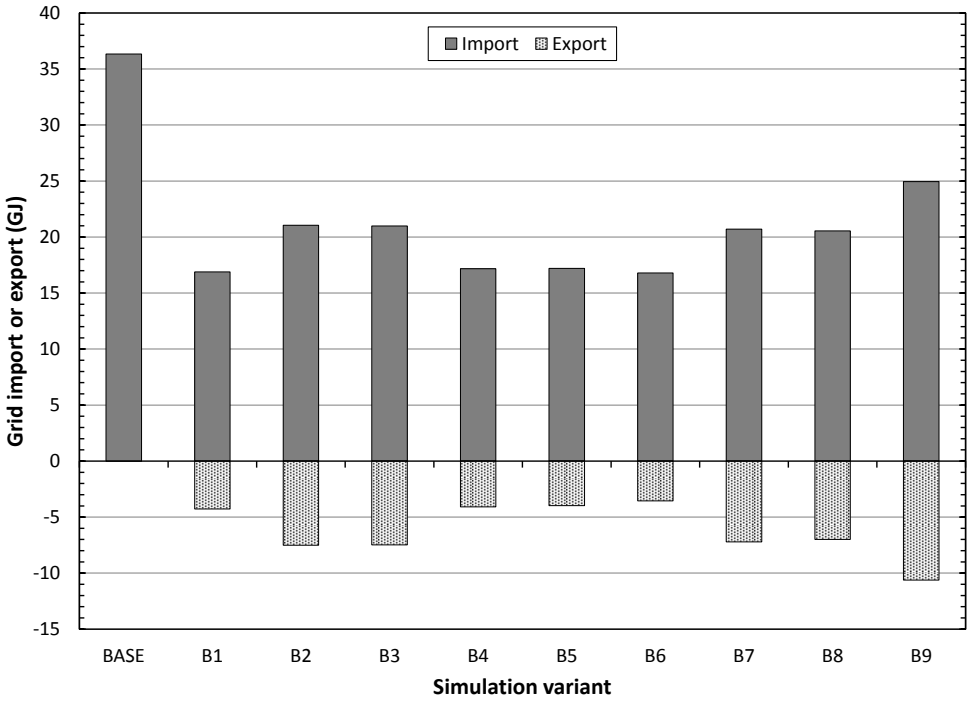

Figure 6.12: Annual grid interaction using a residential PEMFC + RES system for occupant load profile H11.

6.3.1 End-user economic performance

The annual EU economic performance of the PEMFC + RES system for profile H11 is presented in Figure 6.13. As the figure shows, the annual EU cost for each of the simulation variants is given as the sum of the natural gas cost and the net electricity cost after exports are credited. The EU revenue from electricity exports was calculated using the three hypothetical purchase price scenarios described in Section 5.2.1. The net EU cost using these three electricity purchase prices is depicted using three bars for each battery control scenario.

Looking at the net EU cost using EPP1 in Figure 6.13, all scenarios with the PEMFC system reduce the annual EU energy costs compared to the base case. All scenarios which use the PEMFC + RES system (B2-B9) further reduce the annual EU energy costs compared to the PEMFC system alone (B1). This is also true of the annual EU energy costs using EPP3.

EPP3 favours control scenarios which export electricity during on-peak TOU periods, as these exports receive a premium of 5 $¢/kWh$. Control scenarios B2 and B3

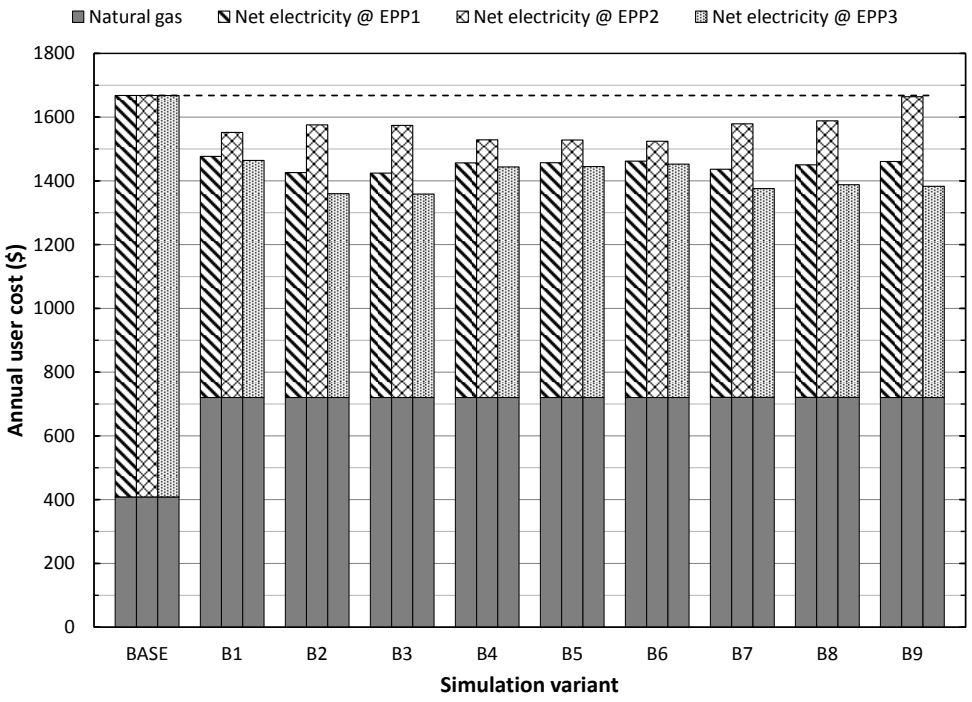

Figure 6.13: Annual end-user energy costs using a residential PEMFC + RES system for occupant load profile H11.

result in the greatest reduction in annual EU energy costs. This is due to the lower RES system rate of discharge which causes fewer internal resistance losses.

Even with an unfavourable purchase price (EPP2) all but one of the control scenarios provide a reduction in annual EU energy costs. The control scenarios which minimize grid interaction (B4-B8) provide the greatest reduction under EPP2. This is because with EPP2 it becomes more advantageous to use the excess electricity stored in the RES system to offset peak electrical demands rather than to export electricity to the grid. This is the basic aim of all of the load-following controllers.

Figures for the annual EU energy costs for profiles H4, H6 and H12 can be found in Appendix C. Comparing these to profile H11 shown in Figure 6.12 it can be seen that for profiles H4 and H6 the annual energy costs using EPP2 are often higher than the base case. It is also shown that B2 and B3 offer the greatest cost reductions when combined with either EPP1 or EPP3 for all occupant load profiles. Control scenario B9 also provides similar cost reduction as these, though only when combined with EPP3.

The economic performance of the PEMFC + RES system from the perspective of

a LDC is described next in Section 6.3.2.

6.3.2 Local distribution company economic performance

The annual LDC economic performance of the PEMFC + RES system for profile H11 is presented in Figure 6.14. As the figure shows, the use of the PEMFC system alone has virtually no effect on the annual LDC energy cost for the assumed NG tariff structure. However, most of the cases with the PEMFC + RES system show at least a minor improvement upon the base case.

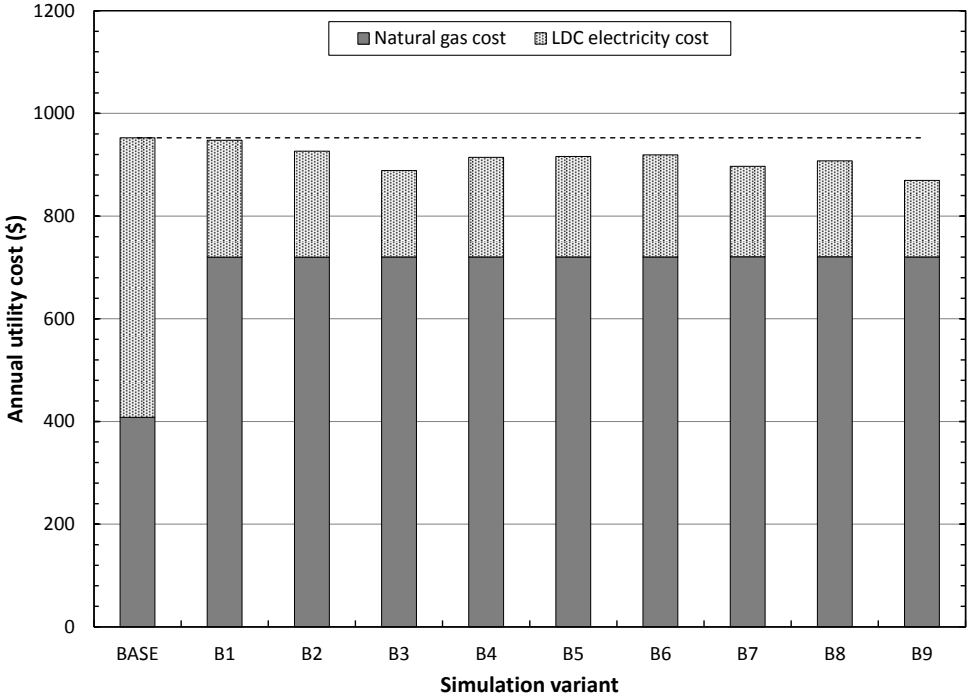

Figure 6.14: Annual LDC energy costs using a residential PEMFC + RES system for occupant load profile H11.

As expected, control scenario B9 provides the greatest reduction to the annual LDC energy cost, as this controller was designed from the LDC's perspective. Interestingly, scenario B3 exhibits a similar reduction to the LDC's annual energy cost despite its simple logic.

Figures for the annual LDC energy costs for profiles H4, H6 and H12 can be found in Appendix D. Comparing these to profile H11 shown in Figure 6.12 it can be seen that for all profiles the LDC control scenario (B9) provides the greatest cost reduction

for the LDC, which is as expected. Similar to the results for H11, scenario B3 provides the second greatest cost reduction for the LDC for all profiles. Scenario B3 was also one of the most favourable scenarios from the EU perspective for all profiles as well.

Chapter 7

Conclusions and Recommendations

7.1 Conclusions

The stated objectives of this research were to:

- model the performance of a residential micro-cogeneration device coupled with a residential electrical storage (RES) system;
- examine the economic potential of the system from the perspective of an end-user and a local energy distribution company;
- assess the system feasibility in the current electricity market as well as in hypothetical scenarios so as to advise on a potential future policy for this technology.

These objectives have been realized by the development of an integrated building envelope, plant, and electrical model within a building performance simulation program. The research conducted to meet these objectives is described in the following sections.

Micro-cogeneration + RES system model

A model of a typical Canadian household containing a micro-cogeneration based heating, ventilation and air-conditioning (HVAC) system coupled to a RES system was developed in the building performance simulation tool ESP-r. A proton exchange membrane fuel cell (PEMFC) was selected as the micro-cogeneration device in this research, and a lithium-ion battery was selected for the RES system. Both the PEMFC and the lithium-ion battery were calibrated with experimental data from literature.

The PEMFC's electrical power output can be modulated between its minimum and maximum settings of 270 W and 980 W, respectively. The lithium-ion battery has a capacity of 8.8 kWh and was calibrated with experimental data from a single lithium-ion cell. This data was applied to a matrix of 4 parallel rows of 14 series-connected cells to provide the desired capacity.

One challenge encountered in the modelling process was the control of many coupled plant and electrical components (e.g. battery storage, thermal storage, PEMFC device, pumps, fans, backup burners).

PEMFC + RES system controller

A customized controller was developed to provide control signals to many plant and electrical components simultaneously. The controller senses multiple simulation variables, such as component temperatures and flow rates, as well as externally read variables such as future outdoor temperatures, domestic hot water (DHW) demands, occupant non-HVAC electrical demands and the future Hourly Ontario Energy Price (HOEP). The non-HVAC electrical demands and HOEP are strongly correlated to the day of the week as well as the outdoor temperature. Caution was necessary in ensuring that the building, plant, and electrical domains, as well as the customized controller, were temporally aligned when referring to the external inputs, as many of these are referred to from separate routines within these domains during each simulation time-step.

The PEMFC electrical output was maintained constant at the maximum power setting during the winter season, and at the minimum setting during the summer season. Nine different control strategies for the RES system were developed in this research, named B1-B9. These strategies demonstrated the potential of the PEMFC + RES system to minimize costs to an end-user (EU) and a local distribution company (LDC), as discussed in the next section. Each of the nine control strategies were simulated for four different non-HVAC load profiles (named H4, H6, H11, H12) to examine the performance of the PEMFC + RES system in residences with various occupant load levels.

Performance metrics

The economic potential of a PEMFC + RES system was examined from the perspective of both an EU and a LDC. This was accomplished by comparing the performance

of the developed system to that of the same household with conventional HVAC and DHW systems.

For the LDC, the total annual cost resulting from a residence's energy demands was calculated as the sum of the natural gas cost and the net electricity cost to the LDC. The cost of electricity for a LDC in Ontario fluctuates hourly and is known as the HOEP. The total electricity costs to the LDC were calculated by summing the net electricity consumption at each hour (e.g. total load less generation) and multiplying this demand by the HOEP at that hour. The natural gas cost was calculated using the current natural gas market price for residential consumers.

For the EU, the total annual cost was calculated as the sum of the natural gas cost and the net EU electricity cost. The cost of electricity for a residential customer in Ontario fluctuates based on a time-of-use (TOU) schedule with a set price for off-peak, mid-peak, and on-peak periods. Three hypothetical export purchase price (EPP) scenarios were examined (named EPP1, EPP2, and EPP3), as there is no current policy in Ontario for electricity exports from micro-cogeneration or battery storage devices. EPP1 represents a neutral scenario where the export price is equal to the cost of electricity at each TOU period, whereas EPP2 represents an unfavourable scenario where the purchase price is equal to half of the cost of electricity. EPP3 is identical to EPP1 with a premium of 5 ¢/kWh paid for exports during on-peak periods. The net EU electricity costs were calculated as the electricity imports multiplied by the TOU price at each hour, less the total exports multiplied by the export purchase price for that hour. The natural gas cost was calculated using the current natural gas market price for residential consumers.

Micro-cogeneration system performance

The annual performance of the PEMFC + RES system was simulated for nine control strategies. This was done for each of the four occupant load profiles. The annual LDC energy cost performance for each simulation variant was then compared to the performance of the base case model. The annual EU cost performance was also compared to the base case for each of the export price scenarios.

Strategy B1

Strategy B1 assessed the performance of the PEMFC device alone, with no RES system use. It was found that for the assumed natural gas tariff structure the use

of the PEMFC system alone had virtually no effect on the annual LDC energy cost. However, it should be noted that this result is for a constant PEMFC output, which can cause excess electricity to be exported when there is little grid demand and the HOEP is low.

Strategy B1 provided an average 10% reduction in annual EU cost when using EPP1 and EPP3. Using EPP2 the PEMFC had virtually no effect on the annual EU cost for occupant load profiles with annual electricity consumptions less than 30 GJ. For load profiles with relatively large base loads (close to PEMFC output power) B1 provided a 10% reduction for all export price scenarios. This is due to the fact that even during off-peak times electricity will be used to offset the base load instead of being exported.

Strategies B2 and B3

Strategies B2 and B3 discharged the RES system at a constant rate during the on-peak period. The discharge rate, which was identical for both B2 and B3, was such that the discharge would be maintained throughout the entire on-peak period (six hours) and that the battery capacity would be fully depleted by the end of this period. Strategy B2 began its charge cycle at the start of the off-peak TOU period (19h00). B3 examined the effect of postponing the charge cycle until after midnight, as the HOEP can still be high during the off-peak hours before midnight.

Strategy B2 provided a modest reduction in annual LDC cost for all occupant load profiles (less than 2%). B3 provided the largest annual LDC cost reductions of all other control strategies but one, with an average 6% reduction observed for all load profiles.

Strategies B2 and B3 also provided the greatest reductions in annual EU cost using EPP1 and EPP3 compared to all other strategies. The results from the EU perspective were virtually identical, as the time of off-peak charge has no effect on the EU cost. The results for B3 are discussed in greater detail in the closing remarks below.

Strategies B4, B5, and B6

Strategies B4, B5 and B6 explored various configurations of an electric load-following RES system discharge, such that the PEMFC electric output + RES output would

supply the total household electrical load. Strategy B4 only incorporated the load-following discharge during on-peak periods, while in B5 and B6 the discharge also occurred during mid-peak periods. If the PEMFC electric output was greater than the total household load during the on-peak and mid-peak periods strategies B4 and B5 would export the excess electricity, while B6 would charge the RES system instead.

The results for strategies B4, B5 and B6 are virtually identical for both the annual LDC cost and the annual EU cost. These strategies provided only modest reductions in annual LDC cost for all occupant load profiles. However, they provided the greatest reductions in annual EU cost when using EPP2. This is because under an unfavourable EPP scenario it becomes more advantageous to use excess electricity to offset the household's peak electricity demands instead of exporting this electricity to the grid. For occupant load profiles with annual electricity consumptions less than 30 GJ these strategies were the only ones to provide a reduction, though modest, in annual EU cost using EPP2. 10-15% reductions in annual EU costs using EPP1 and EPP3 are also seen for these strategies, though these represent the lowest level of EU cost savings among the various control strategies.

It was also observed that the battery capacity was under-utilized with these control strategies, especially in B4 where the RES system was only used during on-peak periods. This suggests that B4 may be a more favourable operating strategy if the RES system is constrained by system size or upfront cost, where a smaller system would be more desirable.

Strategies B7 and B8

Strategies B7 and B8 used a load-following discharge during on-peak periods as well, while simultaneously exporting 1 kW to the grid. From the LDC perspective this is observed as a constant export rate, as opposed to strategies B2 and B3 where the RES system discharge was constant, and the export varied based on the difference between the discharge and total household electrical load. Strategy B8 also introduced a second charge cycle during the winter season mid-peak period, which occurs between two on-peak periods. This was done to provide extra capacity to the battery for the second on-peak period, though it provided no improvement upon strategy B7.

Strategy B7 provided a greater reduction in annual LDC costs than the load following strategies in B4, B5 and B6 due to the grid exports, though did not perform as well as B3 or B9 described next.

B8 may also become advantageous if the system was constrained by size or cost, as the RES system was often under-utilized. Incorporating an extra charge cycle mid-day would allow for a smaller capacity system, though this would only be effective during the winter season.

Strategy B9

Strategy B9 charged and discharged the RES system once daily over one hour each. These hours corresponded to the minimum and maximum HOEP price, respectively. Large charge and discharge rates were used to accommodate this operation, which may be unfeasible within a residential electrical grid, though the strategy represented the most ideal case from a LDC cost perspective.

As expected, strategy B9 provided the greatest reduction in annual LDC cost. A 10-15% reduction in annual EU cost was also observed when using EPP1 or EPP3, though B9 had the worst performance of all strategies when using EPP2. As a result of the high charge-discharge rates, B9 also had the highest losses associated with charge-discharge cycling.

Closing remarks

Strategies B3 (constant discharge) and B9 (HOEP following discharge) were of most interest as they provided the greatest reduction in the annual LDC cost and the annual EU cost (using EPP1 and EPP3). Strategies B3 and B9 offered a $350 and $370 reduction in net LDC electricity costs, respectively, for all studied occupant load profiles, which corresponded to a 50-90% savings in LDC electricity costs depending on the magnitude of occupant non-HVAC loads. However, the natural gas costs for the house are increased by 68-76% due to the PEMFC operation, and so the average LDC cost savings were 6% and 8% for strategies B3 and B9, respectively.

The annual EU cost savings for strategy B3 ranged from 12-16% for EPP1 and from 14-22% for EPP3, depending on the occupant annual electricity consumption. Similarly for strategy B9, savings ranged from 10-14% for EPP1 and from 14-20% for EPP3. For a non-favourable export price scenario (EPP2), where the purchase price that the consumer receives for electricity exports is less than the cost of electricity, the load-following scenarios B4, B5 and B6 provided the greatest reductions. Under such a purchase price scenario it becomes more advantageous to use the excess electricity

stored in the RES system to offset peak electrical demands rather than to export electricity to the grid.

7.2 Recommendations for Future Work

This research represents only the first step in modelling and assessing the performance of a PEMFC + RES system in a Canadian household. Much work still remains in assessing the feasibility of micro-cogeneration and RES systems in Canada. Some recommendations are provided in the following sections.

This research focused mainly on the electrical performance of a PEMFC + RES system and the effect of various control scenarios. However, optimising the use of the PEMFC thermal output will yield further improvements due to less reliance on supplementary heating components (therefore less natural gas use). A stratified tank model with two immersed-coil heat exchangers was used to store the PEMFC thermal output. This model could be improved upon by optimising the tank and immersed-coil heat exchanger sizing and geometry for application with a PEMFC.

It was also noticed that the DHW burner was often fired during the summer season although the supply temperature from the storage tank often exceeded 45^oC. Future systems may benefit from the use of tankless (on-demand) hot water heaters, which are not required to maintain such high temperatures as storage tanks. This could easily be implemented in the developed system by replacing the DHW tank component with a burner.

One plant component that was not addressed in this research is the realistic treatment of a heat rejection device. On rare occasions a minimal amount of heat rejection was required during the summer season to maintain the PEMFC inlet water temperature below the maximum allowable temperature. This heat rejection occurred ideally without consideration of the individual components that would be required. These components and their associated power draws could be included in future models.

This research assessed the performance of a residential PEMFC + RES system under annual occupant electrical demands ranging from 20 GJ to 45 GJ. The developed system could also be implemented in different building models in order to examine the system performance under various thermal demands. Future economic analysis could examine the sensitivity to varying natural gas prices for both the EU and the LDC.

One interesting result from strategy B4 was that its economic performance was comparable to other controllers even though with B4 the battery capacity was often not fully utilized. This suggests that reducing the RES system capacity may not negatively impact the system performance using strategy B4 as much as it would using other control strategies. Future work could assess the capital cost and payback period of various sizes of RES systems and the effect of the sizing on the overall annual performance.

The custom controller developed in this research examined a number of control strategies for the RES system, while the PEMFC output was maintained constant in all of these. The next step would be to incorporate control strategies to modulate the PEMFC thermal output as well. Similar to the current RES system control strategies, some initial PEMFC strategies could modulate the PEMFC output according to a schedule. These results could then be used to inform the development of further PEMFC controls.

Much of the current research into micro-cogeneration system control is regarding predictive control. Currently, only control strategy B9 is predictive, and only in the sense that it uses values for the HOEP one day in advance. However, the framework to import other future variables into the control routine has been implemented. It remains to be seen whether there would be any benefit in applying predictive control to the PEMFC used in this research due to its small thermal output. However, with the improvement of the system thermal performance this could also be examined in future systems.

The data used to calibrate the current lithium-ion battery model was obtained from single-cell experiments of lithium-ion cell prototypes. The lithium-ion battery model currently takes this single cell performance data and extrapolates the results for a matrix of cells in series and parallel. This represents the most ideal scenario of a larger RES system. A more appropriate treatment would be to calibrate the battery model to a prototype residential lithium-ion battery.

These are just examples of some areas where future work is possible. The next step should be to experimentally calibrate the battery model to an appropriately sized RES device. The optimisation of the system's thermal performance could be done simultaneously, which would ensure that the system operates as efficiently as possible to maximize the use of the PEMFC thermal output. A more realistic illustration of the PEMFC + RES system performance could then be drawn.

References

ASHRAE (2011). *BSR/ASHRAE Standard 188P: Prevention of Legionellosis Associated with Building Water Systems*. Atlanta, USA: American Society of Heating, Refrigerating and Air Conditioning Engineers.

Beausoleil-Morrison, I. (2000). *The adaptive coupling of heat and air flow modelling within dynamic whole-building simulation*. Ph. D. thesis, University of Strathclyde, Glasgow, UK.

Beausoleil-Morrison, I. (2007). *Experimental Investigation of Residential Cogeneration Devices and Calibration of Annex 42 Models*. A Report of Subtask B of FC+COGEN-SIM: The Simulation of Building-Integrated Fuel Cell and Other Cogeneration Systems. Annex 42 of the International Energy Agency Energy Conservation in Buildings and Community Systems Programme.

Beausoleil-Morrison, I. (Ed.) (2008). *An Experimental and Simulation-Based Investigation of the Performance of Small-Scale Fuel Cell and Combustion-Based Cogeneration Devices Serving Residential Buildings*. Final report of FC+COGEN-SIM: The Simulation of Building-Integrated Fuel Cell and Other Cogeneration Systems. Annex 42 of the International Energy Agency Energy Conservation in Buildings and Community Systems Programme.

Beausoleil-Morrison, I. (2011). Micro-cogeneration system performance prediction. In J. Hensen and R. Lamberts (Eds.), *Building Performance Simulation for Design and Operation* (1st ed.). Spon Press.

Beausoleil-Morrison, I., M. Mottillo, A. Ferguson, H. Ribberink, L. Yang, and K. Haddad (2006). The simulation of a renewable-energy-powered hydrogen-based residential electricity system. In *Proceedings of SimBuild 2006: Second National IBPSA-USA Conference*, Cambridge, USA.

Beausoleil-Morrison, I. and H. Ribberink (2008). The potential for reducing energy consumption and greenhouse gas emissions in the Ontario (Canada) housing sector with solid-oxide fuel-cell micro-cogeneration. In *Proceedings: Micro-Cogeneration 2008*, Ottawa, CA.

Beausoleil-Morrison, I., A. Weber, F. Maréchal, B. Griffith, A. Ferguson, and N. Kelly (2007). *Specifications for Modelling Fuel Cell and Combustion-Based Residential Cogeneration Devices within Whole-Building Simulation Programs*. A Report of Subtask B of FC+COGEN-SIM: The Simulation of Building-Integrated Fuel Cell and Other Cogeneration Systems. Annex 42 of the International Energy Agency Energy Conservation in Buildings and Community Systems Programme.

Capehart, B. L., W. C. Turner, and W. J. Kennedy (2011). *Guide to Energy Management* (7 ed.). Fairmont Press.

Carbon Trust (2007). Micro-chp accelerator. Technical report, Carbon Trust, London, UK. Accessible online at http://www.carbontrust.com/resources/reports/technology/micro-chp-accelerator.

Clarke, J. A. (2001). *Energy Simulation in Building Design* (2nd ed.). Butterworth-Heinemann.

Cruickshank, C. and S. Harrison (2004). Analysis of a modular thermal storage for solar heating systems. In *Proceedings: Canadian Solar Buildings Conference*, Montreal, CA. NSERC SBRN.

Darcovich, K. and B. Kenney (2012). Experimental lithium-ion cell calibration data, internal report. Technical report, The National Research Council of Canada, Ottawa, CA.

DOE (2011). *Building Technologies Program: Building Energy Software Tools Directory*. Washington, USA: U.S. Department of Energy: Energy Efficiency and Renewable Energy. Accessible online at http://apps1.eere.energy.gov/buildings/tools_directory/alpha_list.cfm.

Douglas, M. (2012). Consumer electricity export purchase price scenarios for residential micro-cogeneration. Email correspondence, Canada Centre for Mineral and Energy Technology (CANMET) Energy Division, Natural Resources Canada.

Edwards, C. (2011). Performance assessment of solar absorption cooling for Ontario housing. Master's thesis, Carleton University, Ottawa, CA.

Enbridge (2012). Residential natural gas rate changes. Enbridge Gas Distribution Incorporated.

Entchev, E., J. Gusdorf, M. Swinton, M. Bell, F. Szadkowski, W. Kalbfleisch, and R. Marchand (2004). Micro-generation technology assessment for housing technology. *Energy and Building 36*, 925–931.

Environment Canada (2008). *Canadian Weather Energy and Engineering Data Sets (CWEEDS Files) Updated Users Manual*. Ottawa, CA: Meteorological Service of Canada (MSC) and The National Research Council of Canada.

ESRU (2000). *The ESP-r system for building energy simulations: User guide version 9 series*. Glasgow, UK: Glasgow: University of Strathclyde. ESRU Manual U00/1.

Gähler, C., M. Gwerder, and R. Lamon (2008). *Optimal Control of CHP Building Energy Systems*. Annex 42 of the International Energy Agency Energy Conservation in Buildings and Community Systems Programme.

Gao, L., S. Liu, and R. A. Dougal (2002). Dynamic lithium-ion battery model for system simulation. *IEEE Transactions on Components and Packaging Technologies 25*(3), 495–505.

Hensen, J. L. (1991). *On the thermal interaction of building structure and heating and ventilation system*. Ph. D. thesis, Eindhoven University of Technology, Eindhoven, NL.

Houwing, M., R. R. Negenborn, M. D. Ilić, and B. D. Schutter (2009). Model predictive control of fuel cell micro-cogeneration systems. In *Proceedings: IEEE International Conference on Networking, Sensing, and Control*, Okayama, Japan.

Hu, S. D. (1985). *Cogeneration* (1st ed.). Reston Publishing Company.

Hydro Ottawa (2012). Residential customers time-of-use periods and rates. Hydro Ottawa Limited, Hydro Ottawa Holding Incorporated.

Ibrahim, H., A. Ilinca, and J. Perron (2008). Energy storage systems: Characteristics and comparisons. *Renewable and Sustainable Energy Reviews 12*, 1221–1250.

IESO (2011). *Introduction to Ontario's Physical Markets*. Toronto, CA: The Independent Electricity System Operator.

IESO (2012). Hourly generator output capability and demand for Ontario on January 27, 2012. Technical report, The Independent Electricity System Operator, Ottawa, CA. Accessible online at http://www.ieso.ca/imoweb/marketdata/genEnergy.asp.

Johnson, G. and I. Beausoleil-Morrison (2012). The calibration and validation of a model for simulating the thermal and electrical performance of a 1 kW_{AC} proton-exchange membrane fuel-cell micro-cogeneration device. *Journal of Power Sources*.

Jordan, U. and K. Vajen (2001). *Realistic Domestic Hot-Water Profiles in Different Time Scales*. Marburg, DE: International Energy Agency Solar Heating and Cooling Programme (IEA SHC), Task 26: Solar Combisystems.

Kelly, N. (1998). *Towards a design environment for building integrated energy systems: The integration of electrical power flow modelling with building simulation*. Ph. D. thesis, University of Strathclyde, Glasgow, UK.

Knight, I., N. Kreutzer, M. Manning, M. Swinton, and H. Ribberink (2007). *European and Canadian non-HVAC Electric and DHW Load Profiles for Use in Simulating the Performance of Residential Cogeneration Systems*. A Report of Subtask A of FC+COGEN-SIM: The Simulation of Building-Integrated Fuel Cell and Other Cogeneration Systems. Annex 42 of the International Energy Agency Energy Conservation in Buildings and Community Systems Programme.

Knight, I., V. I. Ugursal, and I. Beausoleil-Morrison (2005). *Residential Cogeneration Systems: A Review of the Current Technologies*. A Report of Subtask A of FC+COGEN-SIM: The Simulation of Building-Integrated Fuel Cell and Other Cogeneration Systems. Annex 42 of the International Energy Agency Energy Conservation in Buildings and Community Systems Programme.

Kolanowski, B. F. (2011). *Small-Scale Cogeneration Handbook* (4th ed.). Fairmont Press.

Matics, J. and G. Krost (2008). Micro combined heat and power home supply: Prospective and adaptive management achieved by computational intelligence techniques. *Applied Thermal Engineering 28*, 2055–2061.

Mottillo, M., I. Beausoleil-Morrison, A. Ferguson, H. Ribberink, L. Yang, and K. Haddad (2006). *Internal Report: Examining the feasibility of a hydrogen-based renewable-energy-powered residential cogeneration system for grid-connected houses*. Ottawa, CA: Natural Resources Canada CANMET Energy Technology Centre (CETC-Ottawa).

Newton, B. J. (1995). Modeling of solar storage tanks. Master's thesis, University of Wisconsin-Madison, Madison, USA.

NRCan (1994). *R-2000 Standard*. Ottawa, CA: Natural Resources Canada.

NRCan (2012). Energy use data handbook 1990 to 2009. Technical report, Office of Energy Efficiency, Natural Resources Canada. Accessible online at http://oee.nrcan.gc.ca/publications/statistics/handbook11/index.cfm?attr=0.

Onovwiona, H. I. and V. I. Ugursal (2006). Residential cogeneration systems: review of the current technology. *Renewable and Sustainable Energy Reviews 10*, 389–431.

Ontario Power Authority (2010). *Micro Feed-in Tariff Program: Program Overview*. Toronto, CA: Ontario Power Authority.

Ontario Power Authority (2011). *Feed-in Tariff Program: FIT Rules Version 1.5.1*. Toronto, CA: Ontario Power Authority.

Pehnt, M., M. Cames, C. Fischer, B. Praetorius, L. Schneider, K. Schumacher, and J. P. Voß (2006). *Micro Cogeneration: Towards Decentralized Energy Systems* (1st ed.). Springer.

Perlman, M. and B. Mills (1984). Development of hot water use patterns. *ASHRAE Transactions 91*(2), 657–679.

Ribberink, H., D. Bourgeois, I. Beausoleil-Morrison, and A. Ferguson (2007). Performance assessment of residential cogeneration systems in Canada using a whole-building simulation approach. In *Proceedings: Building Simulation*, Beijing, CN, pp. 1946–1953. IBPSA.

Ribberink, H. and W. Wang (2008). Improving esp-r's battery model with active battery life control and coverage of vanadium redox flow batteries. In *Proceedings: eSim 2008 - The 5th IBPSA-Canada Conference*, Quebec, CA.

Saldanha, N. (2010). Towards the assessment of a residential electric storage system: analysis of Canadian residential electricity use and the development of a lithium-ion battery model. Master's thesis, Carleton University, Ottawa, CA.

Saldanha, N. and I. Beausoleil-Morrison (2012). Measured end-use electric load profiles for 12 Canadian houses at high temporal resolution. *Energy and Buildings 49*, 519–530.

Thevenard, D. (2007). *Development of a Stratified Tank Model in ESP-r*. Waterloo, CA: Numerical Logics Inc. Report submitted to NRCan.

Thevenard, D. (2009). *Implementation of a spiral heat exchanger model in the ESP-r building energy analysis software*. Waterloo, CA: Numerical Logics Inc. Report submitted to NRCan.

Thevenard, D. and K. Haddad (2010). Development of a stratified tank model with immersed heat exchangers in esp-r. In *Proceedings: eSim 2010, The 6th IBPSA Canada Conference*, Winnipeg, CA. IBPSA Canada.

Thorsteinson, E., B. Strathearn, G. MacKenzie, and G. Amow (2011). Performance testing of a 1 kW_e PEM fuel-cell cogeneration system. In *Proceedings: MicroGEN '11, The 2nd International Conference on Microgeneration and Related Technologies*, Glasgow, Scotland. IEA/ECBCS.

TRNSYS (2000). *A Transient Simulation Program, Ver. 15*. Solar Energy Laboratory, University of Wisconsin-Madison. Madison, USA.

U.S. Energy Information Administration (2010). International energy outlook. Technical report, U.S. Department of Energy: Office of Integrated Analysis and Forecasting, Washington, USA. Accessible online at http://www.eia.gov/forecasts/ieo/index.cfm.

Wiehagen, J. and J. L. Sikora (2002). Domestic hot water system modeling for the design of energy efficient systems. Technical report, National Renewable Energy Laboratory, Marlboro, USA. NAHB Research Center Inc.

Appendix A

ESP-r finite difference formulation

ESP-r uses FD schemes to simplify the non-linear partial differential equations that govern the energy, mass and momentum flow in buildings, such as the Fourier heat equation or the Navier Stokes equations. Specifically, the Taylor series expansion is used to approximate the derivatives of these equations. For example, the one-dimensional transient Fourier heat conduction equation in the x-direction, which represents the heat transferred across the solid building envelope material, is given as;

$$\rho C_p \frac{\partial T(x,t)}{\partial t} = -\frac{\partial}{\partial x}\left(- k\frac{\partial T(x,t)}{\partial x}\right) + \frac{q_x}{(\delta x \delta y \delta z)} \tag{A.1}$$

where k is the thermal conductivity $[W/mK]$, C_p the specific heat capacity $[J/kgK]$ and ρ the density $[kg/m^3]$ of the building material; T is temperature $[K]$; t is time $[s]$; and q_x is the heat injection in the x-direction $[W]$ such as that from an embedded heating component. δx, δy and δz are small spatial increments in the $x-$, $y-$ and $z-$directions, respectively. Assuming constant thermo-physical properties (material is homogeneous, so k is independent of x) this can be written as;

$$\frac{1}{\alpha}\frac{\partial T}{\partial t} = \frac{\partial^2 T}{\partial x^2} + \frac{q_x}{k(\delta x \delta y \delta z)} \qquad \text{where } \alpha = \frac{k}{\rho C_p} \tag{A.2}$$

The α term is known as the thermal diffusivity $[m^2/s]$. The following expression can be written for a node I at time t using a central difference to approximate the second derivative in x, and a first order forward difference to approximate the time derivative;

$$\frac{1}{\alpha}\frac{T_I^{t+\delta t} - T_I^t}{\delta t} = \frac{T_{I+1}^t - 2T_I^t + T_{I-1}^t}{(\delta x)^2} + \frac{q_I^t}{k(\delta x \delta y \delta z)} \tag{A.3}$$

where δt is a small time increment $[s]$. Equation A.3 can be re-arranged in terms of the unknown future time-step as;

$$T_I^{t+\delta t} = \left(\frac{\alpha\delta t}{(\delta x)^2}\right)T_{I+1}^t + \left(1 - \frac{2\alpha\delta t}{(\delta x)^2}\right)T_I^t + \left(\frac{\alpha\delta t}{(\delta x)^2}\right)T_{I-1}^t + \frac{q_I^{t+\delta t}}{\rho C_p(\delta x\delta y\delta z)} \tag{A.4}$$

This is an explicit scheme, which means the unknown future temperature term ($T_I^{t+\delta t}$) is a function of current temperature terms only. In an implicit scheme the future temperature term is a function of both current and future terms. Explicit schemes are generally easier to formulate and solve, though are unstable in certain cases. It can be seen in the equation above that the coefficient in front of the temperature term at node I at the present time-step can become negative if

$$\frac{2\alpha\delta t}{(\delta x)^2} > 1 \tag{A.5}$$

and so the following stability criterion is imposed:

$$\frac{2\alpha\delta t}{(\delta x)^2} \leq 1 \text{ or } \delta t \leq \frac{1}{2\alpha}(\delta x)^2 \tag{A.6}$$

Implicit schemes are generally more stable than explicit schemes, though are also more complicated to solve. The implicit formulation of the Fourier heat equation A.1 can be developed similarly as;

$$\frac{1}{\alpha}\frac{T_I^{t+\delta t} - T_I^t}{\delta t} = \frac{T_{I+1}^{t+\delta t} - 2T_I^{t+\delta t} + T_{I-1}^{t+\delta t}}{(\delta x)^2} + \frac{q_I^{t+\delta t}}{k(\delta x\delta y\delta z)} \tag{A.7}$$

ESP-r uses a weighted average of the explicit and implicit schemes, known as the Crank-Nicolson method, with an equal weighting for each scheme, given as;

$$\begin{aligned}\left(1 + \frac{\alpha\delta t}{(\delta x)^2}\right)T_I^{t+\delta t} = &\left(\frac{\alpha\delta t}{2(\delta x)^2}\right)(T_{I+1}^t + T_{I-1}^t + T_{I+1}^{t+\delta t} + T_{I-1}^{t+\delta t}) \\ &+ \left(1 - \frac{\alpha\delta t}{(\delta x)^2}\right)T_I^t + \frac{\delta t}{2\rho C_p}\frac{(q_I^{t+\delta t} + q_I^t)}{(\delta x\delta y\delta z)}\end{aligned} \tag{A.8}$$

This formulation is the foundation for the equations used to model the heat transfer through solid building envelope components in ESP-r.

Appendix B

Annual grid interaction

Results for annual grid interaction for houses H4, H6, and H12.

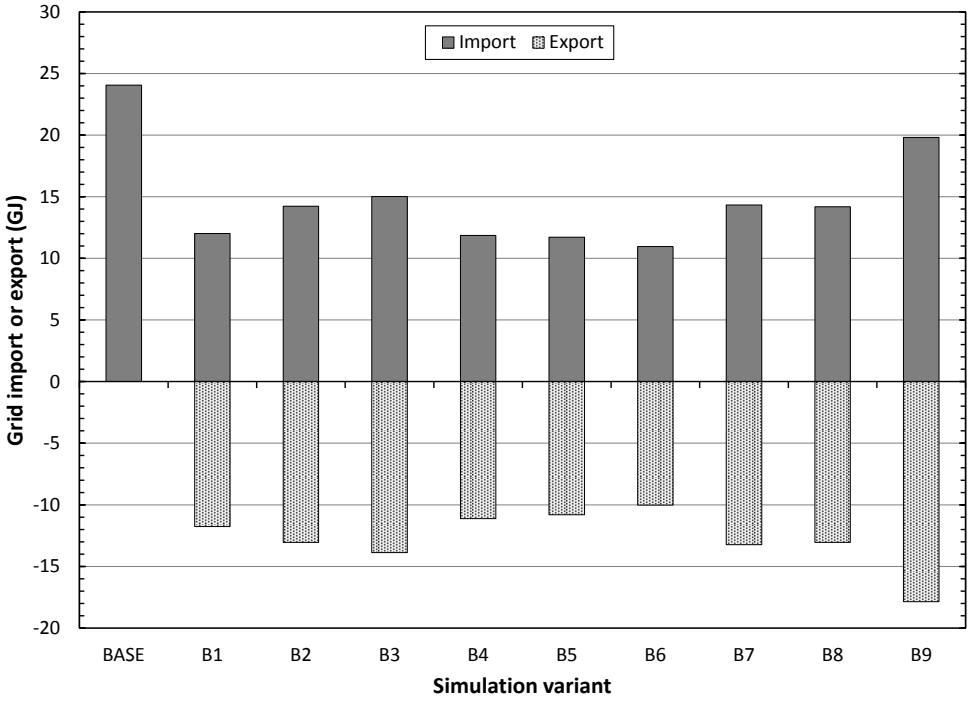

Figure B.1: Annual grid interaction using a residential PEMFC + RES system for occupant load profile H4.

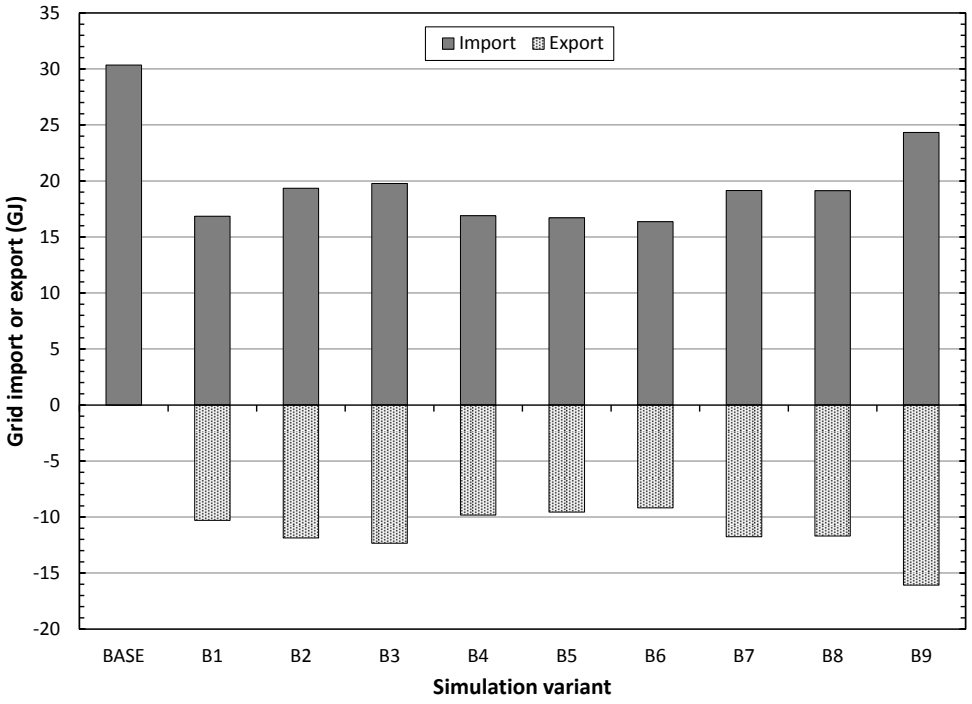

Figure B.2: Annual grid interaction using a residential PEMFC + RES system for occupant load profile H6.

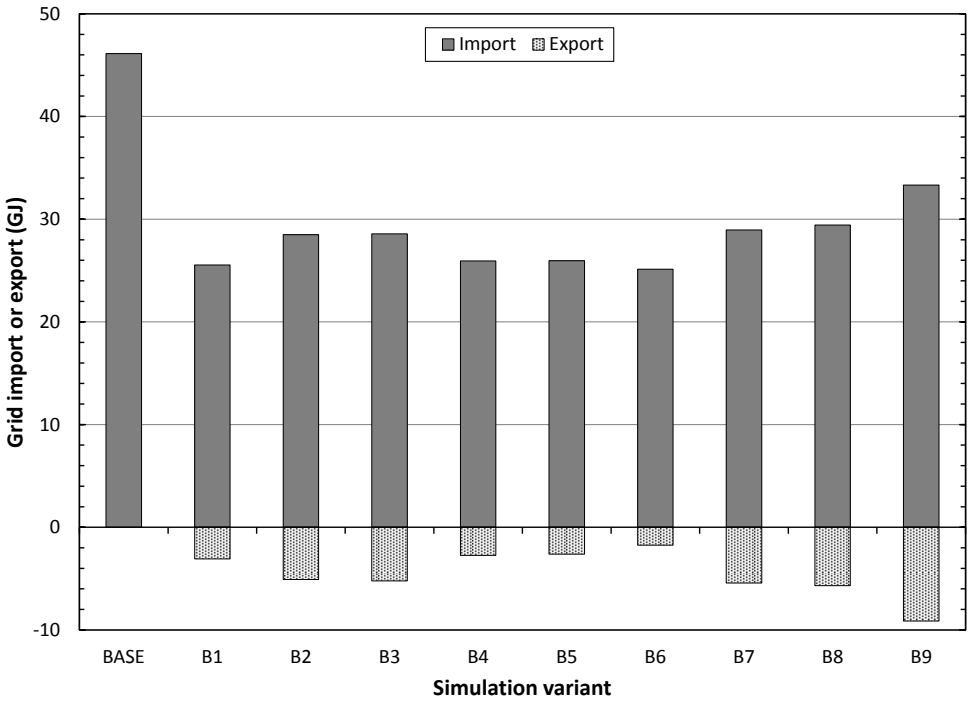

Figure B.3: Annual grid interaction using a residential PEMFC + RES system for occupant load profile H12.

Appendix C

Annual End-user Cost

Results for annual EU cost for houses H4, H6, and H12.

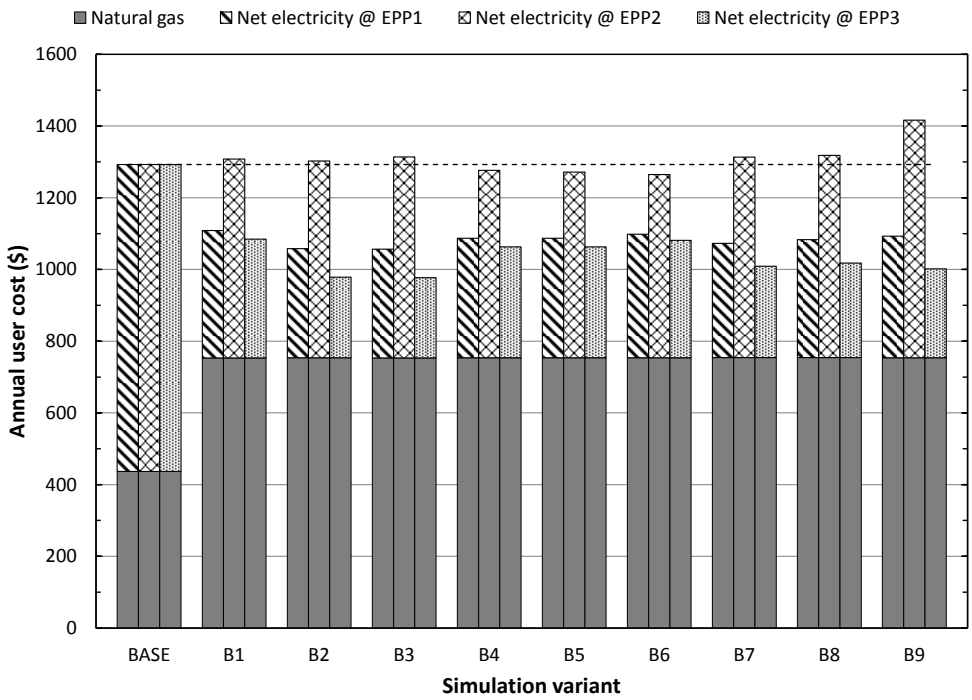

Figure C.1: Annual end-user energy costs using a residential PEMFC + RES system for occupant load profile H4.

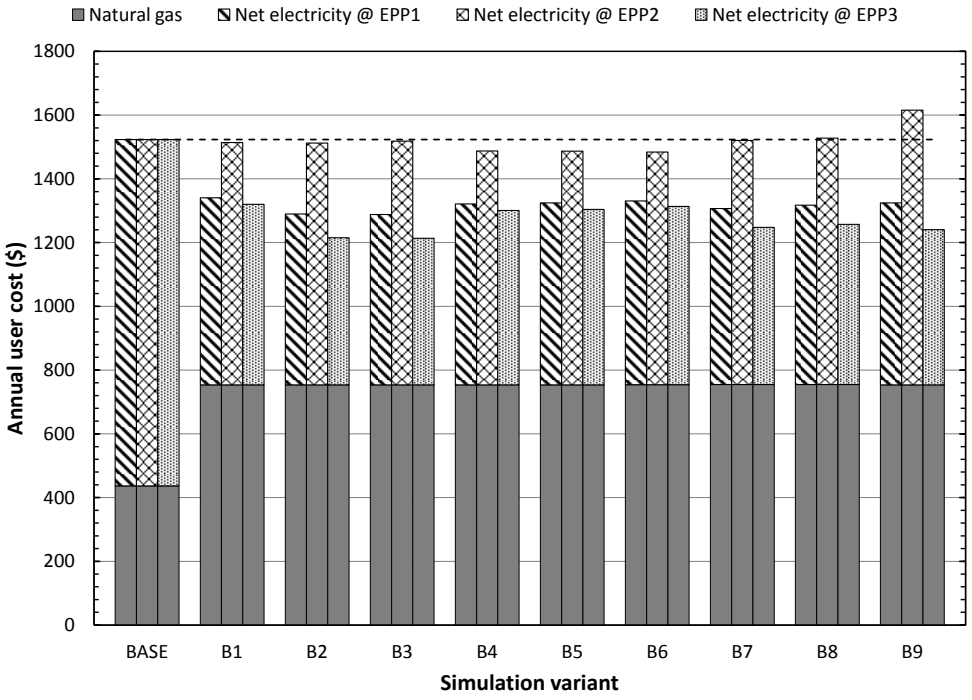

Figure C.2: Annual end-user energy costs using a residential PEMFC + RES system for occupant load profile H6.

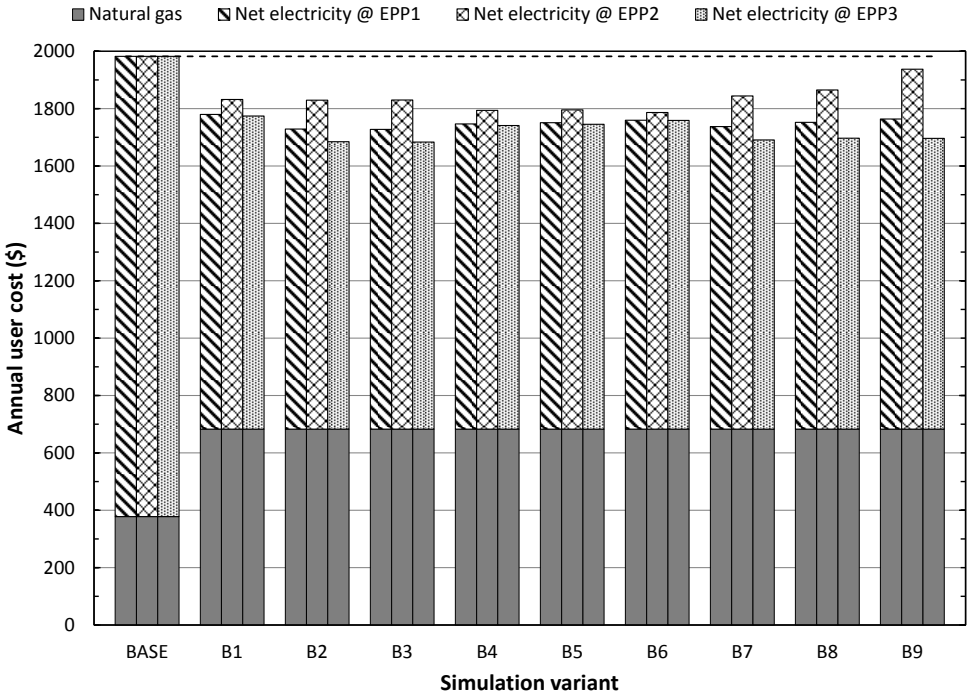

Figure C.3: Annual end-user energy costs using a residential PEMFC + RES system for occupant load profile H12.

Appendix D

Annual Local Distribution Company Cost

Results for annual LDC cost for houses H4, H6, and H12.

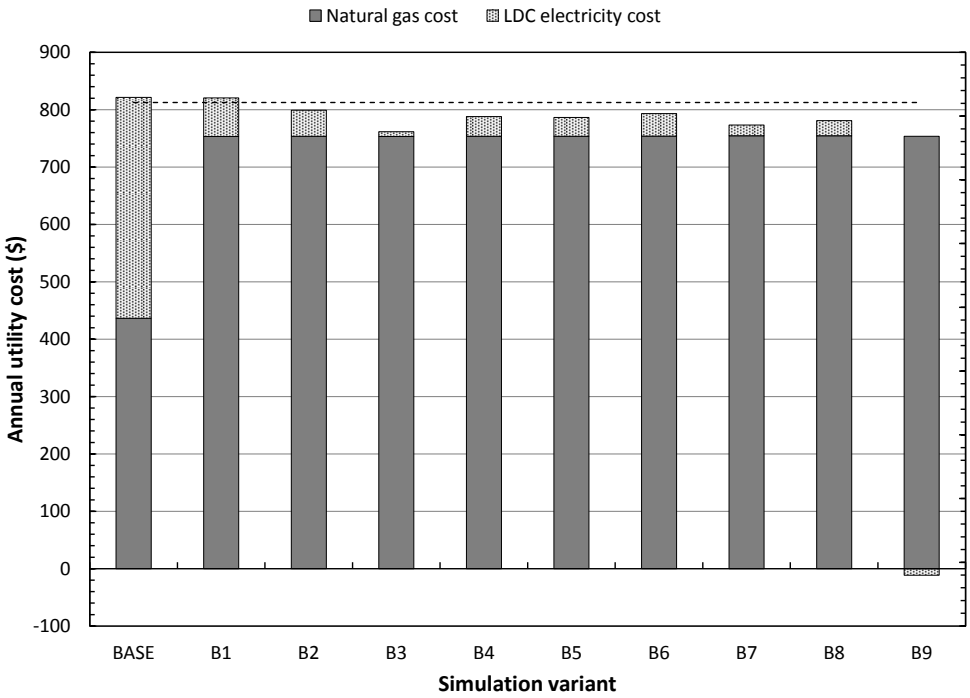

Figure D.1: Annual LDC energy costs using a residential PEMFC + RES system for occupant load profile H4.

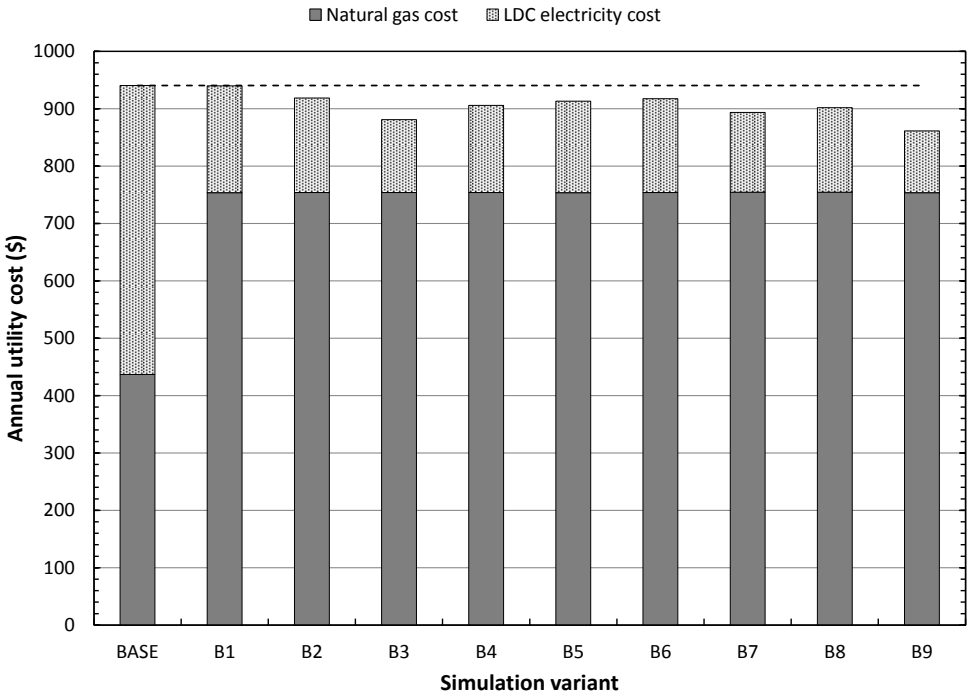

Figure D.2: Annual LDC energy costs using a residential PEMFC + RES system for occupant load profile H6.

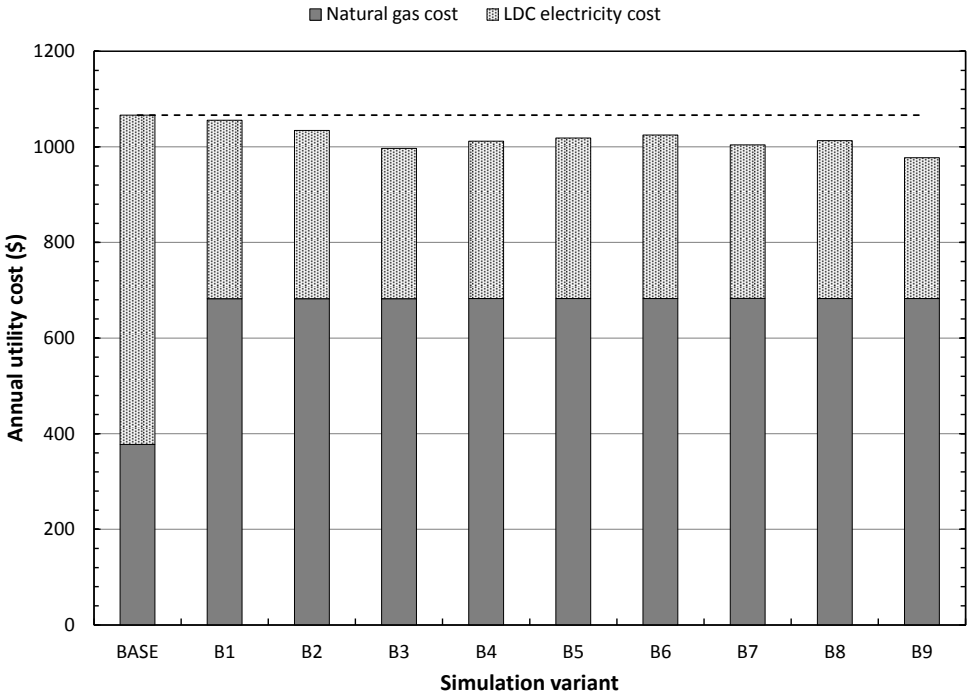

Figure D.3: Annual LDC energy costs using a residential PEMFC + RES system for occupant load profile H12.